Calculation of three-point asymmetric cumulant in high-multiplicity pp collitions at LHC

Ran Segev

Calculation of Three-Point Asymmetric Cumulant in High-Multiplicity Proton-Proton Collisions at the Large Hadron Collider

Research Thesis

Ran Segev

Research Thesis In Partial Fulfillment of the Requirements
for the Degree of Master of Science in Physics

Submitted to the Senate of the Technion - Israel Institute of Technology
Haifa
Adar Aleph, 5782, February, 2022

Instruction

The Research Thesis Was Done Under the Supervision of Professor Blok Boris of the Physics Department.

The generous financial help of the Technion - Israel Institute of Technology is gratefully acknowledged.

List of Publications

- B. Blok, R. Segev, The three point asymmetric cumulants in high-multiplicity pp collisions, Eur. Phys. J. C **81** (2021) 1091, https://doi.org/10.1140/epjc/s10052-021-09886-z [arXiv:2107.11885 [hep-ph]].
- R. Segev, The three point asymmetric cumulants in high-multiplicity pp collisions, 12th International workshop on Multiple Partonic Interactions at the LHC, https://indico.lip.pt/event/688/

Contents

List of Figures

List of Tables

Abstract

The recent detection of nontrivial azimuthal correlation in high-multiplicity proton-proton (pp) collisions at the Large Hadron Collider (the so-called *ridge* phenomenon) has aroused considerable interest because similar correlations were detected previously in heavy-ion collisions at the Large Hadron Collider and the BNL Relativistic Heavy Ion Collier, where they were considered a crucial indicator of the creation of a quark gluon plasma. Although these correlations occur naturally in the quark gluon plasma framework due to the large interactions between the particles emitted in the collisions (final-state interactions), they are absent in pp collisions. This leads to the search for new possible mechanisms for the ridge phenomenon. In particular, a new approach based on quantum interference and the multi-parton interaction was developed. This formalism was recently successfully applied to symmetric correlators.

In this thesis we study how quantum interference and colour flow affect three-point correlations described by asymmetric cumulants in high-multiplicity events in pp collisions. We use the model previously developed to study collectivity in symmetric cumulants to show that the resulting three-point asymmetric cumulant is qualitatively consistent with the experimental data for the same parameters as used in the model to describe the symmetric cumulants. The results show that the initial-state correlations must play a major role and may even dominate the explanation of correlations in high-multiplicity pp events.

We formulate the goals for our research in the introduction, following which Chap. 2 reviews the basic ideas of the approach for high-multiplicity pp collisions based on quantum interference and multi-parton interactions. Chapter 3 computes the three-point cumulant, studies the dependence of the momentum and number of emitted particles and compares the results to experimental data.

List of symbols and abbreviations

pp	:	Proton-proton
LHC	:	Large Hadron Collider
QGP	:	Quark gluon plasma
QCD	:	Quantum chromodynamics
MPI	:	Multi-parton interaction
AA	:	Heavy-ion collisions
GeV	:	Giga electron Volt
sc	:	Symmetric cumulant
ac	:	Asymmetric cumulant
PDF	:	Parton distribution dunction
DGLAP	:	Dokshitzer–Gribov–Lipatov–Altarelli–Parisi
GPD	:	General partonic distribution
DPS	:	Double-parton scattering
LPHD	:	Local parton-hadron duality

Chapter 1

Introduction

Recent studies of high-multiplicity proton-proton (pp) collisions at the Large Hadron Collider (LHC) [1, 2, 3, 4, 5] detected collective behavior (the so-called *ridge* phenomenon) that was considered indicative of the creation of a quark-gluon plasma (QGP) when previously detected in heavy-ion (AA) collisions [5, 6, 7, 8, 9].

The ridge phenomenon occurs naturally in heavy-ion collisions, where it is explained by strong final-state interactions between emitted particles. However, in pp collisions we expect much smaller transverse size and density in the collision, and these collisions are generally well described by Monte Carlo generators that assume independent emitted particles. Consequently, we need a new approach to the ridge phenomenon that is not based on strong final-state interactions.

Such an approach, based on quantum interference and multi-parton interactions (MPIs), was proposed in Refs. [10, 11] to explain this collective behavior. Using this model, we can calculate the azimuthal correlations in pp collisions and explain the ridge phenomenon. Although the studies reported in Refs. [10, 11] were devoted to symmetric cumulants, the ATLAS Collaboration recently measured a new type of correlation in high-multiplicity pp collisions: the three-point asymmetric cumulant [12]. This thesis uses the approach of Refs. [10, 11] to calculate the three-point asymmetric cumulant. We study how emitted particles depend on the momentum and multiplicity, and the results are consistent with the experimental data.

The thesis is organised as follows: Chapter 2 reviews the basic formalism developed in Refs. [10, 11] to study the collective behavior in high-multiplicity pp collisions. In particular, Sec. 2.1 explains the geometry of high-multiplicity pp collisions and the basic experimental and mathematical tools used to describe these correlations (the so-called flow analysis). Section 2.2 reviews the basic ideas of multi-parton interactions, and Sec. 2.3 discusses the model of Refs. [10, 11] used to study correlations in pp collisions.

Chapter 3 calculates the three-point asymmetric cumulant. In particular, Sec. 3.1 establishes the physical problem to be solved, Sec. 3.2 summarises the formalism to be used, Sec. 3.3 finds the three-point asymmetric cumulant for the case of three partonic interactions and three emitted particles and derives the momentum dependence and Sec. 3.4 extends the result to the case of an arbitrary number of partonic interactions and emitted particles and compares the multiplicity dependence with the experimental results.

Finally, Chapt. 4 presents the conclusions.

Chapter 2

Review of Quantum Interference Approach

2.1 Ridge and Cumulants

2.1.1 Heavy-Ion Collisions

Experimentalists have been using heavy-ion (AA) collisions to create and study the QGP since it was discovered in the beginning of the millennium [13]. One way to study the emergence of the QGP in AA collisions is to look at multi-particle-production events and quantify the distribution of the rapidity and azimuthal directions of the emitted particles with respect to reaction-plane angle.[1]

Figure 2.1 shows a simplified diagram taken from Ref. [14] of the geometry of a collision projected onto the plane transverse to the beam axis. To compare measurements of the azimuthal distribution for single particles from different events we need to know the reaction-plane angle for each event and shift the measurements accordingly. One way avoid this is to consider the correlations between particles instead of the distribution of a single particle relative to the reaction plane.

Consider measurements like those shown in Fig. 2.2 (taken from Refs. [6, 7]), where several trends are clear [6, 7]. In particular, we see that, regardless of the azimuthal difference between the particles, the correlation is essentially independent of the pseudorapidity difference, where the pseudorapidity η and rapidity y are defined as follows:

$$\eta \;=\; -\ln\left[\tan\left(\frac{\theta}{2}\right)\right],$$

[1] The reaction plane is the plane that contains the centers of the colliding particles and is parallel to the beam axis.

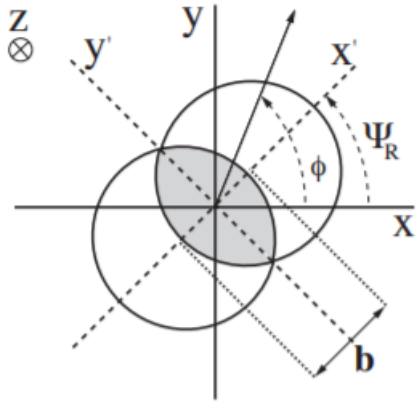

Figure 2.1: Diagram of coordinate system used in flow analysis. The Z axis is the beam axis coming out of the page, the XY plane is the transverse plane, where the X axis, or the azimuthal zero, is chosen arbitrarily. The $X'Y'$ plane is the XY plane rotated by the reaction-plane angle $\mathbf{\Psi}_R$, where the reaction plane is the plane containing the beam axis and the centers of the two nuclei so that both centers are on the X' axis. The impact parameter b is given by the projection of the distance between the centers of the nuclei, and ϕ is the azimuthal angle of an emitted particle. The diagram is taken from Ref. [14].

$$y = \frac{1}{2}\ln\left(\frac{E+p_z}{E-p_z}\right),$$

were θ is the angle between the particle momentum and the beam axis, E is the particle energy and p_z is the particle momentum along the beam axis. Recall that, for massless or ultrarelativistic particles, this is the same as the pseudorapidity that is used in measurements, so $y \approx \eta$.

The phenomenon whereby azimuthal correlations are almost independent of the pseudorapidity difference is called the *ridge* phenomenon. This correlation between particles very distant in rapidity is indicative of collective behavior that reflects the existence of a medium that allows information to be shared between the emitted particles. The existence of such a medium is somewhat expected in AA collisions where we expect the creation of a QGP. As stated at the beginning of the chapter, one of the many topics studied via AA collisions is the existence and properties of the QGP. The collective behavior in Pb-Pb collisions was also reported in Refs. [5, 8, 9, 15, 16].

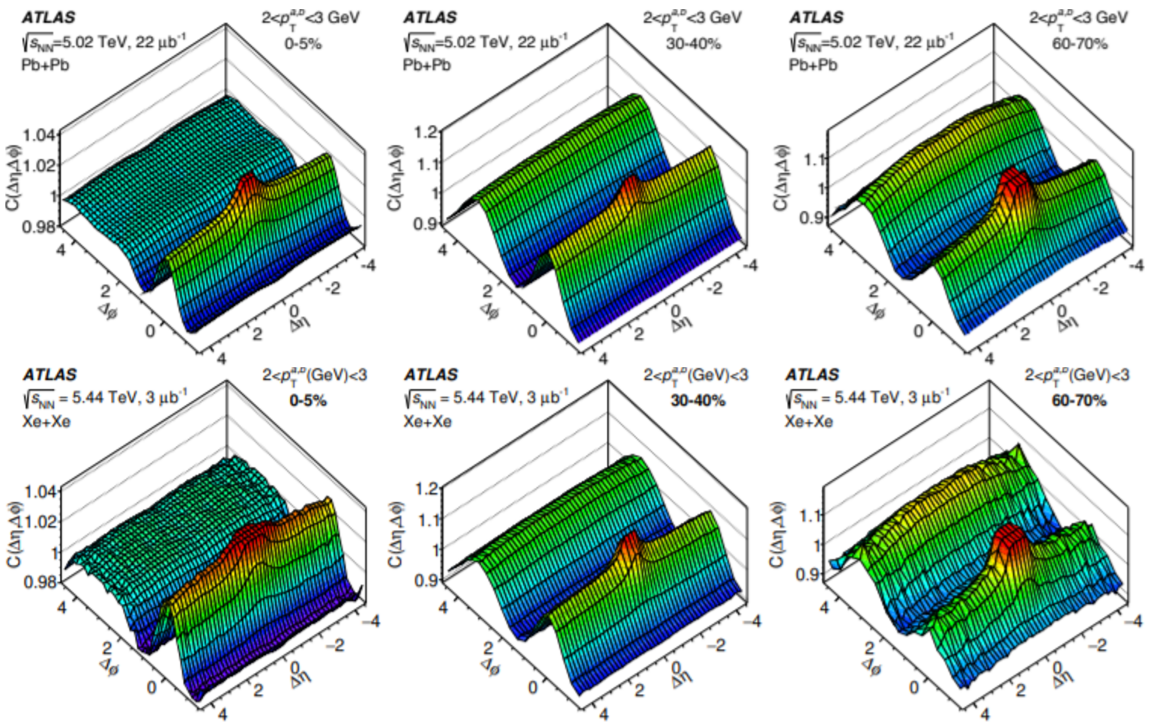

Figure 2.2: Three-dimensional plots of two-particle correlations $C(\Delta\eta, \Delta\phi)$ in AA collisions as a function of $\Delta\phi$, which is the azimuthal difference between the particles, and $\Delta\eta$, which is the pseudorapidity difference between the particles, Pb + Pb on top [6] and Xe + Xe on the bottom [7], for different centrality intervals, 0%–5% (left), 30%–40% (center) and 60%–70% (right). Both experiments considered particles with transverse momentum in the range 2 GeV $< p_t <$ 3 GeV and pseudorapidity in the range $|\eta| < 2.5$ ($\sqrt{s_{NN}}$ is the center-of-mass energy of the collisions in each experiment). Several clear trends appear from these measurements; the most important for us is the apparent independence of the correlation on the pseudorapidity difference. This phenomenon is called the *ridge* phenomenon. The correlations peak around $\Delta\phi = \Delta\eta = 0$ is partly a non-flow contribution that comes from considering particles that originate from the same jet.

2.1.2 High-Multiplicity Proton-Proton Collisions

In high-multiplicity pp collisions, the transverse size of the collision is very small compared with that of AA collisions. For example, for ultrarelativistic Pb + Pb collisions, the ratio of gluon density is much greater than it is for pp collisions, so we do not expect a QGP to be created in such systems (sometimes called *small systems* as opposed to large systems created in AA collisions). Therefore, we cannot explain the correlations between large-rapidity-difference particles by the emergence of a new medium. The particles emitted from a pp collision should act almost as free particles with no sign of collective behavior; in other words, we do not expect the ridge phenomenon in pp collisions.

The CMS Collaboration first observed the ridge phenomenon in pp collisions in 2010 [1], and more measurements have come out since (see, e.g., Refs [2, 3, 4, 5]), as shown in Figs. 2.3 and 2.4. This leads us to ask how particles that are almost completely free embody this collective behavior. We thus need to find an origin other than final-state interactions for correlations in pp collisions.

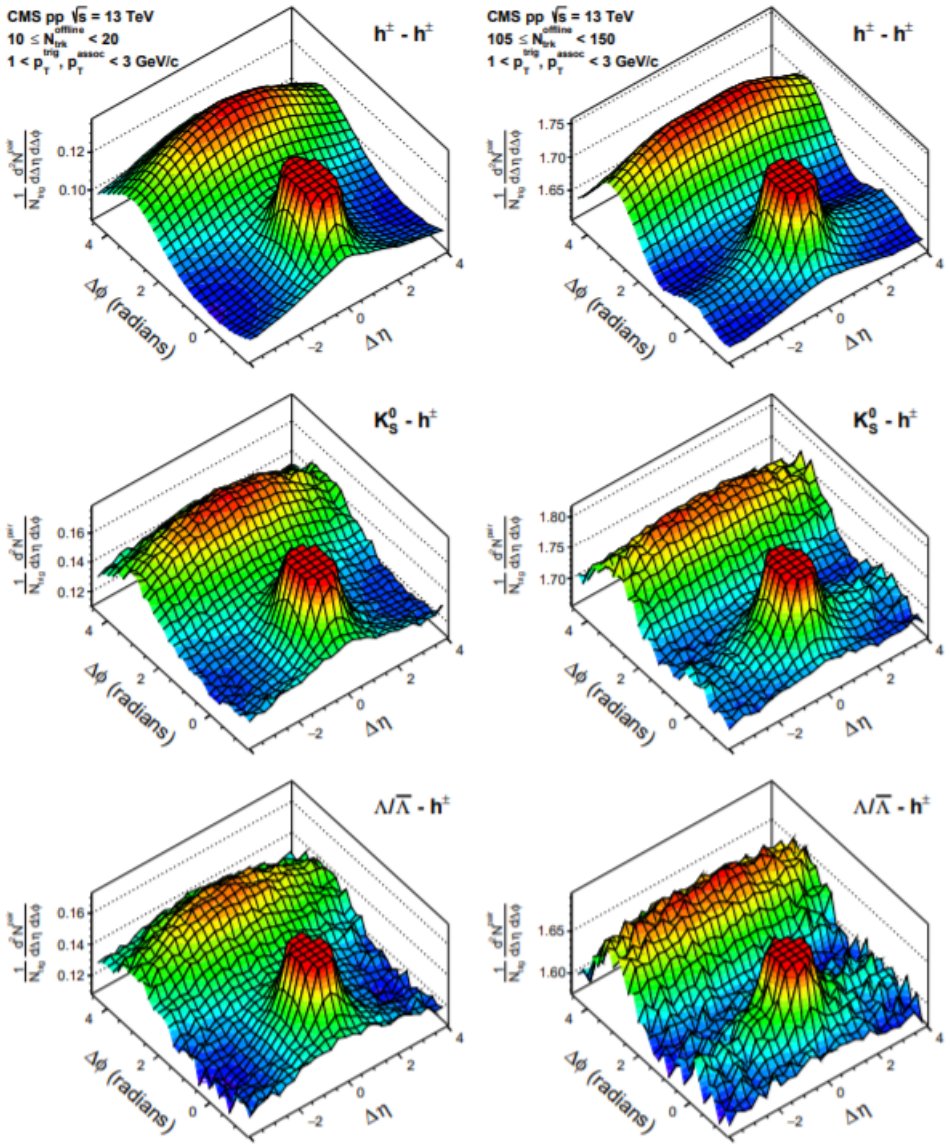

Figure 2.3: Correlations for two particles in a pp collision as a function of $\Delta\phi$, the azimuthal difference, and $\Delta\eta$, the pseudorapidity difference, from Ref. [2]. The plots are for different selection parameters; the figure shows only charged particles (top row), events with kion particles (middle row), and events with lambda (or anti-lambda) particles (bottom row). Low-multiplicity events appear in the left column and high-multiplicity events in the right column. As seen for correlations in AA collisions, the correlations peak in two regions: near $\Delta\phi = \Delta\eta = 0$ a mostly non-flow contribution is due to particles originating from the same jet, as in Fig. 2.2. The peak near $\Delta\phi \approx \pi$ is very similar to the analogous peak for AA collisions, including the very weak dependence on the pseudorapidity difference.

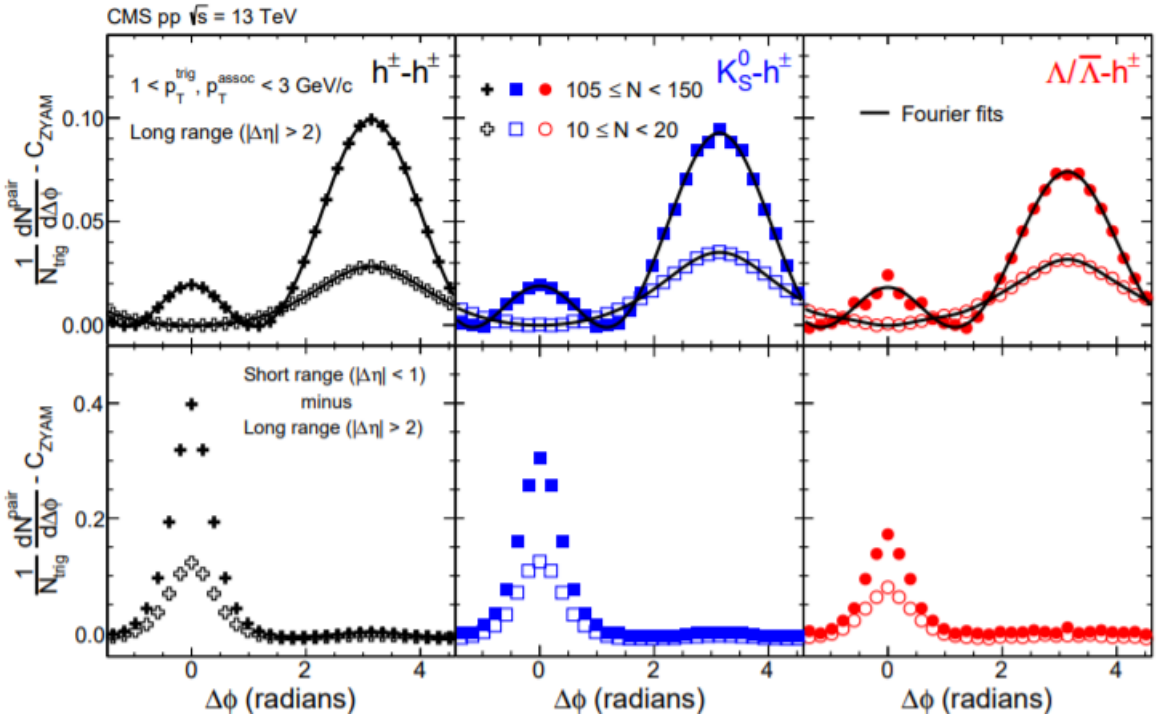

Figure 2.4: Correlations for two protons in a pp collision after applying the zero yield at minimum procedure (which consists of shifting the measurements so that they are zero at the minimum) as a function of $\Delta\phi$, the azimuthal difference (from Ref. [2]). The top row shows long-range correlations for particle pairs with high $\Delta\eta$. The bottom rows show short-range correlations for particles pairs with low $\Delta\eta$; solid symbols are for multiplicities between 105 and 150, open symbols are for multiplicities between 10 and 20. The different colours represent different types of events: only charged particles (black), events with kion particles (blue) and events with lambda (or anti-lambda) particles (red). The black line is a Fourier fit.

2.1.3 Cumulants

When we study correlations between s particles we want to be sure that what we calculate comes from the correlations of *all* particles. To do this we need to define the cumulants. Assume as valid the one-particle momentum distribution function defined in Ref. [17]:

$$f\left(\mathbf{p}\right) \equiv \frac{dN}{d^3p}, \tag{2.1}$$

where dN is the differential multiplicity, or the number of particles within a small momentum space $d^3\boldsymbol{p}$. To calculate the properties of the emitted particles, we can imagine taking the average with respect to the momentum distribution function; for example, we can take the average of a function $F(\mathbf{p})$ over the azimuthal component of the particle momentum, resulting in a function of the transverse momentum and

rapidity:

$$\langle F(\mathbf{p})\rangle(p_t, y) = \frac{\int F(\mathbf{p}) f(\boldsymbol{p})\, d\phi}{\int f(\boldsymbol{p})\, d^3p}, \tag{2.2}$$

where $\langle\ \rangle$ indicates an average. The correlation between two different particles is then defined by the two-particle distribution function,

$$f(\mathbf{p}_1, \mathbf{p}_2) \equiv \frac{d^2N}{d^3p_1 d^3p_2}, \tag{2.3}$$

where $\mathbf{p}_1$ and $\mathbf{p}_2$ are the three-momenta of the two different particles. If the two particles are not correlated, the distribution function factorizes, $f(\mathbf{p}_1, \mathbf{p}_2) = f(\mathbf{p}_1)f(\mathbf{p}_2)$. However, in general we have

$$f(\mathbf{p}_1, \mathbf{p}_2) \equiv f(\mathbf{p}_1) f(\mathbf{p}_2) + f_c(\mathbf{p}_1, \mathbf{p}_2), \tag{2.4}$$

where $f_c(\mathbf{p}_1, \mathbf{p}_2)$ denotes the correlated part of the distribution. For a single particle $f_c(\mathbf{p}) \equiv f(\mathbf{p})$ because we cannot break it down into smaller pieces.

This approach can be generalised to any number of particle correlations; for example, the three-particle distribution is given by

$$\begin{aligned} f(\boldsymbol{p}_1, \boldsymbol{p}_2, \boldsymbol{p}_3) &\equiv \frac{d^3N}{d^3p_1 d^3p_2 d^3p_3} \\ &= f_c(\boldsymbol{p}_1) f_c(\boldsymbol{p}_2) f_c(\boldsymbol{p}_3) + \sum_{j=1}^{3} f_c(\boldsymbol{p}_j) f_c\left(\{\boldsymbol{p}_k\}_{k\neq j}\right) + f_c(\boldsymbol{p}_1, \boldsymbol{p}_2, \boldsymbol{p}_3), \end{aligned} \tag{2.5}$$

where the first term on the right-hand side is the product of the one-particle distributions, the second term comes from the pair correlations within the three particles and the last term is the three-particle true correlation. In general, to decompose the s-particle distribution function we first take all possible partitions of $\{\boldsymbol{p}_1, \boldsymbol{p}_2, \ldots, \boldsymbol{p}_s\}$. For each subset $\{\boldsymbol{p}_{j_1}, \boldsymbol{p}_{j_2}, \ldots, \boldsymbol{p}_{j_m}\}$, we find the corresponding correlated function, $f_c(\boldsymbol{p}_{j_1}, \boldsymbol{p}_{j_2}, \ldots, \boldsymbol{p}_{j_m})$. The contribution of a given partition is the product of the contributions of each subset. Finally, $f(\boldsymbol{p}_1, \boldsymbol{p}_2, \ldots, \boldsymbol{p}_s)$ is the sum of the contributions of all partitions.

By using these relations, we can express the true correlated distributions in terms of the full correlation functions. For example, for one, two and three particles,

$$\begin{aligned} f_c(\boldsymbol{p}) &= f(\boldsymbol{p}), \\ f_c(\boldsymbol{p}_1, \boldsymbol{p}_2) &= f(\boldsymbol{p}_1, \boldsymbol{p}_2) - f(\boldsymbol{p}_1) f(\boldsymbol{p}_2), \\ f_c(\boldsymbol{p}_1, \boldsymbol{p}_2, \boldsymbol{p}_3) &= f(\boldsymbol{p}_1, \boldsymbol{p}_2, \boldsymbol{p}_3) - f(\boldsymbol{p}_1, \boldsymbol{p}_2) f(\boldsymbol{p}_3) - f(\boldsymbol{p}_1, \boldsymbol{p}_3) f(\boldsymbol{p}_2) - f(\boldsymbol{p}_2, \boldsymbol{p}_3) f(\boldsymbol{p}_1) \\ &\quad + 2 f(\boldsymbol{p}_1) f(\boldsymbol{p}_2) f(\boldsymbol{p}_3). \end{aligned} \tag{2.6}$$

The true correlations f_c are called *cumulants*.

2.1.4 Flow Analysis

Studying the azimuthal distributions and correlations of particles gave rise to the subject of *flow analysis*, which studies the anisotropic behavior in the azimuthal direction by decomposing the distribution of emitted particles into a Fourier expansion [14]. For example,

$$f(\boldsymbol{p}) = \frac{1}{2\pi E}\frac{dN}{p_t dp_t dy}\left\{1 + 2\sum_{n=1}^{\infty} v_n(p_t, y)\cos\left[n(\phi - \boldsymbol{\Psi}_R)\right]\right\}, \tag{2.7}$$

where $f(\boldsymbol{p})$ is the one-particle momentum distribution function defined in Eq. (2.1), y is the rapidity of the particle, E is the energy of the particle, p_t is the transverse momentum of the particle, ϕ is the azimuthal coordinate of the particle momentum, $\boldsymbol{\Psi}_R$ is the azimuthal angle between the arbitrarily chosen X axis and the projection of the vector connecting the two centers of the nuclei onto the XY plane (also known as the reaction-plane angle) and v_n are the Fourier coefficients, also known as flow harmonics.

In general, v_n are functions of the transverse momentum and pseudorapidity of the emitted particles, but since we are looking at a ridge case we can neglect the pseudorapidity. The coefficients v_n can be defined by the following average over the azimuthal angle ϕ:

$$v_n(p_t) \equiv \left\langle e^{in(\phi - \boldsymbol{\Psi}_R)}\right\rangle = \langle\cos\left[n(\phi - \boldsymbol{\Psi}_R)\right]\rangle = \frac{\int e^{in(\phi-\boldsymbol{\Psi}_R)} f(\boldsymbol{p})\, d\phi}{\int f(\boldsymbol{p})\, d^3p}. \tag{2.8}$$

In a similar way we can decompose the correlations into a Fourier expansion; for example, the two-particle correlation can be found by using the two-particle distribution function by taking the average over both azimuthal components:

$$\left\langle e^{in(\phi_1 - \boldsymbol{\Psi}_R)} e^{-in(\phi_2 - \boldsymbol{\Psi}_R)}\right\rangle = \left\langle e^{in(\phi_1 - \phi_2)}\right\rangle = \frac{\int e^{in(\phi_1-\phi_2)} f(\boldsymbol{p}_1, \boldsymbol{p}_2)\, d\phi_1 d\phi_2}{\int f(\boldsymbol{p}_1, \boldsymbol{p}_2)\, d^3p_1 d^3p_2}. \tag{2.9}$$

In this way, we get rid of the explicit dependence on the position of the reaction plane.

Flow analysis is the study of the flow harmonics, and v_1 and v_2 are commonly known as the direct flow and the elliptic flow, respectively. v_1 corresponds to a preference for a single direction, and v_2 represents a symmetry by a 180° rotation around the Z axis. This symmetry is expected in a AA-collision system. In general, v_n depend on the collision geometry, which is why higher-order flow harmonics ($n > 2$) are also important in studying the collision structure.

By using the approach of the previous section, the correlations between many particles can be reduced to sums of correlations between fewer particles, like the

s-particle distribution functions. In other words, the two-particle correlation can be reduced to

$$\left\langle e^{in(\phi_1-\phi_2)}\right\rangle = \left\langle e^{in\phi_1}\right\rangle \left\langle e^{-in\phi_2}\right\rangle + \left\langle e^{in(\phi_1-\phi_2)}\right\rangle_c , \tag{2.10}$$

were $\langle e^{in(\phi_1-\phi_2)}\rangle_c$ is just the two-particle cumulant defined in the previous section.

If we assume a perfect detector, $\langle e^{in\phi_j}\rangle$ vanishes due to the axial symmetry of the system for any $n \neq 0$ because it implies an average over the reaction-plane angle. Therefore, it is not the same as v_n. In the same way, all the correlations of the form $\langle \exp(i\sum_{j=1}^{s} n_j\phi_j)\rangle$ where $\sum_{j=1}^{s} n_j \neq 0$ also vanish.

2.1.5 Calculating Cumulants from Data

The s-particle cumulant is determined from measurements in a few steps. First, we calculate the single-event multi-particle correlations; for example, the two- and four-particle single-event correlations are given by

$$\begin{aligned} \langle 2\rangle_n &\equiv \left\langle e^{in(\phi_1-\phi_2)}\right\rangle = \frac{1}{P_{m,2}}{\sum_{i,j}}' e^{in(\phi_i-\phi_j)}, \\ \langle 4\rangle_n &\equiv \left\langle e^{in(\phi_1+\phi_2-\phi_3-\phi_4)}\right\rangle = \frac{1}{P_{m,4}}{\sum_{i,j,k,l}}' e^{in(\phi_i+\phi_j-\phi_k-\phi_l)}, \end{aligned} \tag{2.11}$$

where $\langle s\rangle_n$ is the s-particle correlation of single event n, m is the multiplicity or number of particles emitted in the event, $P_{m,s} \equiv m!/(m-s)!$ and the sum $\sum'$ means all the indices are different. We then average over all events:

$$\langle\langle s\rangle\rangle_n \equiv \frac{\sum_{\text{events}} \left(W_{\langle s\rangle}\right)_i \langle s\rangle_n}{\sum_{\text{events}} \left(W_{\langle s\rangle}\right)_i}, \tag{2.12}$$

where $\langle\langle s\rangle\rangle_n$ denotes the averaged nth s-particle correlation, where the average is first over all particles and then over all events. $(W_{\langle s\rangle})_i$ is the weight of event i and is used to account for variations in multiplicity between different events. We can use $(W_{\langle s\rangle})_i = \delta_{m_i,M}$ to consider only events with a fixed multiplicity M, or $(W_{\langle s\rangle})_i = P_{m_i,s}$ for general multiplicity. Picking this option leads to $\langle\langle s\rangle\rangle_n$, which is independent of multiplicity, or to many other functions.

The connection between the double-bracketed correlations and the cumulants is discussed in detail in Ref. [18]. Here, we write only the cumulants for $s = 2, 4, 6$, denoted $c_n\{s\}$, which are functions of the transverse momentum and pseudorapidity of all s particles being correlated. Examples are helpful to see the patterns:

$$\begin{aligned} c_n\{2\} &= \langle\langle 2\rangle\rangle_n , \\ c_n\{4\} &= \langle\langle 4\rangle\rangle_n - 2\left(\langle\langle 2\rangle\rangle_n\right)^2 , \end{aligned}$$

$$c_n\{6\} = \langle\langle 6\rangle\rangle_n - 9\langle\langle 4\rangle\rangle_n\langle\langle 2\rangle\rangle_n + 12\left(\langle\langle 2\rangle\rangle_n\right)^3. \tag{2.13}$$

These examples assume both large average multiplicity and a detector with uniform acceptance (more general definitions can be found in Refs. [14, 18]). The cumulants are defined in such a away that, for all $c_n\{2k\}$ for $k > 1$, they vanish unless there is a sizable $s = 2k$ correlation. For example, if we assume that there are no four-particle correlations we could expand as follows $\langle\langle 4\rangle\rangle_n$ into a product of a pair two-particle correlations:

$$\langle\langle 4\rangle\rangle_n = \left\langle\left\langle e^{in(\phi_1+\phi_2-\phi_3-\phi_4)}\right\rangle\right\rangle \approx 2\left\langle\left\langle e^{in(\phi_1-\phi_3)}\right\rangle\right\rangle\left\langle\left\langle e^{in(\phi_2-\phi_4)}\right\rangle\right\rangle = 2\left(\langle\langle 2\rangle\rangle_n\right)^2. \tag{2.14}$$

Plugging this result back into $c_n\{4\}$ in Eq. (2.13), we see that it vanishes identically. The same occurs for $c_n\{6\}$ and any other $c_n\{s\}$ for $s > 2$.

By using the cumulants, we can approximate the flow harmonics, with $c_n\{s\}$ giving us better approximation for higher values of s. The results of Ref. [18] allow us to write the approximations

$$\begin{aligned}
\left(v_n\{2\}\right)^2 &\approx c_n\{2\}, \\
\left(v_n\{4\}\right)^4 &\approx -c_n\{4\}, \\
\left(v_n\{6\}\right)^6 &\approx c_n\{6\}/4.
\end{aligned} \tag{2.15}$$

The fact that $v_n\{2k\} \propto (-1)^{k+1}c_n\{2k\}$ is called collectivity.

2.1.6 Three-Particle Cumulant

So far we have only talked about symmetric cumulants, for which all particles have the same flow harmonic index, but this forces us to only consider an even number of particles so that the dependence on the reaction-plane angle cancels out. We can extend the notion of the cumulant to odd numbers of particles by allowing correlations between flow harmonics with different indices. For three-particle correlations it is common to define them in a way similar to four-particle correlations, where the two particles with a negative weight are chosen to be the same:

$$\left\langle e^{in(\phi_1+\phi_2-2\phi_3)}\right\rangle \equiv \frac{\int e^{in(\phi_1+\phi_2-2\phi_3)}\frac{d^3N}{d^3\boldsymbol{p}_1 d^3\boldsymbol{p}_2 d^3\boldsymbol{p}_3}d\phi_1 d\phi_2 d\phi_3}{\int \frac{d^3N}{d^3\boldsymbol{p}_1 d^3\boldsymbol{p}_2 d^3\boldsymbol{p}_3}d^3p_1 d^3p_2 d^3p_3}. \tag{2.16}$$

To calculate Eq. (2.16) from data we define the single-event average by

$$\langle 3\rangle_{n,n|2n} \equiv \left\langle e^{in(\phi_1+\phi_2-2\phi_3)}\right\rangle = \frac{1}{P_{m,3}}{\sum_{i,j,k}}' e^{in(\phi_i+\phi_j-2\phi_k)}. \tag{2.17}$$

We can also consider taking the harmonic indices with the opposite sign, but if we assume a perfect detector we find that correlation is just the complex conjugate of the one we defined, $\langle 3\rangle_{n,n|2n} = (\langle 3\rangle_{-n,-n|-2n})^* = (\langle 3\rangle_{2n|n,n})^*$, and since the correlations are real, from the symmetry between the particles, they are the same. Taking this correlation and averaging over many events gives us the average correlation, $\langle\langle 3\rangle\rangle_{n,n|2n}$, from which we get the three-particle cumulant, which is also known as the three-particle asymmetric cumulant:

$$ac_{n,n|2n}\{3\} = \langle\langle 3\rangle\rangle_{n,n|2n}\,. \tag{2.18}$$

Like the two-particle cumulant, the asymmetric three-particle cumulant is the same as the three-particle average correlation because it is impossible to break the correlations down into pairs without separating the angle with greater weight from itself. The three-particle cumulant is called an asymmetric cumulant because it breaks the symmetry between the flow harmonic indices, but this property is not limited to three-particle correlations—we can define cumulants with different flow indices for any number of particles. For example, Ref. [12] studies four-particle correlations defined as $\langle\langle 4\rangle\rangle_{n,m|n,m}$. Provided the sums of the positive and negative indices are equal, the correlation and associated cumulants are well defined. But even then it is common to call the cumulant for an even (odd) number of particles the symmetric (asymmetric) cumulant. For the sake of brevity and to follow naming conventions, it is common to write $ac_{n,n|2n}\{3\}$ as $ac_n\{3\}$.

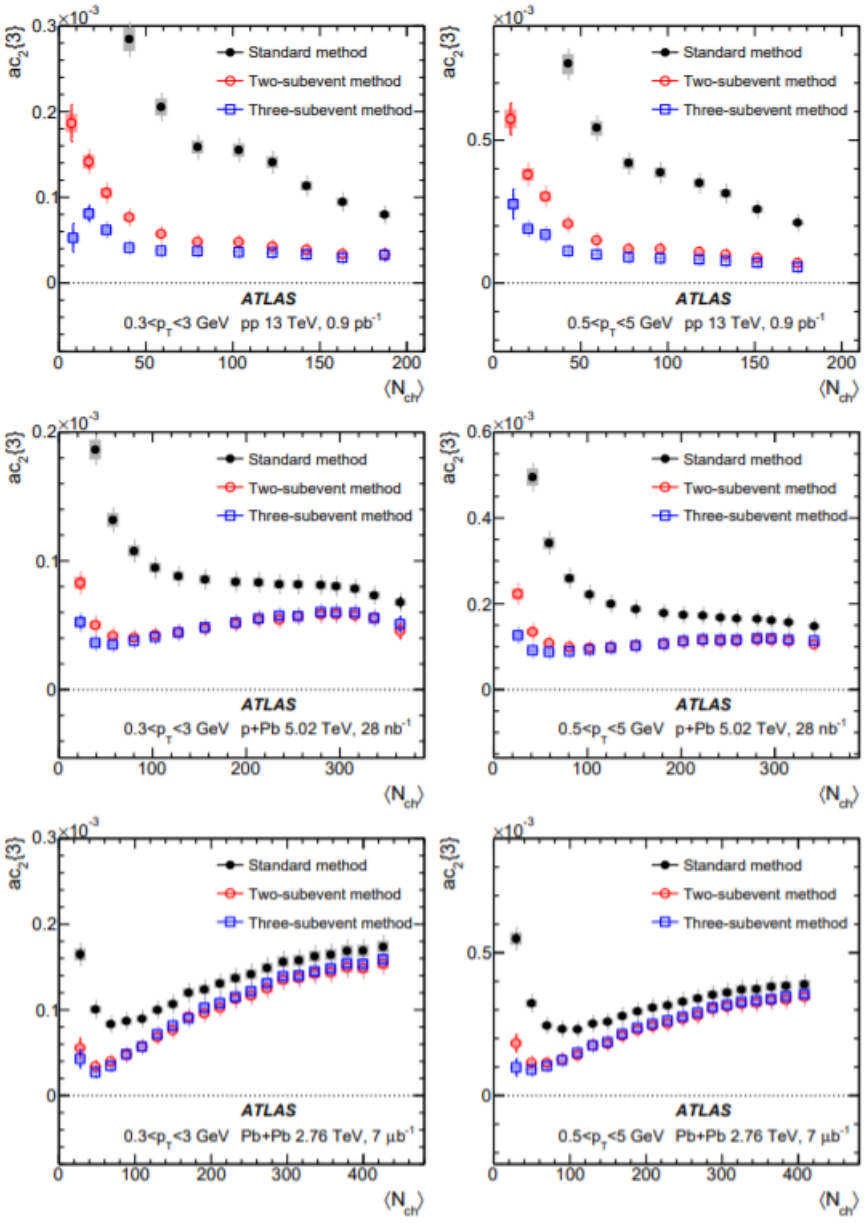

Figure 2.5: The second asymmetric cumulant for three particles, $ac_2\{3\}$, or the azimuthal correlations $\langle e^{i2(\phi_1+\phi_2-2\phi_3)}\rangle$ as a function of $\langle N_{ch}\rangle$, the number of charged particles detected, in (top) pp, (middle) p + Pb and (bottom) collisions for different ranges of transverse momentum of emitted particles, 0.3 GeV $< p_T <$ 3 GeV (left) and 0.5 GeV $< p_T <$ 5 GeV (right), as measured by Ref. [12]. The 2 (3) subevent methods refer to dividing the detector into 2 (3) equal parts in the range $|\eta| < \eta_{max} = 2.5$ and taking the particles from the different parts. This gives us more confidence that the correlations are due to the ridge phenomenon as opposed to taking particles out of the same jet (see Figs. 2.2 and 2.3).

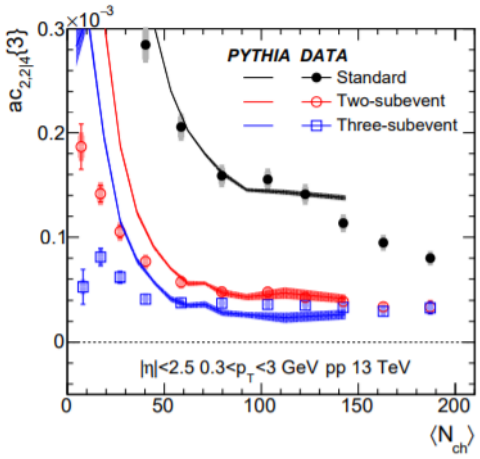

Figure 2.6: The second asymmetric cumulant for three particles $ac_2\{3\}$, or the azimuthal correlations $\langle e^{i2(\phi_1+\phi_2-2\phi_3)}\rangle$ as a function of the number $\langle N_{ch}\rangle$ of charged particles detected in pp collisions for emitted particles with transverse momentum in the range 0.3 GeV $< p_T <$ 3 GeV with the non-flow contributions reduced. The reduction of the non-flow contribution was done by Ref. [19].

2.2 Multi-Parton Interactions

The processes in which several partons from one nucleon collide with several partons from another nucleon are called multi-parton interactions (MPIs). Figure 2.7 (right) shows a diagram of a MPI with an arbitrary number of partonic interactions. Each partonic interaction involves one parton from hadron h_a and one parton from hadron h_b and results in a hard event, producing two or more hard out-going partons. In each collision there can be any number of MPIs. Figure 2.7 (left) shows an example of a collision with only two hard processes, which is usually called double-parton scattering (DPS) and is discussed in detail later in this chapter.

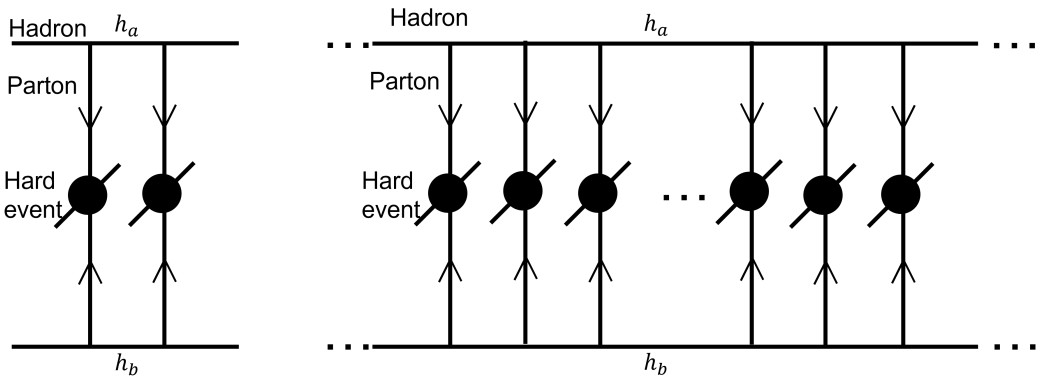

Figure 2.7: Two diagrams of amplitudes for a two-hadron collision. The horizontal lines represent the hadrons h_a and h_b, the vertical arrows represent the hard partons, the circles represent different hard events, and the diagonal lines represent out-going particles. The cross section of the process is the square of the diagrams. On the left is an event with only two partonic interactions and on the right is an event with an arbitrary number of partonic interactions, where the points indicate the possibility of many more partonic interactions not shown on the diagram.

2.2.1 Hard Process in Quantum Chromodynamics

This section discusses the example of a collision with a single partonic interaction and defines tools that will help us work with partonic interactions. An important parameter in a hadronic interaction is the hard scale Q^2, which characterises the transverse scale of the hard event.

The behavior of a parton inside a hadron is only defined in a quasi-probabilistic manner. For each parton we define the parameter x, called the longitudinal fraction, or the light-cone hadron's momentum fraction of the parton. Given a hadron with

four-momentum P^μ and a parton with initial four-momentum p^μ, we define

$$x \equiv \frac{p_0 + p_z}{P_0 + P_z}. \tag{2.19}$$

This parameter was first defined by Bjorken and is often denoted x_{B}, where the index z indicates the momentum component along the beam axis, and x goes from zero to one. Assuming the parton is massless, its momentum is defined by x and its transverse momentum.

As seen in Fig. 2.8, the two hadrons are a bundle of many partons. In this example, a parton from h_a with momentum $x, \vec{k}$ and a parton from h_b with momentum of $x', \vec{k}'$ interact and two new particles with momentum q_i and q_j are emitted. Here we must separate the two types of cross sections: The first is the hadronic cross section, which is the cross section for the two hadrons to produce the particles q_i and q_j, or any other products. This is the cross section of the entire diagram and can be measured. The grey dashed rectangle contains a diagram of two partons interacting with no connection to the hadrons, this is the partonic cross section that can be calculated via QCD with fundamental particles but never measured directly.

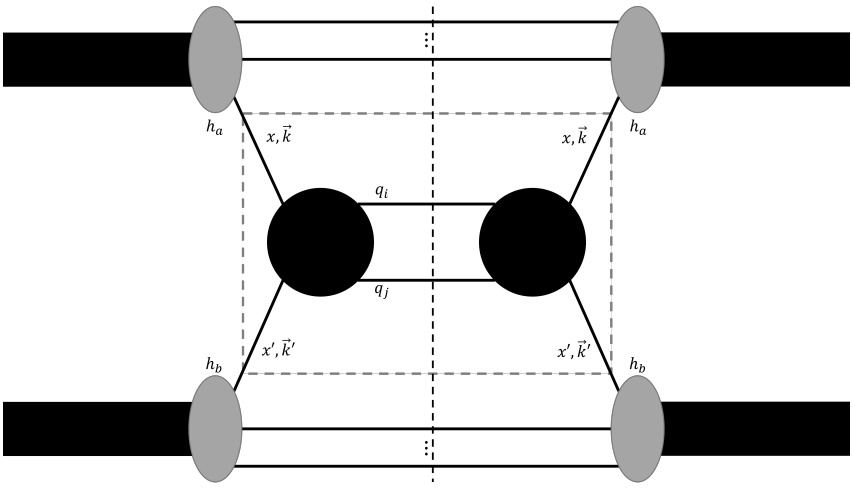

Figure 2.8: A diagram of the hadronic cross section of two hadrons colliding via a single partonic interaction. Each parton contributes a parton that interacts with the other parton, and the black circles represent the QCD processes that originate from the two partons and emit two new particles. The grey dashed rectangle encloses the diagram of a partonic cross section.

To find the hadronic cross section of this process we must know the probability to find a parton with momentum fraction x inside a hadron and use it to reduce the problem to the diagram of a partonic cross section. Such probabilities depend on the hard scale Q^2 of the process and on the QCD processes inside the hadron. When

we consider an event of hard scale Q^2, we say that the quasi-probability to find a parton of type j with momentum fraction x inside a hadron is given by $f_j(x, Q^2)$, where f is the standard parton distribution function (PDF).

PDFs satisfy the following two sum rules: The first is the valence rule, which states that, for every hadron, the integral over x for the valence partons must give the number of partons in the given hadron. For example, in a proton there are two valence up quarks and one valence down quark, so we write

$$\int_0^1 dx \left[f_u\left(x, Q^2\right) - f_{\overline{u}}\left(x, Q^2\right)\right] = 2, \quad \int_0^1 dx \left[f_d\left(x, Q^2\right) - f_{\overline{d}}\left(x, Q^2\right)\right] = 1. \quad (2.20)$$

For all other flavors of quarks (i.e. $f \neq u, d$), we write $f_j(x, Q^2) = f_{\overline{j}}(x, Q^2)$. This implies that, for every hadron, we need a different set of PDFs, but we only work with protons so we need not index the hadron type.

The other sum rule is the condition that the total momentum fraction is unity,

$$\int_0^1 dx\, x \left\{ f_g\left(x, Q^2\right) + \sum_f \left[f_f\left(x, Q^2\right) + f_{\overline{f}}\left(x, Q^2\right)\right] \right\} = 1. \quad (2.21)$$

To define how the PDF varies as a function of hard scale, we define the splitting functions $P_{j\leftarrow i}(z)$, which are proportional to the quasi-probability of a parton of type i with momentum fraction x/z to split into two partons, with one being a real particle of type j with momentum fraction z. QCD proposes three diagrams that contribute to finding the splitting functions: $q \to q + g$, $g \to q + \bar{q}$ and $g \to g + g$.

To calculate the splitting functions, we must avoid the pole at $z = 1$, so we define the function

$$\frac{1}{(1-z)_+} = \lim_{\varepsilon \to 0} \left[\frac{1}{1-z} \Theta\left(1 - \varepsilon - z\right) - \delta\left(1 - z\right) \int_0^{1-\varepsilon} \frac{dz'}{1-z'} \right], \quad (2.22)$$

where Θ is the step function [$\Theta(x < 0) = 0$ and $\Theta(x \geq 0) = 1$].

Leveraging Θ, we define the splitting functions as follows:

$$\begin{aligned}
P_{q\leftarrow q}\left(z\right) &= \frac{4}{3}\left[\frac{1+z^2}{(1-z)_+} + \frac{3}{2}\delta\left(1-z\right)\right], \\
P_{g\leftarrow q}\left(z\right) &= \frac{4}{3}\left[\frac{1+(1-z)^2}{z}\right], \\
P_{q\leftarrow g}\left(z\right) &= \frac{1}{2}\left[z^2 + (1-z)^2\right], \\
P_{g\leftarrow g}\left(z\right) &= 6\left[\frac{1-z}{z} + \frac{z}{(1-z)_+} + z\left(1-z\right) + \left(\frac{11}{12} - \frac{n_f}{18}\right)\delta\left(1-z\right)\right], \quad (2.23)
\end{aligned}$$

where n_f is the number of light quarks with mass less than the hard scale Q.

The diagrams that define the splitting functions also include a factor $\alpha_s(Q^2)/\pi$, where $\alpha_s(Q^2)$ is the QCD running coupling, which in the one-loop approximation is expressed as

$$\alpha_s\left(Q^2\right) = \frac{4\pi}{\left(\frac{11}{3}N_c - \frac{2}{3}n_f\right)\ln\left(Q^2/\Lambda_{\mathrm{QCD}}\right)}. \tag{2.24}$$

where N_c is the number of colours (for QCD, $N_c = 3$), n_f is the number of light quarks, and $\Lambda_{\mathrm{QCD}} \approx 0.3$ GeV is the QCD scale parameter.

Exploiting the splitting functions allows us to write the Dokshitzer–Gribov–Lipatov–Altarelli–Parisi (DGLAP) equations that describe perturbative QCD in the leading logarithmic approximation:

$$\begin{aligned}
\frac{d}{d\log Q} f_g\left(x,Q^2\right) &= \frac{\alpha_s\left(Q^2\right)}{\pi}\int_x^1 \frac{dz}{z}\Bigg\{P_{g\leftarrow q}\left(z\right)\sum_f\left[f_f\left(\frac{x}{z},Q^2\right) + f_{\overline{f}}\left(\frac{x}{z},Q^2\right)\right] \\
&\quad + P_{g\leftarrow g}\left(z\right) f_g\left(\frac{x}{z},Q^2\right)\Bigg\}, \\
\frac{d}{d\log Q} f_f\left(x,Q^2\right) &= \frac{\alpha_s\left(Q^2\right)}{\pi}\int_x^1 \frac{dz}{z}\left\{P_{q\leftarrow q}\left(z\right) f_f\left(\frac{x}{z},Q^2\right) + P_{q\leftarrow g}\left(z\right) f_g\left(\frac{x}{z},Q^2\right)\right\}, \\
\frac{d}{d\log Q} f_{\overline{f}}\left(x,Q^2\right) &= \frac{\alpha_s\left(Q^2\right)}{\pi}\int_x^1 \frac{dz}{z}\left\{P_{q\leftarrow q}\left(z\right) f_{\overline{f}}\left(\frac{x}{z},Q^2\right) + P_{q\leftarrow g}\left(z\right) f_g\left(\frac{x}{z},Q^2\right)\right\}.
\end{aligned} \tag{2.25}$$

Because the derivation of the DGLAP equations respects the conservation laws of QCD (namely, conservation of flavor and longitudinal momentum), they obey the summation rules in Figs. 2.20 and 2.21.

We now give the connection between the hadronic and partonic cross sections. To produce two particles i and j with momenta q_i and q_j, the inclusive hadronic cross section σ_h for colliding hadrons h_a with momentum P and h_b with momentum P' is given by

$$\begin{aligned}
\sigma_h\left(h_a\left(P\right) + h_b\left(P'\right) \to i + j + X\right) &= \int_0^1 dx \int_0^1 dx' \sum_{\alpha,\beta} f_\alpha\left(x,Q^2\right) f_\beta\left(x',Q^2\right) \\
&\quad \times \sigma_p\big(\alpha\left(x\right) + \beta\left(x'\right) \to i + j\big),
\end{aligned} \tag{2.26}$$

where σ_p is the hard partonic cross section of the process $\alpha(x) + \beta(x') \to i + j$ and the indices α and β span all types of partons (i.e. quarks and anti-quarks for each flavor, or gluons).

Hereinafter, we do not write the type index for the PDF because, at high hard scales, such as at the LHC, gluons dominate the proton structure [20], which means that we assume that all partons are gluons.

Recall that the PDFs do not give real probabilities, which instead are defined via the parton wave function. However, we can define many other quasi-distributions that can be useful.

A natural framework for visualising the MPI is the impact-parameter representation of the collision (see Fig. 2.1). In the high-energy limit, conservation of angular momentum implies that the impact parameter b is a constant for the collision. In addition, hard collisions have the hard scale that localise them in a transverse area $1/Q^2$.

To describe the transverse geometry of pp collisions it is convenient to consider the quasi-probability to find a parton with a given x and transverse distance $\vec{r}$ from the hadron transverse center of mass, in hard scale Q^2: $\rho(x, \vec{r}|Q^2)$. This quantity is called the diagonal generalised parton distribution (GPD) and is related to the PDF by

$$f\left(x, Q^2\right) = \int d^2r \rho\left(x, \vec{r}|Q^2\right). \tag{2.27}$$

The inclusive cross section does not depend on the transverse structure of the colliding hadrons in the leading twist perturbative-QCD regime. The cross section is expressed through the convolution of parton densities. In fact, we can write the connection between the hadronic and partonic cross sections as

$$\begin{aligned}\sigma_h\left(h_a + h_b \to Y + X\right) \;&\propto\; \int d^2b d^2r d^2r' \delta^{(2)}\left(\vec{r} - \vec{r}' - \vec{b}\right) \rho\left(x, \vec{r}|Q^2\right) \rho\left(x', \vec{r}'|Q^2\right) \\ &\quad \times \sigma_p\big(\alpha\left(x\right) + \beta\left(x'\right) \to Y\big) \\ &= \; f\left(x, Q^2\right) f\left(x', Q^2\right) \sigma_p\big(\alpha\left(x\right) + \beta\left(x'\right) \to Y\big),\end{aligned} \tag{2.28}$$

which is equivalent to Eq. (2.26).

2.2.2 Double-Parton Scattering

This section considers the example of DPS and uses it to define the tools used for the general MPI.

In DPS, each of the two colliding hadrons contribute two partons that collide and create two independent hard processes. DPS is normally parameterised as

$$\sigma^{(\mathrm{DPS})} = \frac{\sigma_1 \sigma_2}{\sigma_{\mathrm{eff}}}, \tag{2.29}$$

were $\sigma^{(\mathrm{DPS})}$ is the total hadronic cross section of the process of two partons with each hadron coming in and making two hard processes. The quantities σ_1 and σ_2 are the hadronic cross sections of a process with only one partonic interaction. Finally, σ_{eff} characterises the geometry of the DPS process.

Note that $\sigma^{(\mathrm{DPS})}$ and σ_{eff} are functions of the hard scale Q_i^2 and of x_i and ${x'}_i$, the light-cone hadron's momentum fractions for both hard processes ($i = 1, 2$), whereas σ_i is a function only of variables with the same index, meaning that they are assumed to be independent.

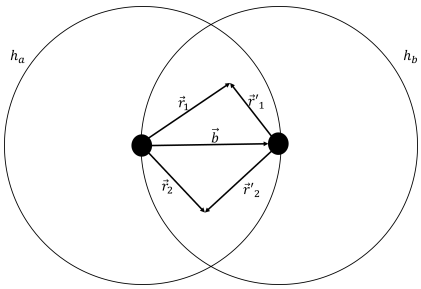

Figure 2.9: Geometry of a DPS process in the transverse plane. The two big circles represent the hadrons h_a and h_b, the two small circles are their centers and $\vec{b}$ is the impact parameter vector. The vectors $\vec{r}_1,\ \vec{r}'_1,\ \vec{r}_2$ and $\vec{r}'_2$ are the transverse positions of the four partons that interact.

Figure 2.9 shows the geometry of this process in the transverse plane. In the transverse plane, the two hadrons are almost circles, and the vector connecting their centers is the impact parameter $\vec{b}$, as seen in Fig. 2.1. To simplify our calculations, we use the single-parton transverse position distribution functions to treat the partons as point-like particles that can only interact with partons from other hadrons if they are in the same transverse position.

Denoting the transverse position of a parton from h_a as $\vec{r}$ with respect to the center of h_a, and the transverse position of a parton from h_b as $\vec{r}'$ with respect to the center of h_b, then for both of them to be in the same transverse position the vectors need to satisfy the condition $\vec{b} = \vec{r} - \vec{r}'$.

The diagonal GPD allows us to write σ_{eff} by averaging over all possible hard-process positions for all possible impact parameters:

$$(\sigma_{\mathrm{eff}})^{-1} = \int d^2b \left[\prod_{i=1}^{2} d^2r_i d^2r'_i \rho\left(x_i, \vec{r}_i | Q_i^2\right) \rho\left({x'}_i, \vec{r}'_i | Q_i^2\right) \delta^{(2)}\left(\vec{r}_i - \vec{r}'_i - \vec{b}\right) \right]. \quad (2.30)$$

2.2.3 Generalised Parton Distribution

To find the cross section of a hard process with N parton interactions, we introduce a new physical quantity, the N-particle generalised parton distribution, normally denoted ${}_N$GPD.

The ${}_N$GPD can be defined by using the light-cone wave function of the hadron:

$$\begin{aligned} D_h\left(\left\{x_i, Q_i^2, \vec{\Delta}_i\right\}_{i=1}^{N}\right) \equiv & \sum_{p=N+1}^{\infty} \int \left(\prod_{l=1}^{N} \frac{d^2k_l}{(2\pi)^2}\Theta\left(Q_l^2 - k_l^2\right)\right)\left(\prod_{l=N+1}^{p} \frac{d^2k_l}{(2\pi)^2} dx_l\right) \\ & \times (2\pi)^3\, \delta\left(\left(\sum_{m=1}^{p} x_m\right) - 1\right) \delta^{(2)}\left(\sum_{m=1}^{p} \vec{k}_m\right) \delta^{(2)}\left(\sum_{m=1}^{p} \vec{\Delta}_m\right) \\ & \times \psi_p\left(\left\{x_l, \vec{k}_l\right\}_{l=1}^{p}\right) \psi_p^{\dagger}\left(\left\{x_l, \vec{k}_l + \vec{\Delta}_l\right\}_{l=1}^{N}, \left\{x_l, \vec{k}_l\right\}_{l=N+1}^{p}\right), \end{aligned} \tag{2.31}$$

where h is an index for the hadron, x_i is the light-cone hadron momentum fraction of parton i, the integral over x_l for $l > N$ goes from zero to one, Q_i^2 is the hard scale of partonic interaction i, $\vec{\Delta}_i$ is the Fourier conjugate to the transverse positions of parton i, p is the number of partons in the hadron, $\vec{k}_l$ is the transverse momentum of parton l and $\Theta(Q_l^2 - k_l^2)$ is the step function (one for $Q_l^2 \geq k_l^2$ and zero for $Q_l^2 < k_l^2$). In the second line, the first delta function enforces the condition that the sum over the light-cone fraction of all partons is one, the second delta function enforces the condition that the sum over the transverse momentum is zero and ψ_p is the wave function of parton p normalised to one.

Unlike the diagonal GPD that we defined in Sec. 2.1 in coordinate space, we define ${}_N$GPD here in transverse-momentum space. The definitions may be shown to be equivalent via a Fourier transform. This connection is shown in Sec. 2.4.

For a MPI with N partonic interactions, we can generalise the parameterisation of the cross section from Eq. (2.29) to

$$\sigma_N^{(\mathrm{MPI})} = \frac{\prod_{i=1}^{N} \sigma_i\left(x_i, x_i', Q_i^2\right)}{K_N\left(\{x_i, x_i', Q_i^2\}_{i=1}^{N}\right)}, \tag{2.32}$$

where $\sigma_N^{(\mathrm{MPI})}$ is the total hadronic MPI cross section, i is an index spanning all N partonic interactions in the process, σ_i is the hadronic cross section of a single independent hard process and K_N is a dimensionful function, $K_N \propto (\text{area})^{N-1}$ with the parameters x_i and x_i', which are the light-cone hadron momentum fractions of the partons, the unprimed index comes from hadron h_a and the primed index comes from hadron h_b and Q_i^2 is the hard scale of hard process i. For $N = 2$ we get $K_2 = \sigma_{\mathrm{eff}}$.

Using the ${}_N$GPD, we can see that the total cross section for N partonic interactions is

$$\sigma_N^{(\mathrm{MPI})} \propto \int D_a\left(\left\{x_i, Q_i^2, \vec{\Delta}_i\right\}_{i=1}^{N}\right) D_b\left(\left\{x'{}_i, Q_i^2, -\vec{\Delta}_i\right\}_{i=1}^{N}\right) \delta^{(2)}\left(\sum_{i=1}^{N} \vec{\Delta}_i\right) \prod_{i=1}^{N} \frac{d^2\Delta_i}{(2\pi)^2}. \tag{2.33}$$

To compare this to our example of DPS, we take $N = 2$ and use the delta function $\delta^{(2)}(\sum_{i=1}^{2} \vec{\Delta}_i)$ to write

$$\begin{aligned} D_h\left(x_1, x_2, Q_1^2, Q_2^2, \vec{\Delta}\right) \equiv & \sum_{p=3}^{\infty} \int \left(\prod_{l=1}^{p} \frac{d^2 k_l}{(2\pi)^2}\right) \left(\prod_{l=3}^{p} dx_l\right) \Theta\left(Q_1^2 - k_1^2\right) \Theta\left(Q_2^2 - k_2^2\right) \\ & \times (2\pi)^3 \delta\left(\left(\sum_{m=1}^{p} x_m\right) - 1\right) \delta^{(2)}\left(\sum_{m=1}^{p} \vec{k}_m\right) \\ & \times \psi\left(\left\{x_l, \vec{k}_l\right\}_{l=1}^{p}\right) \psi^{\dagger}\left(x_1, \vec{k}_1 + \vec{\Delta}, x_2, \vec{k}_2 - \vec{\Delta}, \left\{x_l, \vec{k}_l\right\}_{l=3}^{p}\right). \end{aligned} \tag{2.34}$$

The DPS cross section is then given by

$$\begin{aligned} \sigma_2^{(\mathrm{MPI})} = & \int \frac{d^2\Delta}{(2\pi)^2} d\Omega_1 d\Omega_2 D_a\left(x_1, x_2, Q_1^2, Q_2^2, \vec{\Delta}\right) D_b\left(x'_1, x'_2, Q_1^2, Q_2^2, -\vec{\Delta}\right) \\ & \times \frac{d\sigma\left(x_1, x'_1, Q_1^2\right)}{d\Omega_1} \frac{d\sigma\left(x_2, x'_2, Q_2^2\right)}{d\Omega_2}. \end{aligned} \tag{2.35}$$

From this we find that σ_{eff} is given by

$$\left(\sigma_{\mathrm{eff}}\right)^{-1} = \int \frac{d^2\Delta}{(2\pi)^2} \frac{D_a\left(x_1, x_2, Q_1^2, Q_2^2, \vec{\Delta}\right) D_b\left(x'_1, x'_2, Q_1^2, Q_2^2, -\vec{\Delta}\right)}{f\left(x_1, Q_1^2\right) f\left(x_2, Q_2^2\right) f\left(x'_1, Q_1^2\right) f\left(x'_2, Q_2^2\right)}, \tag{2.36}$$

where $f\left(x, Q^2\right)$ is the standard PDF. For general N we can write

$$\frac{1}{K_N} = \int \left(\prod_{j=1}^{N} \frac{d^2\Delta_j}{(2\pi)^2}\right) \frac{D_a\left(\left\{x_j, Q_j^2, \vec{\Delta}_j\right\}_{j=1}^{N}\right) D_b\left(\left\{x'_j, Q_j^2, -\vec{\Delta}_j\right\}_{j=1}^{N}\right) \delta^{(2)}\left(\sum_{j=1}^{N} \vec{\Delta}_j\right)}{\prod_{j=1}^{N} \left[f\left(x_j, Q_j^2\right) f\left(x'_j, Q_j^2\right)\right]}. \tag{2.37}$$

Note that a hard parton can split perturbatively and the resulting partons interact with the partons from the other hadrons, producing a different dependence on the transverse momentum. Such a process is represented in Fig. 2.10 on the right and is denoted a $1 \otimes 2$ process.

When we calculate the GPD we need to take into account the possibility of the splitting process, which is done by summing over all possible splitting combinations. For example, for the two-parton GPD we can write

$$\begin{aligned} D_h\left(x_1, x_2, Q_1^2, Q_2^2, \vec{\Delta}_1, \vec{\Delta}_2\right) = & {}_{[2]}D_h\left(x_1, x_2, Q_1^2, Q_2^2, \vec{\Delta}_1, \vec{\Delta}_2\right) \\ & + {}_{[1]}D_h\left(x_1, x_2, Q_1^2, Q_2^2, \vec{\Delta}_1, \vec{\Delta}_2\right), \end{aligned} \tag{2.38}$$

where the index $_{[2]}$ indicates the non-perturbative part of the production of two hard partons from the wave function, as in the diagram on the left in Fig. 2.10, and the index $_{[1]}$ indicates the perturbation-theory part of the production of one hard parton from the wave function that then splits into two, as in the diagram on the right in Fig. 2.10.

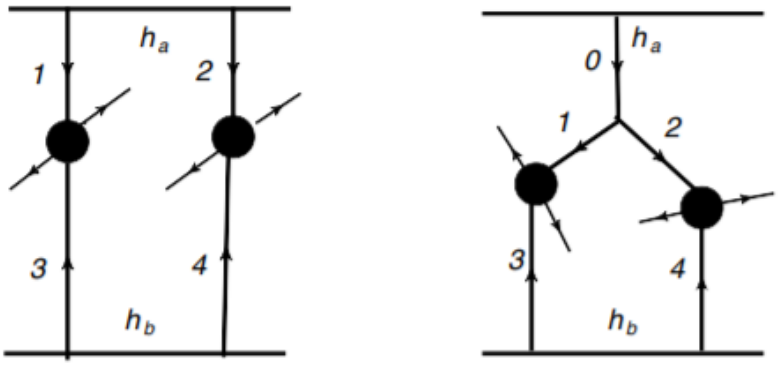

Figure 2.10: Two diagrams representing collisions between two hadrons h_a and h_b with two partonic interactions. On the left, each of interacting partons originates in the hadron's wave function. On the right is an example of a $1 \otimes 2$ process, where the parton from h_a splits into two partons that each undergo their own partonic interaction with a parton from h_b. The diagrams are taken from Ref. [21].

2.2.4 Single-Parton Distribution

We now define the generalised single-parton distribution and the two-gluon form factor and use them to parameterise the diagonal GPD in coordinate space, $\rho(x, \vec{r}|Q^2)$.

The generalised single-parton distribution is denoted G_1 and is the non-forward parton correlator. It is defined by using the light-cone wave function of the hadron:

$$\begin{aligned} G_1\left(x, Q^2, \vec{\Delta}\right) \equiv & \sum_{p=2}^{\infty} \int \left(\prod_{l=1}^{p} \frac{d^2 k_l}{(2\pi)^2}\right) \left(\prod_{l=2}^{p} dx_l\right) \Theta\left(Q_1^2 - k_1^2\right) \\ & \times (2\pi)^3 \, \delta\left(\left(\sum_{m=1}^{p} x_m\right) - 1\right) \delta^{(2)}\left(\sum_{m=1}^{p} \vec{k}_m\right) \\ & \times \psi\left(\left\{x_l, \vec{k}_l\right\}_{l=1}^{p}\right) \psi^{\dagger}\left(x_1, \vec{k}_1 + \vec{\Delta}, \left\{x_l, \vec{k}_l\right\}_{l=2}^{p}\right). \end{aligned} \tag{2.39}$$

This function can be parametrised by using processes similar to those shown in Fig. 2.11, where a parton with momentum x_1, $\vec{k}_1$ inside a proton interacts with a virtual photon γ^*, emitting a vector meson V^0. A new parton with momentum x_1, $\vec{k}_1 + \vec{\Delta}$ is absorbed into the proton.

This function is related to the diagonal GPD in coordinate space via a Fourier transform over the transverse position:

$$G_1\left(x, Q^2, \vec{\Delta}\right) = \int d^2 r e^{-i\vec{\Delta}\cdot\vec{r}} \rho\left(x, \vec{r}|Q^2\right). \tag{2.40}$$

For $\vec{\Delta} = \vec{0}$, the use of Eq. (2.27) gives

$$G_1\left(x, Q^2, \vec{0}\right) = \int d^2 r \rho\left(x, \vec{r}|Q^2\right) = f\left(x, Q^2\right). \tag{2.41}$$

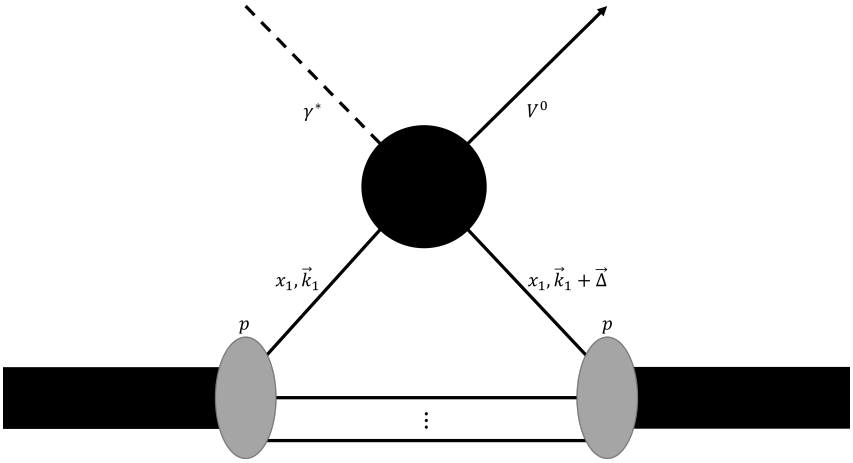

Figure 2.11: A diagram of the process measured by HERA [22] of a proton interacting with a virtual photon γ^* and emitting a vector meson V^0. The particles connected to the protons are partons, and we see one parton with parameters x_1, $\vec{k}_1$ participate in the interaction. A parton with x_1, $\vec{k}_1 + \vec{\Delta}$ is absorbed back into the proton.

It is common to parametrise G_1 as a product of two functions:

$$G_1\left(x, Q^2, \vec{\Delta}\right) = f\left(x, Q^2\right) F_{2g}\left(x, Q^2, \vec{\Delta}\right), \tag{2.42}$$

were $f(x, Q^2)$ is the standard PDF and $F_{2g}(x, Q^2, \vec{\Delta})$ is the two-gluon form factor.

Two common parameterisations exist for the two-gluon form factor and are referred to as 'exponential' and 'dipole' parameterisations. They are written as

$$F_{2g}\left(x, \Delta | Q^2\right) = \begin{cases} e^{\frac{-B\left(x, Q^2\right)\Delta^2}{2}} \\ \left[1 + \Delta^2 / m_g^2\left(x, Q^2\right)\right]^{-2}, \end{cases} \tag{2.43}$$

where the first is the exponential parameterisation and the second is the dipole parameterisation. B and m_g are functions of x and Q^2. The two parameterisations give very similar results for the right choices of B and m_g and both can be fitted to the data, as seen in Ref. [23], which uses the relation $B = 3.24/m_g^2$.

For our calculations it is much easier to work with the exponential parameterisation, so we consider only this parameterisation herein.

We also find the diagonal GPD in coordinate space $\rho(x, \vec{r}|Q^2)$:

$$\rho\left(x, r | Q^2\right) = \int \frac{d^2\Delta}{(2\pi)^2} e^{i(\Delta \cdot r)} G_1\left(x, Q^2, \vec{\Delta}\right) = f\left(x, Q^2\right) \int \frac{d^2\Delta}{(2\pi)^2} e^{i(\Delta \cdot r)} F_{2g}\left(x, Q^2, \vec{\Delta}\right). \tag{2.44}$$

Taking the exponential parameterisation $F_{2g}(x,Q^2,\vec{\Delta}) = \exp[-\frac{1}{2}B(x,Q^2)\Delta^2]$ gives

$$F_{2g}\left(x,r|Q^2\right) = \frac{1}{2\pi B\left(x,Q^2\right)} e^{-\frac{r^2}{2B(x,Q^2)}}, \quad \rho\left(x,r|Q^2\right) = f\left(x,Q^2\right) F_{2g}\left(x,r|Q^2\right). \tag{2.45}$$

Note that both the spatial and momentum forms of F_{2g} depend on x and Q^2 only via B. Analysis of the HERA data gives us a parameterisation for B [21] of the form

$$B\left(x\right) = B_0 + 2\alpha' \ln\left(x_0/x\right), \tag{2.46}$$

where, for $Q^2 \approx 3$ GeV^2 fitting to the HERA data, the parameters take the values $B_0 = 4 \pm 0.4$ GeV^{-2}, $\alpha' = 0.14 \pm 0.08$ GeV^{-2} and $x_0 = 0.0012$. For fixed x we can use DGLAP evolution [Eq. (2.25)] to see that $B(x,Q^2)$ varies slowly with Q^2, so we can take B to be constant and write F_{2g} as a function of Δ or r only, neglecting its x and Q^2 dependence.

2.2.5 Mean-Field Approximation

In the mean-field approximation we consider partons as independent particles. The light-cone wave function then factorises to

$$\psi\left(\left\{x_l,\vec{k}_l\right\}_{l=1}^{p}\right) = \prod_{l=1}^{p} \psi\left(x_l,\vec{k}_l\right). \tag{2.47}$$

Assuming this, we express the ${}_N$GPD functions as

$$D_h\left(\left\{x_i,Q_i^2,\vec{\Delta}_i\right\}_{i=1}^{N}\right) \simeq \prod_{i=1}^{N} G_1\left(x_i,Q_i^2,\Delta_i\right) \simeq \prod_{i=1}^{N} f\left(x_i,Q_i^2\right) F_{2g}\left(\Delta_i\right), \tag{2.48}$$

where $G_1(x_i,Q_i^2,\Delta_i)$ is the generalised single-parton distribution as defined by Eq. (2.39), $f(x_i,Q_i^2)$ is the standard PDF and $F_{2g}(\Delta_i)$ is the two-gluon form factor.

This approximation is not perfect; for starters, it loses the property of the GPD: $D_h(\sum_{i=1}^{N} x_i > 1) = 0$, meaning that we cannot work in regions where x_i are too big. Conversely, if x_i are too small we start to look at the region where the $1 \otimes 2$ process is non-perturbative. Reference [10] states that this approximation should hold for $10^{-1} > x_i > 10^{-3}$.

For DPS we write ${}_2$GPD and σ_{eff} as

$$\begin{aligned} D_h\left(x_1,x_2,Q_1^2,Q_2^2,\vec{\Delta}\right) &= G_1\left(x_1,Q_1^2,\vec{\Delta}\right) G_1\left(x_2,Q_2^2,\vec{\Delta}\right) \\ &\simeq f\left(x_1,Q_1^2\right) f\left(x_2,Q_2^2\right) F_{2g}^2\left(\Delta\right) \\ \Rightarrow \sigma_{\text{eff}} &= \left(\int \frac{d^2\Delta}{\left(2\pi\right)^2} F_{2g}^4\left(\Delta\right)\right)^{-1} = 8\pi B. \end{aligned} \tag{2.49}$$

For general N we get

$$K_N \simeq \left[\int \left(\prod_{j=1}^{N} \frac{d^2\Delta_j}{(2\pi)^2} F_{2g}^2(\Delta_j) \right) \delta^{(2)} \left(\sum_{j=1}^{N} \vec{\Delta}_j \right) \right]^{-1} = N (4\pi B)^{N-1} . \tag{2.50}$$

2.2.6 Soft-Gluon Emission

In addition to hard out-going particles (jets), partons in the hard process can also emit soft gluons. Since these gluons are important we note that, for a collision with N partonic interactions, the cross section to emit m gluons with transverse momenta $\{\mathbf{k}_i\}_{i=1}^m$ using the approximations above is given by

$$\frac{d^m\sigma_N(\{\boldsymbol{k}_j\},\{\boldsymbol{\Delta}_i\})}{d^2k_1\cdots d^2k_m} \sim |\mathcal{M}(\{\boldsymbol{k}_j\},\{\boldsymbol{\Delta}_i\})|^2 \left(\prod_{i=1}^{N} F_{2g}^2(\Delta_i)\,\sigma_i \right) \delta^{(2)} \left(\sum_{i=1}^{N} \vec{\Delta}_i \right), \tag{2.51}$$

where $\mathcal{M}(\{\boldsymbol{k}_j\},\{\boldsymbol{\Delta}_i\})$ is the amplitude for the production of m gluons by N partons in the hadron wave function, and σ_i is the cross section for partonic interaction i. The corresponding m-particle spectrum is obtained by normalising this expression with the cross section

$$\sigma_N = \int \left(\prod_{i=1}^{N} d^2\Delta_i F_{2g}^2(\Delta_i)\,\sigma_i \right) \delta^{(2)} \left(\sum_{i=1}^{N} \vec{\Delta}_i \right). \tag{2.52}$$

The m-particle spectrum can now be written in coordinate space representation as

$$\frac{d^m\sigma_N(\{\boldsymbol{k}_j\})}{\sigma_N d^2k_1\cdots d^2k_m} = \frac{\int \left(\prod_{i=1}^{N} d^2r_i\right) d^2b\,|\mathcal{M}(\{\boldsymbol{k}_j\},\{\boldsymbol{r}_i\})|^2\,\rho(\{\boldsymbol{r}_i\},\boldsymbol{b})}{\int \left(\prod_{i=1}^{N} d^2r_i\right) d^2b\rho(\{\boldsymbol{r}_i\},\boldsymbol{b})}, \tag{2.53}$$

where $\rho(\{\boldsymbol{r}_i\},\boldsymbol{b})$ is a quasi-probability distribution of the impact parameter $\boldsymbol{b}$ and the hard partons' transverse positions $\{\boldsymbol{r}_i\}$, as seen in Fig. 2.9. $\rho(\{\boldsymbol{r}_i\},\boldsymbol{b})$ is given by

$$\rho(\{\boldsymbol{r}_i\},\boldsymbol{b}) = \prod_{i=1}^{N} \int \left(\frac{d^2\Delta_i d^2r'_i}{(2\pi)^2} F_{2g}^2(\Delta_i)\, e^{i\vec{\Delta}_i\cdot(\boldsymbol{r}_i+\boldsymbol{r}'_i)} \delta^{(2)}(\boldsymbol{b}-\boldsymbol{r}_i+\boldsymbol{r}'_i) \right). \tag{2.54}$$

For the exponential parameterisation we have chosen for $F_{2g}(\Delta_i)$, we get

$$\rho(\{\boldsymbol{r}_i\},\boldsymbol{b}) = \frac{1}{(4\pi B)^N} \prod_{i=1}^{N} e^{-\frac{r_i^2}{4B}} e^{-\frac{(\boldsymbol{r}_i-\boldsymbol{b})^2}{4B}}. \tag{2.55}$$

2.2.7 Effective Cross Section

By using the mean-field approach, the clear connection between σ_{eff} and B in Eq. (2.49) allows us to use experimental data to find the values of B that we should consider.

For pp collisions at the LHC [24, 25, 26], σ_{eff} was found to be about 15 ± 5 mb, which means that we should look at $B = 1.5 \pm 0.5$ GeV^{-2}, so in this thesis we use the two values $B = 1$ and 2 GeV^{-2}.

2.3 Quantum Interference model

This section reviews the basic ideas of the quantum interference model [10, 11] and explains how to find the azimuthal cumulant in the corresponding framework.

First, we define the normalisation that we work with:

$$\left\langle e^{i\left(\sum_{j=1}^{s} n_j \phi_j\right)} \right\rangle \left(\{k_j, y_j\}_{j=1}^{s}\right) = M_s \frac{\int_\rho \int \left(\prod_{j=1}^{s} d\phi_j\right) e^{i\left(\sum_{j=1}^{s} n_j \phi_j\right)} f\left(\{\boldsymbol{k}_j\}_{j=1}^{s}\right)}{(2\pi)^s \prod_{j=1}^{s} \int_\rho f\left(\boldsymbol{k}_j\right)}, \tag{2.56}$$

where $M_s = m^s / \binom{m}{s}$ is a normalisation factor, the integral $\int_\rho$ means $\int_\rho \equiv \int (\prod_{i=1}^{N} d^2 r_i)\, \rho(\{\boldsymbol{r}_i\})$, $f(\boldsymbol{k}_j)$ is the one-particle momentum distribution function defined in Eq. (2.1) and $f(\{\boldsymbol{k}_j\}_{j=1}^{s})$ is the s-particle momentum distribution function defined as $f(\{\boldsymbol{k}_j\}_{j=1}^{s}) \equiv \frac{d^s N}{d^3 k_1 \cdots d^3 k_s}$, and n_j is the flow harmonic index of particle j, where we only consider the case where $\sum_{j=1}^{s} n_j = 0$. All that we need to to find then is the one- and three-particle differential multiplicity. This is a generalised form of the normalisation used by Ref. [11], which only considers even s.

2.3.1 Defining the Model

We model multi-particle production in pp collisions as events of N partonic interactions at transverse positions $\{\mathbf{r}_i\}_{i=1}^{N}$. Each partonic process is represented by a line source with initial $SU(N_c)$ adjoint representation index $\{b_i\}_{i=1}^{N}$ at the rapidity of one of the colliding hadrons, emitting gluons with $SU(N_c)$ adjoint representation index $\{a_j\}_{j=1}^{m}$ and transverse momentum of $\{\mathbf{k}_j\}_{j=1}^{m}$ in the intermediate rapidity window and ending at the rapidity of the other hadron with final $SU(N_c)$ adjoint representation index $\{c_i\}_{i=1}^{N}$. Each multi-particle production amplitude is therefore of the type given in Fig. 2.12, where we account for any selection of sources emitting any of the gluons.

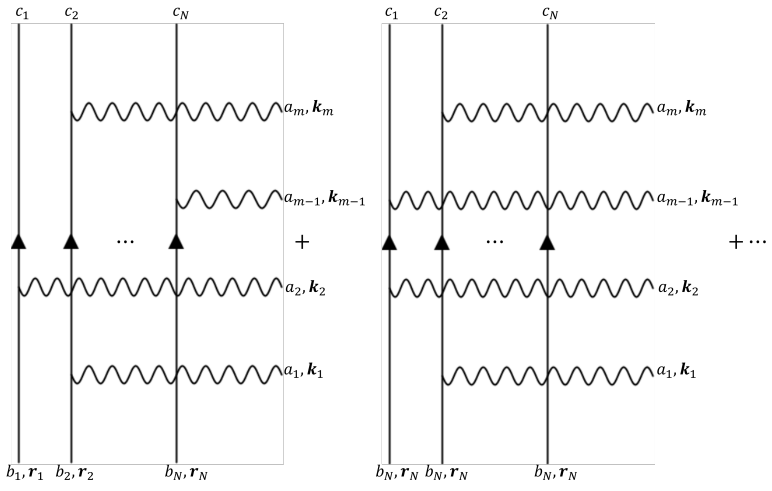

Figure 2.12: Example diagrams for N sources emitting m gluons. The vertical lines are the N sources with initial conditions of $\{\mathbf{r}_i, b_i\}_{i=1}^{N}$ and final colour index of c_i. The horizontal waves are the m emitted gluons with colour index and transverse momenta of $\{a_j, \mathbf{k}_j\}_{j=1}^{m}$. Each diagram in the sum represents a different choice of which gluons are emitted from which source, and to find the total amplitude we must sum over all of these choices.

The emission vertex for a soft gluon is given by an eikonal vertex. If the source is positioned at $\mathbf{r}_i$ with a colour index of b'_i before emission and b''_i after emission, and the emitted gluon has transverse momentum of $\mathbf{k}_j$ and colour index a_j, then the eikonal vertex is given by

$$T^{a_j}_{b'_i,b''_i}\vec{f}\,(\mathbf{k}_j)\, e^{i\mathbf{r}_i\cdot\mathbf{k}_j}, \tag{2.57}$$

where T^a is the adjoint representation of the $SU(N_c)$ generator, and $\vec{f}(\mathbf{k})$ is the vertex form function. $\vec{f}(\mathbf{k})$ is a two-dimensional vector in the transverse plane, which in the cross sections is dotted into another vertex function of the same momentum. We do not assume a specific functional shape of the vertex function because it does not impact the results in any meaningful way, but we do assume two of its properties: First, we normalise it to so that $\int d^2k|\vec{f}(\boldsymbol{k})|^2 = 1$, and, second, we assume that $|\vec{f}(\boldsymbol{k})|^2$ is independent of the momentum azimuthal angle. An example of a function that fits what we need is Coulombic radiation: $\vec{f}\,(\boldsymbol{k}) \propto \frac{1}{k^2}\boldsymbol{k}$.

When calculating cross sections of event samples we use the quasi-probability distribution of the impact parameter $\mathbf{b}$ and the transverse position of the hard partons, $\{\boldsymbol{r}_i\}_{i=1}^{N}$, given in Eq. (2.55). Denoting coordinates as the complex-conjugate amplitude with primes, this means that initial and final data $\{\mathbf{r}_i, b_i, c_i\}_{i=1}^{N}$ and $\{\mathbf{r'}_i, b'_i, c'_i\}_{i=1}^{N}$ are averaged with the weight

$$\rho\left(\{\boldsymbol{r}_i\}, \boldsymbol{b}\right)\delta^{(2)}\left(\boldsymbol{r}_i - \boldsymbol{r'}_i\right)\delta_{b_i b'_i}\delta_{c_i c'_i}. \tag{2.58}$$

To find the emission spectrum of m soft gluons from a collision with N partonic interactions for general N and m, we use the following simplifications:

- Neglect longitudinal phase factors.

  We only account for transverse momenta and transverse coordinates. We supplement the model with longitudinal phase factors in the definition of the vertex function in Eq. (2.57) by the replacement $\vec{f}(\mathbf{k})e^{i\mathbf{r}\cdot\mathbf{k}} \to \vec{f}(\mathbf{k})e^{i\mathbf{r}\cdot\mathbf{k}}e^{-i(k^+r^- + k^-r^+)}$, where the indices $\pm$ denote components of light-cone coordinates and momenta. For high collision energy, when both the emitting sources and the emitted gluons propagate close to the light-cone, we get $k^- \approx 0$. Identifying the particle-emitting source with an energetic parton of light-cone momentum fraction p^+, it follows from the uncertainty relation that $r^- \; 1/p^+$,

in the soft-gluon limit $k^+ \ll p^+$, gives a negligible total longitudinal phase: $k^+r^- + k^-r^+ \approx k^+/p^+ \approx 0$.

- Emitted gluons do not cross.

  We assume that multi-gluon radiation is dominated by ladder-type diagrams, in which the emitted gluons do not cross each other, and that the emitted gluons are ordered the same way in rapidity. The model is made to retain relevant features of QCD but that are simple enough to allow for the explicit calculation of soft multi-gluon interference for large m and N.

- Symmetrization in the m emitted particles.

  We find that interference contributions to multi-particle-emission cross sections are not always symmetric under interchange of final-state momentum $\mathbf{k}_j$. This arises from different colour constraints on the gluons that we identify with a low index ($j \ll m$ or $j \approx m$) and those near the center. Although these differences are small and unimportant for our discussion, they lead to much longer expressions for higher-order cumulants, so we often randomize the final results by averaging over all permutations of the m outgoing momenta.

- No modelling of hadronization.

  This model only allows us to calculate partonic spectra and momentum correlations. We assume that hadronization satisfies local parton-hadron duality (LPHD) and use it to compare our results with measured hadron spectra and correlations. However, the simple LPHD prescription may not be phenomenologically viable for multi-particle correlations at soft transverse momentum, which may constitute an unaccounted-for source of error.

Using these assumptions allows us to find the spectrum given by Eq. (2.53), the connection between this spectrum and the s-particle differential multiplicity is

$$\frac{d^s N}{d\Gamma_1 \cdots d\Gamma_s} = \frac{d^s \sigma_N \left(\{\boldsymbol{k}_j\}_{j=1}^s\right)}{\sigma_N d\Gamma_1 \cdots d\Gamma_s}, \tag{2.59}$$

where $d\Gamma_j = d^2k_j = k_j dk_j d\phi_j$ is the transverse phase space of particle j. Note that the differential multiplicity is independent of rapidity under the first simplification (i.e. neglecting the longitudinal phase factor).

2.3.2 Dipole Interference Term

This section considers an example of a pp collision with $N = 2$ sources and $m = 2$ emitted gluons and finds the two-particle spectrum. We use this example to define terminology that will help us understand the more general cases.

Sixteen diagrams contribute to the $N = m = 2$ cross section (see Fig. 2.13). In each diagram the gluons are emitted from the sources on the left side of the diagram and are absorbed by the sources on the right side of the diagram.

We define two types of gluons: the first consists of *diagonal* gluons, which are absorbed by the same source that emitted them, and the second consists of *off-diagonal* gluons, which are absorbed by a source other than the one that emitted them. We divide the diagrams shown in Fig. 2.13 into three groups depending on how many *off-diagonal* gluons are in them. The four diagrams on the top line have no off-diagonal gluons, the four diagrams on the second line from the top have two off-diagonal gluons, and the two bottom lines have one diagonal gluon and one off-diagonal gluon. Each diagram makes a different contribution to the cross section.

Each diagram contributes to the cross section in a manner proportional to the trace of the product of the $SU(N_c)$ adjoint representation of the gluon colour indices connected to each source. This factor is called the *colour factor* and, for the top-left diagram, it is given by

$$\mathrm{Tr}\left[T^b T^a T^a T^b\right] \mathrm{Tr}\left[I\right] = N_c^2 \left(N_c^2 - 1\right)^2 , \tag{2.60}$$

where I is the $(N_c^2 - 1) \times (N_c^2 - 1)$ identity matrix, summing over repeating indices is implied and we use the identities $T^a T^a = N_c I$ and $\mathrm{Tr}[I] = N_c^2 - 1$. The colour factors for all diagrams in the top row are the same, which can be shown by using the latter identity. The identity $\mathrm{Tr}\left[T^a T^b\right] = N_c \delta^{ab}$ allows us to obtain the colour factor for the diagrams on the second row from the top, which is

$$\mathrm{Tr}\left[T^b T^a\right] \mathrm{Tr}\left[T^a T^b\right] = N_c^2 \left(N_c^2 - 1\right). \tag{2.61}$$

This result means that a couple of off-diagonal gluons gives us a factor of $(N_c^2 - 1)^{-1}$. The colour factor for the bottom two rows is proportional to the trace of a single generator, $\propto \mathrm{Tr}[T^a] = 0$, meaning that the diagrams with only one off-diagonal gluon do not contribute to the cross section.

The other factor that changes between diagrams is the phases that come from the vertices, $e^{\mp i \mathbf{k}_j \cdot \mathbf{r}_i}$, where the positive (negative) phase come from the complex conjugate amplitude. These phases cancel for a diagonal gluon, leaving us with phases only for off-diagonal gluons.

To find the spectrum for $N = m = 2$, we need the amplitude squared, $|\mathcal{M}(\{\boldsymbol{k}_j\}, \{\boldsymbol{r}_i\})|^2$, and the quasi-probability distribution of the impact parameter and the source positions [the latter is given in Eq. (2.55)]. The amplitude squared is the sum over all 16 diagrams discussed, so all together we can write

$$\left|\mathcal{M}\left(\{\boldsymbol{k}_j\}, \{\boldsymbol{r}_i\}\right)\right|^2 \;\propto\; \left|\vec{f}\left(\boldsymbol{k}_1\right)\right|^2 \left|\vec{f}\left(\boldsymbol{k}_2\right)\right|^2 N_c^2 \left(N_c^2 - 1\right)^2$$

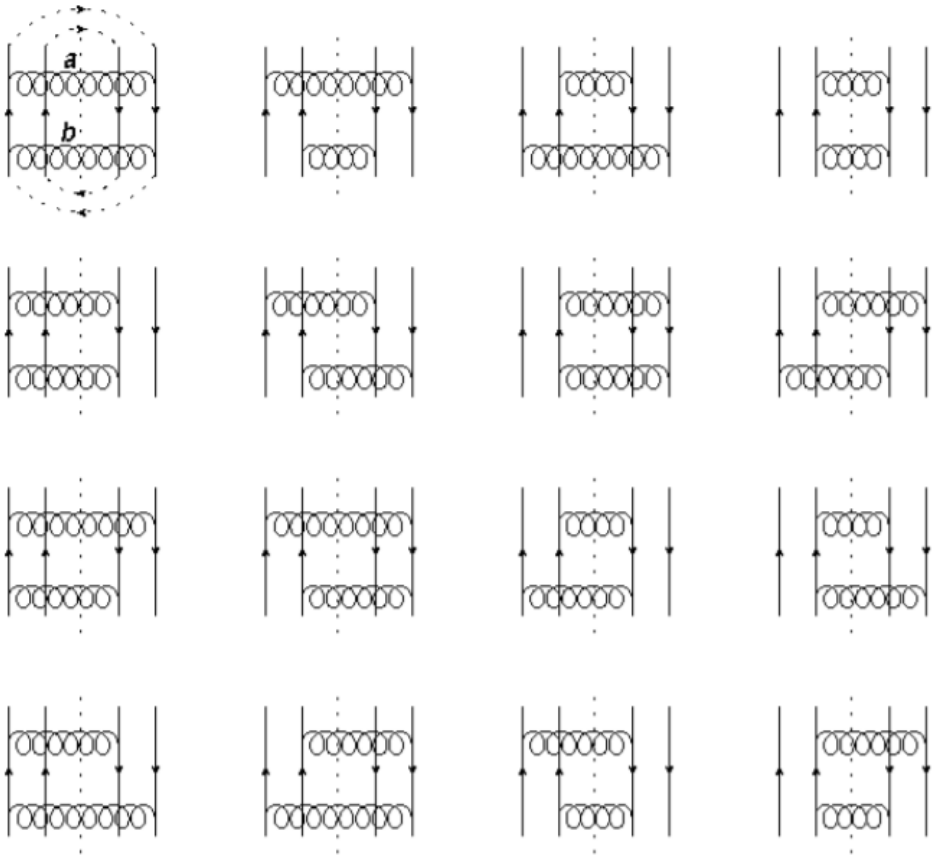

Figure 2.13: Sixteen diagrams for the cross section of $N = m = 2$. The horizontal arrows are the two sources, the two arrows pointing down are the conjugation of the two arrows pointing up, where the outermost arrows are from the same source and the inner arrows are from other sources, as indicated by the dashed arrows on the top, leftmost diagram. The two emitted gluons connect the sources to the conjugated sources. The upper gluon has colour index a and the lower gluon has colour index b. We say that they are emitted from the sources on the left side of the diagram and are absorbed by the sources on the right side. This diagram is taken from Ref. [10].

$$\times \left\{ 4 + \frac{1}{N_c^2 - 1} \left(e^{i(\boldsymbol{k}_1 + \boldsymbol{k}_2)\cdot(\boldsymbol{r}_1 - \boldsymbol{r}_2)} + e^{i(\boldsymbol{k}_1 - \boldsymbol{k}_2)\cdot(\boldsymbol{r}_1 - \boldsymbol{r}_2)} + \text{c.c.} \right) \right\}, \tag{2.62}$$

where the four are the phase factors of the two diagonal gluon diagrams, the phases shown are from the two leftmost diagrams of the second row from the top and c.c. stands for 'complex conjugate'. The two rightmost diagrams on the second row from the top are the complex conjugate of the leftmost diagrams.

To simplify the quasi-probability distribution in Eq. (2.55) we can take the impact parameter to be $\vec{b} = 0$ and normalise it to integrate to unity by making the following replacement:

$$\int d^2b \rho\left(\{\boldsymbol{r}_i\}, \boldsymbol{b}\right) \to \rho\left(\{\boldsymbol{r}_i\}\right) = \int d^2b 2^N \rho\left(\{\boldsymbol{r}_i\}, \boldsymbol{b}\right) \delta^{(2)}\left(\boldsymbol{b}\right), \tag{2.63}$$

which also allows us to write $\rho(\{\boldsymbol{r}_i\}) = \prod_{i=1}^{N} \rho(\boldsymbol{r}_i) = \prod_{i=1}^{N} \frac{1}{2\pi B} e^{\frac{-r_i^2}{2B}}$, so as to separate the dependence on the sources.

The spectrum can now be found by using Eq. (2.53). The resulting spectrum is first order in powers of $(N_c^2 - 1)^{-1}$, so

$$\frac{d^2\sigma_2\left(\boldsymbol{k}_1, \boldsymbol{k}_2\right)}{\sigma_2 d\Gamma_1 d\Gamma_2} \approx \left|\vec{f}\left(\boldsymbol{k}_1\right)\right|^2 \left|\vec{f}\left(\boldsymbol{k}_2\right)\right|^2 \left(1 + \frac{e^{-B(\boldsymbol{k}_1 + \boldsymbol{k}_2)^2} + e^{-B(\boldsymbol{k}_1 - \boldsymbol{k}_2)^2}}{2\left(N_c^2 - 1\right)} \right). \tag{2.64}$$

This spectrum characterises QCD dipole radiation because interference effects decrease, as for larger B or a larger distance between the sources.

Recall that we assumed that $|\vec{f}(\boldsymbol{k})|^2$ is independent of the azimuthal angle of the momentum, which leaves completely isotropic the first term of the diagrams for only-diagonal gluons, which means that this term does not contribute to the azimuthal correlation. The correlations thus arise from interference between different amplitudes, where the gluons are emitted from different sources. However, recall that this does not imply interference between the gluons.

In addition, this spectrum is symmetric upon replacing any of the momenta by $\mathbf{k} \to -\mathbf{k}$, which means that correlations of the form $\langle e^{in(\phi_1 - \phi_2)} \rangle$ vanish identically for odd n.

2.3.3 Diagonal Gluon Corrections to the Dipole

This section investigates what happens when we consider processes with more sources ($N > 2$) and more emitted gluons ($m > 2$). We discuss how diagonal gluons affect the spectrum and the two point cumulants.

To leading order in powers of $(N_c^2-1)^{-1}$ we have two types of diagrams: those with m diagonal gluons, and those with $m-2$ diagonal gluons.

The diagrams with only diagonal gluons do not change drastically. Each of their contributions to the spectrum is proportional to a colour factor $(N_c^2-1)^N N_c^m$ and to the product of the squares of the vertex functions for all the emitted gluons, $\prod_{j=1}^m |\vec{f}(\boldsymbol{k}_j)|^2$. Since by definition diagonal gluons connect each source to its conjugate each gluon can be emitted by any of the sources; however, this also determines which source absorbs the gluon. Thus, in total, we have N^m choices for diagonal diagrams. The result is that the contribution to the spectrum of diagonal diagrams is given by

$$\frac{d^m\sigma_N^{(diagonal)}}{d\Gamma_1\cdots d\Gamma_m} \propto N^m\left(N_c^2-1\right)^N N_c^m \prod_{j=1}^m \left|\vec{f}(\boldsymbol{k}_j)\right|^2. \tag{2.65}$$

The diagrams with two off-diagonal gluons do not vanish if the gluons are shared between a pair of sources, as in Fig. 2.14. This diagram reveals three types of relationships between the diagonal and off-diagonal gluons, which we now use as an example for how each type of relationship affects the colour factor of the diagram.

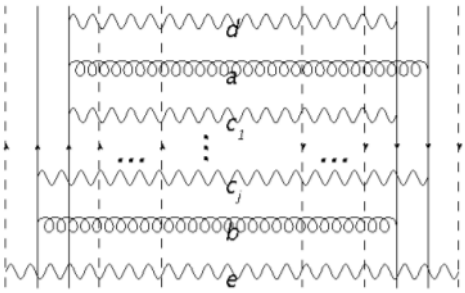

Figure 2.14: Example diagram for single-dipole term for the general N and m case. The curly lines a and b are the two off-diagonal gluons that create the dipole, and the wavy lines $c_1,\ldots,c_j,d$ and e, are diagonal gluons with different relationships to the dipoles. The colour factor for this diagram shows that gluon e does not share a source with the off-diagonal gluons, gluons c_1 and c_j are sandwiched between the off-diagonal gluons in the trace, and gluon d gives a trivial factor of $T^dT^d = N_cI$. This diagram is taken from Ref. [10].

The total colour factor of the diagram, assuming no other sources or gluons, is given by

$$\mathrm{Tr}\left[T^eT^e\right]\mathrm{Tr}\left[T^{c_j}T^bT^{c_j}T^a\right]\mathrm{Tr}\left[T^{c_1}T^aT^dT^dT^{c_1}T^b\right]\left(\mathrm{Tr}\left[I\right]\right)^2. \tag{2.66}$$

We can sum over d and e by using the identity $T^aT^a = N_cI$ when e does not share a source with the dipole pair, and d appears next to itself (so they are both trivial).

The gluons c_1 and c_j differ, but we use the identity $T^bT^aT^b = \frac{N_c}{2}T^a$ to compute this trace. Each of them then gives a factor of $\frac{1}{2}$ that we did not have before. A diagonal gluon that shares its source with off-diagonal gluons and is between them on the diagram is sandwiched by the off-diagonal gluons. These types of gluons contribute a factor of $\frac{1}{2}$ to the diagram and to the colour factor.

It will be useful to sum over all diagrams with a single pair of off-diagonal gluons, since they all have the same source position and gluon-momentum dependence. Thus, by summing over all such diagrams we define a factor that accounts for the factors of $\frac{1}{2}$. This factor is denoted $F^{(2)}_{\text{corr}}(N,m)$. The total contribution to the spectrum of diagrams with single pairs of off-diagonal gluons is proportional to this correction factor.

To find $F^{(2)}_{\text{corr}}(N,m)$, we use the method established in Ref. [10]. For an ordered list of m gluons with one off-diagonal pair, $m-1-j$ ways exist to have $j = 1,2,\ldots,m-2$ diagonal gluons between the two off-diagonal gluons. For each configuration with j diagonal gluons between the two off-diagonal gluons, $\binom{j}{l}2^l(N-2)^{j-l}$ ways exist to have l of them share a source with the off-diagonal gluons, making them sandwiched. Each such contribution is then suppressed by a correction factor of $(\frac{1}{2})^l$.

Ignoring the factor $(\frac{1}{2})^l$ would be like assuming that all $m-2$ diagonal gluons are incoherently superimposed to form the interference pattern of the two off-diagonal gluons. The number of such incoherent superpositions is

$$N_{\text{incoh}} = \sum_{j=0}^{m-2} N^{m-2-j}\,(m-1-j)\sum_{l=0}^{j}\binom{j}{l}2^l\,(N-2)^{j-l} = \frac{m\,(m-1)}{2}N^{m-2}. \quad (2.67)$$

When we account for the factor $(\frac{1}{2})^l$, we get the real colour factor, but we want to average it over all the diagrams that we are counting, so the colour correction factor is given by

$$\begin{aligned} F^{(2)}_{\text{corr}}\,(N,m) &= \frac{1}{N_{\text{incoh}}}\sum_{j=0}^{m-2} N^{m-2-j}\,(m-1-j)\sum_{l=0}^{j}\binom{j}{l}2^l\,(N-2)^{j-l}\,\frac{1}{2^l} \\ &= \frac{2}{m\,(m-1)}N^{1-m}\left[N\,(N-1)^m + mN^m - N^{1+m}\right]. \end{aligned} \quad (2.68)$$

We now note few properties of $F^{(2)}_{\text{corr}}(N,m)$ that can be useful to us. First, $F^{(2)}_{\text{corr}}(N,m) \leq 1$ where full equality occurs only for $m = 2$. Three interesting limits are considered:

- The limit of $m = \text{const.}$ and $N \to \infty$.

Increasing the number of sources at fixed multiplicity m favors incoherent particle production, so we find

$$\lim_{N\to\infty} F_{\text{corr}}^{(2)}(N,m)\Big|_{m=\text{const.}} = 1. \tag{2.69}$$

- The limit of $m \to \infty$ for fixed average multiplicity per source $\bar{m} = m/N$.

  This limit is consistent with analyses of LHC pp data that indicate that the multiplicity of hard processes is proportional to the soft multiplicity [27]. For any finite value of $\bar{m} = m/N$, the limit is also finite:

$$\lim_{m\to\infty} F_{\text{corr}}^{(2)}(m/\overline{m},m)\Big|_{\overline{m}=\text{const.}} = \frac{2\overline{m}+2e^{-\overline{m}}-2}{\overline{m}^2}. \tag{2.70}$$

- The limit of $N = \text{const.}$ and $m \to \infty$.

  For a fixed number of sources, the colour correction factor behaves asymptotically like

$$\lim_{m\to\infty} F_{\text{corr}}^{(2)}(N,m)\Big|_{N=\text{const.}} \approx \frac{2N}{m} + O\left(\frac{N^2}{m^2}\right). \tag{2.71}$$

  Therefore, increasing the multiplicity for a fixed number of sources decreases the correlation.

We cannot write the total contribution to the spectrum of the diagrams with single pairs of off-diagonal gluons:

$$\begin{aligned}\frac{d^m\sigma_N^{(\text{dipole})}}{d\Gamma_1\cdots d\Gamma_m} \;\propto\; & N^m\left(N_c^2-1\right)^N N_c^m\left(\prod_{j=1}^{m}\left|\vec{f}\,(\boldsymbol{k}_j)\right|^2\right)\\ & \times\frac{F_{\text{corr}}^{(2)}(N,m)}{N^2\left(N_c^2-1\right)}\sum_{(ab)}\sum_{(ij)} 2^2\cos\left[\boldsymbol{k}_a\left(\boldsymbol{r}_i-\boldsymbol{r}_j\right)\right]\cos\left[\boldsymbol{k}_b\left(\boldsymbol{r}_i-\boldsymbol{r}_j\right)\right].\end{aligned} \tag{2.72}$$

Here the factor of N^{-2} comes from having two fewer diagonal gluons, the factor of $(N_c^2-1)^{-1}$ comes from the difference between the colour factors of an all-diagonal diagram and two off-diagonal diagrams, the sum over (ab) sums over all possible ordered pair of choices of which m gluons are the two off-diagonal ones, the sum over (ij) is the sum over unordered pairs of sources, and the factor $2^2\cos[\boldsymbol{k}_a(\boldsymbol{r}_i - \boldsymbol{r}_j)]\cos[\boldsymbol{k}_b(\boldsymbol{r}_i-\boldsymbol{r}_j)]$ is the same sum over phases we had for the case $N = m = 2$.

Since we end up randomizing the gluons and the sources are interchangeable, we can use these symmetries to transform the sums into a factor that only depends on N and m, the sum over the gluons give us a factor of $\sum_{(ab)} \to 2!\binom{m}{2}$, and the sum

over the sources gives us a factor of the form $\sum_{(ij)} \to \binom{N}{2}$. We can now rewrite the two-particle spectrum as

$$\begin{aligned}\frac{d^m\sigma_N}{\sigma_N d\Gamma_1 \cdots d\Gamma_m} &= \left(\prod_{j=1}^{m}\left|\vec{f}\left(\boldsymbol{k}_j\right)\right|^2\right) \\ &\times\left[1+\frac{2^2 F_{\mathrm{corr}}^{(2)}(N,m)}{N^2\left(N_c^2-1\right)}\binom{m}{2}2!\binom{N}{2}\cos\left(\boldsymbol{k}_1\cdot\boldsymbol{r}_{12}\right)\cos\left(\boldsymbol{k}_2\cdot\boldsymbol{r}_{12}\right)\right],\end{aligned} \tag{2.73}$$

where $\boldsymbol{r}_{12} \equiv \boldsymbol{r}_1 - \boldsymbol{r}_2$ is the displacement between the two sources.

The leading order in powers of $(N_c^2-1)^{-1}$ of the single-particle differential multiplicity comes from the diagonal term of the cross section:

$$\frac{dN}{d\Gamma_j} = m\left|\vec{f}\left(\boldsymbol{k}_j\right)\right|^2. \tag{2.74}$$

To find the azimuthal correlations, we integrate over a phase, so we can ignore the diagonal contribution to the two-particle differential multiplicity and write it as

$$\begin{aligned}\frac{d^2N}{d\Gamma_1 d\Gamma_2} &= \left(\prod_{j=1}^{2}\left|\vec{f}\left(\boldsymbol{k}_j\right)\right|^2\right) \\ &\times\frac{2^3 F_{\mathrm{corr}}^{(2)}(N,m)}{N^2\left(N_c^2-1\right)}\binom{m}{2}\binom{N}{2}\cos\left(\boldsymbol{k}_1\cdot\boldsymbol{r}_{12}\right)\cos\left(\boldsymbol{k}_2\cdot\boldsymbol{r}_{12}\right),\end{aligned} \tag{2.75}$$

where, again, this is only the non-isotropic part to leading order in powers of $(N_c^2-1)^{-1}$. We can now use Eq. (2.56) to find the two-particle azimuthal correlations, remembering that, for two particles, the two-particle azimuthal correlation is the same as the two-particle symmetric cumulant [Eq. (2.13)]. We can thus write

$$sc_n\{2\} = \frac{2F_{\mathrm{corr}}^{(2)}(N,m)\binom{N}{2}}{N^2\left(N_c^2-1\right)}(-1)^n\left[1+(-1)^n\right]^2\int_\rho J_n\left(k_1 r_{12}\right)J_n\left(k_2 r_{12}\right), \tag{2.76}$$

where $J_n(z)$ are Bessel functions of the first kind that we get from the integral over the phases:

$$\int_0^{2\pi} d\phi e^{in\phi}\cos\left(z\cos\left[\phi-\alpha\right]\right) = \pi i^n e^{in\alpha}\left[1+(-1)^n\right]J_n\left(z\right). \tag{2.77}$$

Here, α is a general phase shift, but for us it is the azimuthal angle of the vector $\Delta\boldsymbol{r}_{12}$, where the final phase cancels, giving $e^{in\alpha}e^{i(-n)\alpha} = 1$.

Equation (2.76) shows that, for any odd n, the cumulant vanishes due to the factor of $[1+(-1)^n]^2$, which agrees with Eq. (2.64) that the dipole symmetry for $\mathbf{k} \to -\mathbf{k}$ means that all odd harmonics vanish.

In addition, the two-particle cumulant is not separable for general momenta. For small momenta $k \ll B^{-1/2}$, also called the hydrodynamic approximation, we can write $J_n(k_j \Delta r_{12}) \approx \frac{(k_j \Delta r_{12})^n}{2^n n!}$, resulting in an integral that can be solved analytically. For even n we obtain

$$sc_n\{2\} \approx \frac{2^3 F_{\text{corr}}^{(2)}(N,m)\binom{N}{2}}{N^2\left(N_c^2-1\right)n!}\left(\sqrt{B}k_1\right)^n\left(\sqrt{B}k_2\right)^n. \tag{2.78}$$

The cumulant dependence on N and m is fully expressed in the factor $\frac{F_{\text{corr}}^{(2)}(N,m)\binom{N}{2}}{N^2}$, meaning that it behaves very similarly to what we saw in the three limits we discussed for $F_{\text{corr}}^{(2)}(N,m)$.

2.3.4 General Cross Section

This section determines the cross section for any number N of sources and m of emitted gluons.

Before we can find the general cross section, we discuss diagrams with more then two off-diagonal gluons. For a diagram with off-diagonal gluons to have a non-vanishing colour factor, each source cannot emit only a single off-diagonal gluon, which means that the off-diagonal gluons must come in sets of two or more that create close source loops. The case of a dipole is the two-loop, $1 \to 2 \to 1$, but more off-diagonal gluons can create loops of as many sources as the number of off-diagonal gluons, although not necessarily as equal. A dipole is a two-source loop, a tripole is a three source loop, $1 \to 2 \to 3 \to 1$, and a loop of a sources is called an a-pole. A diagram of a tripole appears in Fig. 2.15 on the left; going from top to bottom, the source pairs of each gluon are $(12) \to (23) \to (31)$, where '1' stands for the innermost source and '3' sands for the outermost source.

Loops smaller then the number of off-diagonal gluons exist for two reasons: The first reason is that, given four or more off-diagonal gluons, they can group up in smaller chains (i.e. four off-diagonal gluons can form a four-pole or two dipoles, but not a tripole and a single off-diagonal gluon on its own). The second reason is that any part in the loop can be connected by any number of off-diagonal gluons (i.e. three off-diagonal gluons can create a dipole with an extra off-diagonal gluon). Figure 2.15 (right) shows a diagram of a three-gluon dipole with three sources. Going from top to bottom, the source pair for each gluon is $(12) \to (21) \to (12)$, where '1' stands for the innermost source and '3' stands for the outermost source. This is a dipole: only two sources are connected, with an additional gluon.

Each type of diagram has different arrangements of off-diagonal gluons and will produce different colour factors and correction factors, but in the limit of $m \to \infty$

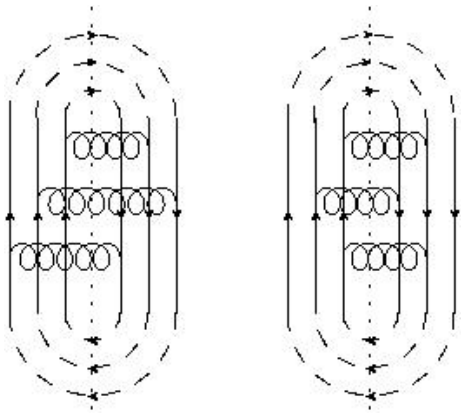

Figure 2.15: Two of the diagrams that contribute to the three-point asymmetric cumulant for the case of $N = m = 3$. On the left is the diagram of a tripole, where each of the three gluons is connected to a different pair of sources. On the right is a three-gluon dipole, where only two of the sources are connected by three off-diagonal gluons.

for fixed average multiplicity per source ($\bar{m} = m/N$), we can find the different contributions and sum them. Each off-diagonal gluon gives a factor of N^{-1}, so off-diagonal loops with more gluons than sources will be suppressed compared with loops with the sources but no extra gluons. In addition, each off-diagonal gluon with momentum $\mathbf{k}$ that connects the sources one and two gives as a factor of $2\cos(\mathbf{k}\cdot\mathbf{r}_{12})$, where $\mathbf{r}_{12} \equiv \mathbf{r}_1 - \mathbf{r}_2$.

Each a-pole comes with a colour factor of $N_c^m(N_c^2-1)^{N-(a-1)}$ regardless of the number of gluons in it (this is true in general only in the limit of $m \to \infty$ for fixed average multiplicity per source $\bar{m} = m/N$), so higher poles will be suppressed by powers of $(N_c^2 - 1)$.

Two factors must be considered to compute the cross section: N and $(N_c^2 - 1)$. In addition, each diagram type with a different number of loops of different lengths and containing different numbers of gluons will produce a different correction factor.

The first few terms of the total cross section are

$$\begin{aligned}\frac{d^m\sigma_N}{d\Gamma_1\cdots d\Gamma_m} \;\propto\; & N^m\left(N_c^2-1\right)^N N_c^m\left(\prod_{j=1}^{m}\left|\vec{f}\,(\boldsymbol{k}_j)\right|^2\right) \\ & \times\left\{1+\frac{F_{\mathrm{corr}}^{(2)}(N,m)}{N^2\left(N_c^2-1\right)}\sum_{(ab)}\sum_{(lm)}2^2\cos\left(\boldsymbol{k}_a\cdot\boldsymbol{r}_{lm}\right)\cos\left(\boldsymbol{k}_b\cdot\boldsymbol{r}_{lm}\right)\right. \\ & \left.+\frac{F_{\mathrm{corr}}^{(3,2)}(N,m)}{4N^3\left(N_c^2-1\right)}\sum_{(abc)}\sum_{(lm)}2^3\cos\left(\boldsymbol{k}_a\cdot\boldsymbol{r}_{lm}\right)\cos\left(\boldsymbol{k}_b\cdot\boldsymbol{r}_{lm}\right)\cos\left(\boldsymbol{k}_c\cdot\boldsymbol{r}_{lm}\right)\right.\end{aligned}$$

$$+\frac{F_{\text{corr}}^{(3)}(N,m)}{N^3\left(N_c^2-1\right)^2}\sum_{(abc)}\sum_{(lm)(mn)(ln)}2^3\cos\left(\boldsymbol{k}_a\cdot\boldsymbol{r}_{lm}\right)\cos\left(\boldsymbol{k}_b\cdot\boldsymbol{r}_{mn}\right)\cos\left(\boldsymbol{k}_c\cdot\boldsymbol{r}_{ln}\right)$$

$$+O\left(\frac{1}{N^4\left(N_c^2-1\right)^2}\right)\Bigg\}. \tag{2.79}$$

The sums $\sum_{(ab)}$ and $\sum_{(abc)}$ over the gluons are over ordered sets of gluons. In diagrams with m_{off} off-diagonal gluons there are $\binom{m}{m_{\text{off}}}m_{\text{off}}!$ terms in the sum. In the terms shown, the sums $\sum_{(lm)}$ and $\sum_{(lm)(mn)(ln)}$ over the sources go over non-ordered sets of sources: for an a-pole the sum has $\binom{N}{a}$ terms, for diagrams with l loops the loop lengths are denoted $\{a_i\}_{i=1}^{l}$ and we find

$$\binom{N}{a_1}\binom{N-a_1}{a_2}\cdots\binom{N-\sum_{i=1}^{l-1}a_i}{a_l}=\frac{N!}{\prod_{i=1}^{l}\left(a_i!\right)\left(N-\sum_{i=1}^{l}a_i\right)!}$$

terms in the sum.

The first line in Eq. (2.79) contains the factors of the fully diagonal diagrams, the terms in the second line are the fully diagonal gluon diagrams and diagrams with a single two-gluon dipole, the terms in the third line are the diagrams with only a three-gluon dipole, the terms in the fourth line are the three-gluon tripole diagrams, and the last line indicates that we are neglecting terms of higher orders in powers of N^{-1} and $(N_c^2-1)^{-1}$, such as double-dipole diagrams and four-gluon tripoles.

The factor of 4^{-1} from the three-gluon diagram comes from the colour factor. The correction factors $F_{\text{corr}}^{(3,2)}(N,m)$ and $F_{\text{corr}}^{(3)}(N,m)$ can be obtained in the same way as we got $F_{\text{corr}}^{(2)}(N,m)$. The details of the calculation are in Appendix B; the result is $F_{\text{corr}}^{(3,2)}(N,m)=F_{\text{corr}}^{(3)}(N,m)$, with

$$F_{\text{corr}}^{(3)}(N,m)=\frac{(m-3)!}{m!}\left[6\left(m-2N\right)N^2+6\left(N-1\right)^{m-1}N^{3-m}\left(m+2N-2\right)\right]. \tag{2.80}$$

This correction factor is very similar to $F_{\text{corr}}^{(2)}(N,m)$ in the three limits discussed above. For the limit $m\to\infty$ for fixed average multiplicity per source ($\bar{m}=m/N$), we get

$$\lim_{m\to\infty}F_{\text{corr}}^{(2)}\left(m/\overline{m},m\right)\Big|_{\overline{m}=\text{const.}}=6\frac{e^{-\overline{m}}\left(\overline{m}+2\right)}{\overline{m}^3}+6\frac{\overline{m}-2}{\overline{m}^3}. \tag{2.81}$$

2.3.5 The Real Expansion Parameter

The way we express the cross section in Eq. (2.79) is somewhat misleading. The diagrams with more off-diagonal loops with more gluons than sources are suppressed by a factor of N^{-1} for each additional gluon. Reference [11] shows that we need to add a factor $\frac{m^a}{(N_c^2-1)^{a-1}}$ for each a-pole, which implies that the expansion is only valid

for small m. Because m is finite, this parameter series can be explicitly summed, giving a genuine $\frac{1}{N_c}$ and $\frac{1}{N}$.

Chapter 3

Three-Point Asymmetric Cumulant

3.1 Introduction

Sizeable nth harmonic coefficients v_n for azimuthal momentum asymmetries have been observed at the LHC in nucleus-nucleus (AA), proton-nucleus (pA) and proton-proton (pp) collisions [8, 9, 28, 5, 29, 30]. These asymmetries reflect a collective mechanism that relates all particles produced in a given collision. The dynamic origin of these collectivity phenomena continues to be sought in competing and potentially contradicting pictures.

There are two basic approaches to explain this collective behaviour. The first approach is based on the final-state interactions, like viscous fluid dynamics simulations [31] or kinetic transport models of heavy-ion collisions [32, 33, 34, 35, 36]. In AA collisions, the jet-quenching phenomenon provides an alternative confirmation for such a approach. However, jet quenching is absent in smaller pp and pA collision systems. Moreover, in marked contrast with any final-state explanation of flow anisotropies v_n in pp collisions, the phenomenologically successful modelling of soft multi-particle production in modern multi-purpose pp event generators [37] are based on free-streaming partonic final-state distributions supplemented by independent fragmentation into hadrons. Efforts to go beyond this picture are relatively recent (see, e.g., Refs. [38, 39]). Therefore, two contradictory pictures to describe the multi-particle dynamics in small systems currently exist: one based on the final-state interactions, and the another that does not involve final-state interactions. One approach in the second direction corresponds to the recent works within the framework of colour glass condensates [40, 41, 42] (see Ref. [43] for a recent review), which is based on the parton-saturation hypothesis and recently made significant

progress towards a phenomenological description of correlations in small systems.

Recently, a simple QCD model based on theory of MPIs in pp collisions [44, 45, 46, 47, 48, 49, 50, 51, 52, 53] and not involving saturation effects was proposed in Refs. [10, 11] to study the effects of quantum interference and colour flow in high-multiplicity pp events. The strong simplification of the model involves neglecting a dynamically explicit formulation of the scattering process: all gluons in the incoming wave function are assumed to be freed in the scattering process with the same (possibly small) probability. The model pictures the incoming hadronic wave function as a collection of N colour sources in an adjoint representation distributed in transverse space according to a classical density $\rho(\vec{r}_i)$. On the amplitude level, emission of a gluon is taken into account in the soft-gluon eikonal approximation.

Reference [11] calculates the flow coefficients $v_n\{2s\}$ determined by $2s$ point symmetric cumulants:

$$sc_n\{2s\} \equiv \left\langle\left\langle \exp\left\{in\left(\sum_{i=1}^{i=s}\phi_i - \sum_{i=s+1}^{i=2s}\phi_i\right)\right\}\right\rangle\right\rangle, \tag{3.1}$$

where $\langle\langle\cdots\rangle\rangle$ indicates averaging over the multi-particle final states and taking the cumulant. The phases ϕ_i are the azimuthal angles of measured soft hadrons.

The model from Refs. [10, 11] predicts both the collectivity phenomenon and the qualitatively correct scale of correlations as well as their behaviour as functions of transverse momentum. Consequently, it makes sense to study the other recently measured flow phenomenon in high-multiplicity pp collisions within the framework of this model.

One group of potentially interesting cumulants are the three-point asymmetric cumulants. The corresponding cumulants are often denoted $ac_n\{3\}$, where

$$ac_n\{3\} \equiv \left\langle\left\langle e^{in(\phi_1-\phi_3)}e^{in(\phi_2-\phi_3)}\right\rangle\right\rangle = \left\langle\left\langle e^{in(\phi_1+\phi_2-2\phi_3)}\right\rangle\right\rangle. \tag{3.2}$$

These cumulants were recently studied experimentally [12]. Since we consider herein only $ac_n\{3\}$ cumulants, we simply denote them as ac_n below.

The purpose of the chapter is to calculate the three-point correlations [Eq. (3.2)] and to compare these correlators with experimental data [12]. The results are qualitatively consistent with the experimental data, although insufficient experimental data are available for a detailed comparison.

We make detailed predictions of the transverse-momentum dependence and of the scale (characteristic magnitude) of the three-point cumulant, and we also discuss how this cumulant depends on multiplicity.

Recall that the model from Refs. [10, 11] is based on large N_c and N expansion, following which the results are extrapolated to $N_c = 3$.

3.2 Basic Formalism

3.2.1 The Model [10, 11]

Each pp collision is considered as an event consisting of N emitting sources characterized by two-dimensional transverse positions $\boldsymbol{r}_j$ and the initial colours in the adjoint representation b_j. Physically, these sources correspond to MPIs. In other words, each source is a collision of two partons—one from each of the colliding nucleons.

The emission amplitude of the gluon with colour a and transverse momentum $\vec{k}$ from a source at transverse position $\vec{r}_j$ is given by an eikonal vertex

$$T^a_{b_j c_j} \overrightarrow{f}(\boldsymbol{k})\, e^{i\boldsymbol{k}\cdot\boldsymbol{r}_j}, \tag{3.3}$$

where $T^a_{b_j c_j}$ are the adjoint generators of $SU(N_c)$ and $\overrightarrow{f}(\boldsymbol{k})$ is a vertex function. The concrete form of $\vec{f}$ does not influence the results (see below). For example, for Coulombic radiation we have $\vec{f} = \vec{k}/k^2$. However, since the relevant momenta are small the function f must be taken to be non-perturbative. In the cross section, the emitted gluon can be absorbed by the same source in the complex-conjugated amplitude ('diagonal gluons') or by different sources ('off-diagonal gluons'), leading to multi-particle correlations. The simplest diagrams contributing to the multi-particle cross section and to correlations are presented in Fig. 3.1. The left image in the figure shows a diagram with two sources and two diagonal gluons, and the right image shows two sources but with off-diagonal gluons that are emitted by one source and absorbed by another, leading to azimuthal correlations.

After calculating cross sections for given source positions we average over the source positions with a classical probability distribution $\rho(\{\boldsymbol{r}_j\})$ corresponding to the distribution of MPIs in the pp collision [45]:

$$\frac{d\hat{\sigma}}{d^2\vec{k}_1 \cdots d^2\vec{k}_m} = \prod_{i=1}^{N} \int d^2\boldsymbol{r}_i \rho(\boldsymbol{r}_i) \hat{\sigma}(\vec{k}_i, \boldsymbol{r}_i), \tag{3.4}$$

where $\sigma(k_i, \boldsymbol{r}_i)$ is the cross section for producing m gluons from sources at fixed transverse positions $\boldsymbol{r}_i$. Herein we neglect the so-called $1 \to 2$ mechanism for MPIs [45, 48, 50] and do all calculations in the mean-field approximation. In this case, the source or MPI distribution in the pp system has a Gaussian form:

$$\rho\left(\{\boldsymbol{r}_j\}\right) = \prod_{i=1}^{i=N} \frac{1}{2\pi B} e^{\frac{-r_i^2}{2B}}, \tag{3.5}$$

where the parameter B is determined by analysing the one-particle GPD data from HERA [54]. As noted in Ref. [10], the mean-field approach to MPIs corresponds

to $B = 4$ GeV^{-2}, which is the actual experimental data reparameterised in the mean-field form; that is, assuming that the factorization of MPI cross sections corresponds to $B = 2$ GeV^{-2}, and the best fit to the experimental data for symmetric correlators sc_n considered in Refs. [10, 11] corresponds to $B = 1$ GeV^{-2}, which was justified (although not proven) in Ref. [10] based on arguments leveraging the possible contribution of very small dipoles formed by the so-called $1 \to 2$ mechanism in MPIs [45, 48, 50]. Herein, the value of B influences only the transverse-momentum dependence, and the value $B = 1$ GeV^{-2} seems to be the most consistent with the experimental data.

We work in the limit of a large number N of sources with m finite, $N \to \infty$ [10, 11] and $N_c \to \infty$ and with all diagrams classified in powers of $1/N_c$ and $1/N$.

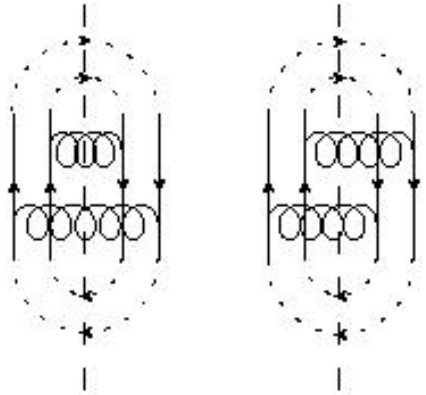

Figure 3.1: The simplest diagrams contributing to the total cross section and to correlations. The left diagram shows two diagonal gluons, the right diagram shows interference corresponding to two off-diagonal gluons forming a dipole.

The Correlation Functions

The correlation functions we are interested in have the general form

$$K^{(n)}(k_1, \ldots, k_s) = M_s \frac{\int_\rho d\phi_1 \cdots d\phi_s \exp\left[i(\sum_{i=1}^{i=s} n_i \phi_i)\right] \frac{d^s N}{d\Gamma_1 \cdots d\Gamma_s}}{(2\pi)^s \prod_{i=1}^{i=s} \int_\rho \frac{dN}{d\Gamma_i}}, \tag{3.6}$$

where $\sum_i n_i = 0$, and $\int_\rho = \int \prod_i d^2 y_i \rho(\vec{y}_i)$ is the average over the position of the sources. The standard s-particle spectrum has the form

$$\frac{d^s N}{d\Gamma_1 \cdots \Gamma_s} = \binom{m}{s} \frac{d^s \hat{\sigma}}{\hat{\sigma} d\Gamma_1 \cdots d\Gamma_s}, \tag{3.7}$$

where $\hat{\sigma}$ is the cross section for the production of s gluons, and the normalisation factor M is

$$M_s = m^s \Big/ \binom{m}{s}, \tag{3.8}$$

where m is the total multiplicity, and s is the number of measured gluons. We assume LPHD [54], so radiated-gluon correlations and multiplicities coincide with correlations and multiplicities in the soft-hadronic spectrum. The number of radiated gluons is in one-to-one correspondence with the number of radiated soft hadrons.

Herein we are interested in the case $s = 3$, $n_1 = n$, $n_2 = n$, $n_3 = -2n$. In other words,

$$K^{(n)}(k_1, k_2, k_3) = M_3 \frac{\int_\rho d\phi_1 d\phi_3 \exp\left[in(\phi_1 + \phi_2 - 2\phi_3)\right] \frac{d^3N}{d\Gamma_1 \cdots \Gamma_3}}{(2\pi)^s \prod_{i=1}^{i=3} \int_\rho \frac{dN}{d\Gamma_i}}. \tag{3.9}$$

3.2.2 The Differential Cross Section

The relevant differential cross section was calculated in Ref. [10], so we can now write $\hat{\sigma}$ explicitly in the limit $N \to \infty$, that is, omitting terms that go to zero as $N \to \infty$:

$$\begin{aligned}
\hat{\sigma} \quad \propto \quad & N_c^m (N_c^2 - 1)^N N^m \prod_{i=1}^{m} \left| \overrightarrow{f}\left(\boldsymbol{k}_i\right) \right|^2 \\
& \times \Bigg[1 + \frac{F_{\mathrm{corr}}^{(2)}(N,m)}{N^2(N_c^2-1)} \sum_{ab} \sum_{lm} 2^2 \cos\left(\mathbf{k}_a \cdot \Delta\mathbf{r}_{lm}\right) \cos\left(\mathbf{k}_b \cdot \Delta\mathbf{r}_{ml}\right) \\
& + \frac{F_{\mathrm{corr}}^{(3)}(N,m)}{4N^3\left(N_c^2-1\right)} \sum_{(abc)} \sum_{(lm)} 2^3 \cos\left(\mathbf{k}_a \cdot \Delta\mathbf{r}_{lm}\right) \cos\left(\mathbf{k}_b \cdot \Delta\mathbf{r}_{lm}\right) \cos\left(\mathbf{k}_c \cdot \Delta\mathbf{r}_{lm}\right) \\
& + \frac{F_{\mathrm{corr}}^{(3)}(N,m)}{N^3\left(N_c^2-1\right)^2} \sum_{(abc)} \sum_{(lm)(mn)} 2^3 \cos\left(\mathbf{k}_a \cdot \Delta\mathbf{r}_{lm}\right) \cos\left(\mathbf{k}_b \cdot \Delta\mathbf{r}_{mn}\right) \cos\left(\mathbf{k}_c \cdot \Delta\mathbf{r}_{nl}\right) \\
& + O\left(N^{-4}\right) \Bigg].
\end{aligned} \tag{3.10}$$

The sums span over all ordered combinations of off-diagonal gluons and non-ordered combinations of sources. By using Eq. (3.10), we can find any correlation function for any number of particles.

The first term in Eq. (3.10) corresponds to diagonal gluons, and the second is a dipole term, which is a leading contribution to symmetric cumulants [11]. The leading contribution to the asymmetric correlator [Eq. (3.2)] comes from the third and fourth terms in the expansion [Eq. (3.10)], which corresponds to a three-gluon dipole (which is actually $1/N$-suppressed relative to the second term) and a tripole diagram, as depicted in Fig. 3.2. Note that the tripole diagram has a finite value in the limit $N \to \infty$.

The factors $F_{\mathrm{corr}}^{(2)}(N,m)$ and $F_{\mathrm{corr}}^{(3)}(N,m)$ correspond to the contribution of diagonal gluons to the interference diagrams. As shown in Ref. [10], the diagonal gluons

lead to multiplicative renormalisation of the correlators, as given by the corresponding coefficients F_{corr}.

3.2.3 $1/N_c$ Expansion

Recall the structure of the expansion discussed in Refs. [10, 11] for even harmonics for symmetric cumulants. The expansion is in two parameters: $1/(N_c^2-1)$ and $1/N$. The leading contribution comes from the dipole diagram, which is of order $1/(N_c^2-1)$, and the leading approximation in $1/(N_c^2-1), 1/N$ is considered so that we may discard all $1/N$-suppressed diagrams. Note, however, that odd harmonics appear only due to $1/N$-suppressed terms in the differential-cross-section expansion. Reference [10] shows that the real parameters of the expansion for a given multiplicity are $m^2/[(N_c^2-1)N]$, where N is the number of sources and m is the multiplicity. However, the leading terms in this expansion can be resummed as done in Ref. [11]. The corresponding diagrams are built from up to $[N/2]$[1] sources and correspond to non-intersecting dipoles.

For three-point cumulants the situation is more complicated. For symmetric cumulants we have shown that the $1/N$-suppressed diagrams can be neglected. Conversely, for a three-point cumulant, the leading diagram in the limit $N \to \infty$ is a tripole (see Fig. 3.3). However, this diagram is suppressed by $1/(N_c^2-1)^2$ in the large-N_c limit. In contrast, the diagram corresponding to the dipole with three off-diagonal gluons (Fig. 3.3) has zero limit for large N; in other words, it is $1/N$-suppressed, whereas it is only $1/(N_c^2-1)$-suppressed in the large-N_c limit. We thus expect that $1/N$ corrections will play a significant role in the three-point correlator if we extrapolate to finite $1/N_c$.

In fact, we see below that the dipole with three gluons dominates numerically up to a rather large number of sources, so we consider both the tripole and the dipole with three off-diagonal gluons. We also consider the leading terms in the expansion in $m^2/(N_c^2-1)$ for both leading and subleading ($1/N$, i.e. a dipole with three off-diagonal gluons) terms in the expansion. This is in analogy with the symmetric case [11] in which such an expansion corresponds to the inclusion of up to $[N/2]$ non-intersecting integrated-out dipoles with two off-diagonal gluons.[2] All other diagrams are subleading, namely, suppressed by higher powers of $1/(N_c^2-1)$ or $1/N$ (i.e. as $1/(N_c^2-1)^a 1/N^b$, $a+b \geq 3$).

For numerical calculations we extrapolate the results to finite $N_c = 3$ and to

[1] [] means the integer part.

[2] By 'integrated out' we mean that we integrate over momenta of the corresponding non-observable off-diagonal gluons.

finite N, actually fixing $\bar{m} = m/N$ in the limit $m, N \to \infty$ as the parameter of the model. We use the same values of $\bar{m}$ as was done for symmetric cumulants in Ref. [11].

3.3 Tripole and Three-Gluon Dipole

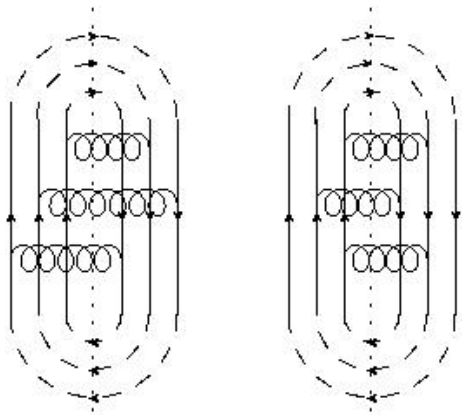

Figure 3.2: (left) Tripole diagram for $N = m = 3$. (right) Three-gluon dipole diagram for $N = m = 3$.

This section considers the simplest case of $N = m = 3$, for which there are two contributions: one from the tripole diagram and one from the dipole with three gluons. Note that each diagram is a building block for the case of arbitrary m, N.

We start by analysing the single-tripole term, which corresponds to the case $N = m = 3$. The corresponding diagram is depicted in Fig. 3.2 (left). In this case there are $3! = 6$ ordered combinations of gluons and there are three ways to assign the phases to the three available gluons. By using Eq. (3.10), we obtain the multiplier 144:

$$\begin{aligned} ac_n^{(3,3)} &\equiv \frac{T_n}{(N_c^2-1)^2} \\ &= \frac{144}{(N_c^2-1)^2 3^3} \int_\rho \int d\phi_1 d\phi_2 d\phi_3 e^{in(\phi_1+\phi_2-2\phi_3)} \cos\left(\mathbf{k}_1 \cdot \Delta\mathbf{r}_{12}\right) \cos\left(\mathbf{k}_2 \cdot \Delta\mathbf{r}_{23}\right) \cos\left(\mathbf{k}_3 \cdot \Delta\mathbf{r}_{31}\right), \end{aligned} \tag{3.11}$$

where $ac^{3,3}$ is the contribution of the tripole diagram to the total ac.

Consider now the contribution of the three-gluon dipole to the asymmetric three-point cumulant. Figure 3.2 (right) shows the corresponding diagram. For the three-gluon dipole, only two of the three sources are involved, so the multiplier gains a

factor of

$$\begin{pmatrix} 3 \\ 2 \end{pmatrix}$$

and a factor of 4^{-1} from the colour trace, and the multiplier becomes 108:

$$\begin{aligned} ac_n^{(3,2)} &\equiv \frac{\tilde{T}_n}{N_c^2-1} \\ &= \frac{144\binom{3}{2}/4}{(N_c^2-1)3^3}\int_\rho\int d\phi_1 d\phi_2 d\phi_3 e^{in(\phi_1+\phi_2-2\phi_3)}\cos\left(\mathbf{k}_1\cdot\Delta\mathbf{r}_{12}\right)\cos\left(\mathbf{k}_2\cdot\Delta\mathbf{r}_{12}\right)\cos\left(\mathbf{k}_3\cdot\Delta\mathbf{r}_{12}\right) \\ &= \frac{108}{(N_c^2-1)3^3}\int_\rho\int d\phi_1 d\phi_2 d\phi_3 e^{in(\phi_1+\phi_2-2\phi_3)}\cos\left(\mathbf{k}_1\cdot\Delta\mathbf{r}_{12}\right)\cos\left(\mathbf{k}_2\cdot\Delta\mathbf{r}_{12}\right)\cos\left(\mathbf{k}_3\cdot\Delta\mathbf{r}_{12}\right), \end{aligned} \tag{3.12}$$

where $ac^{3,2}$ is the dipole contribution to the cumulant. Below we denote the asymmetric cumulant for a tripole as T_n and the asymmetric cumulant for a three-gluon dipole as $\tilde{T}_n$, while reserving the notation ac_n for total asymmetric three-point cumulant for general N, m. The total value of the three-point cumulant is

$$ac_n = ac_n^{3,2} + ac_n^{3,3}. \tag{3.13}$$

3.3.1 Tripole Momentum Dependence

We start by defining α_{ij} to be the azimuthal phase of $\overrightarrow{r}_{ij} \equiv \overrightarrow{r}_i - \overrightarrow{r}_j$. We can now take the integral over the three azimuthal angles of vectors $\vec{k}_1$, $\vec{k}_2$, $\vec{k}_3$ by using

$$\int_0^{2\pi} d\phi_1 e^{in\phi_1}\cos\left[k_1\Delta r_{12}\cos\left(\phi_1-\alpha_{12}\right)\right] = \pi i^n e^{in\alpha_{12}}\left[1+(-1)^n\right]J_n\left(k_1\Delta r_{12}\right), \tag{3.14}$$

where $J_n(z)$ is the nth Bessel function of the first kind. By using Eq. (3.14), we obtain

$$T_n(k_1,k_2,k_3) = \frac{2^4\pi^3 2\left[1+(-1)^n\right]^2}{3\left(2\pi\right)^3}\int_\rho e^{in(\alpha_{12}+\alpha_{23}-2\alpha_{31})}J_n\left(k_1\left|\mathbf{r}_{12}\right|\right)J_n\left(k_2\left|\mathbf{r}_{23}\right|\right)J_{2n}\left(k_3\left|\mathbf{r}_{31}\right|\right). \tag{3.15}$$

Due to the antisymmetry $\vec{k}\to-\vec{k}$, all correlation functions with odd n vanish.

Consider now the integral over the sources:

$$\left(\begin{array}{ccc}\overrightarrow{r}_1 & \overrightarrow{r}_2 & \overrightarrow{r}_3\end{array}\right) \to \left(\begin{array}{ccc}\overrightarrow{r}_{12} & \overrightarrow{r}_{23} & \overrightarrow{r}_3\end{array}\right) = \left(\begin{array}{ccc}\overrightarrow{r}_1-\overrightarrow{r}_2 & \overrightarrow{r}_2-\overrightarrow{r}_3 & \overrightarrow{r}_3\end{array}\right). \tag{3.16}$$

We can simplify the latter expression since the integral over d^2r_3 is a simple Gaussian integral:

$$\int d^2r_3 \frac{e^{-\frac{r_1^2+r_2^2+r_3^2}{2B}}}{(2\pi B)^3} = \int d^2r_3 \frac{e^{-\frac{\left(\overrightarrow{r}_{12}+\overrightarrow{r}_{23}+\overrightarrow{r}_3\right)^2+\left(\overrightarrow{r}_{23}+\overrightarrow{r}_3\right)^2+r_3^2}{2B}}}{(2\pi B)^3} = \frac{e^{-\frac{r_{12}^2+\overrightarrow{r}_{12}\cdot\overrightarrow{r}_{23}+r_{23}^2}{3B}}}{3\,(2\pi B)^2}. \tag{3.17}$$

By using Eq. (3.17), we obtain the final expression for T_n:

$$\begin{aligned} T_n \;\equiv\; & \frac{2^4}{3^2\,(2\pi B)^2}\int dr_{12}dr_{23}d\alpha_{12}d\alpha_{23}r_{12}r_{23} \\ & \times \exp\left[-\frac{r_{12}^2+r_{12}r_{23}\cos(\alpha_{12}-\alpha_{23})+r_{23}^2}{3B}+in\,(\alpha_{12}+\alpha_{23})\right] \\ & \times \left(\frac{r_{12}\cos(\alpha_{12})+r_{23}\cos(\alpha_{23})-i\,[r_{12}\sin(\alpha_{12})+r_{23}\sin(\alpha_{23})]}{\sqrt{r_{12}^2+2r_{12}r_{23}\cos(\alpha_{12}-\alpha_{23})+r_{23}^2}}\right)^{2n} \\ & \times J_n\,(k_1r_{12})\,J_n\,(k_2r_{23})\,J_{2n}\left(k_3\sqrt{r_{12}^2+2r_{12}r_{23}\cos(\alpha_{12}-\alpha_{23})+r_{23}^2}\right), \end{aligned} \tag{3.18}$$

where we use $e^{in\alpha}=[(x+iy)/|\overrightarrow{r}|]^n$ to find α_{31} in terms of α_{12}, α_{23} [here, $\vec{r}=(x,y)$, so $x+iy=re^{i\alpha}$].

For very small momenta (i.e. all $k_i \ll 1/B^{1/2}$), we obtain

$$T_n \simeq \frac{2^{4-2n}\,[B^2\mathrm{Sym}(k_1k_2k_3^2)]^n}{3\,(n!)^2}, \tag{3.19}$$

where 'Sym' means symmetrization over three gluons (and division by 1/3). The details of calculation are given in Appendix A.

3.3.2 Dependence on Three-Gluon Dipole Momentum

In the same way as we did with T_n, we can get a simplified form of $\tilde{T}_n$. Taking the integral over the phases gives

$$\begin{aligned} \tilde{T}_n(k_1,k_2,k_3) &= \frac{2^2\times\left[1+(-1)^n\right]^2}{(2\pi)^3}\int_\rho e^{in(\alpha_{12}+\alpha_{12}-2\alpha_{12})}J_n\,(k_1r_{12})\,J_n\,(k_2r_{12})\,J_{2n}\,(k_3r_{12}) \\ &= \frac{2^4\times\left[1+(-1)^n\right]^2}{(2\pi)^3}\int_\rho J_n\,(k_1r_{12})\,J_n\,(k_2r_{12})\,J_{2n}\,(k_3r_{12})\,. \end{aligned} \tag{3.20}$$

Again due to the antisymmetry $\vec{k}\to-\vec{k}$, all correlation functions with odd n vanish. The integral over the source positions is now a Gaussian with two vector variables. By using the transformation

$$\left(\begin{array}{cc}\overrightarrow{r}_1 & \overrightarrow{r}_2\end{array}\right) \to \left(\begin{array}{cc}\overrightarrow{r}_{12} & \overrightarrow{r}_2\end{array}\right) = \left(\begin{array}{cc}\overrightarrow{r}_1-\overrightarrow{r}_2 & \overrightarrow{r}_2\end{array}\right), \tag{3.21}$$

we can take the integral over d^2r_2 and over the azimuthal part of $\overrightarrow{r}_{12}$:

$$\int d^2r_2 d\alpha_{12} \frac{e^{-\frac{r_1^2+r_2^2}{2B}}}{(2\pi B)^2} = \int d^2r_2 d\alpha_{12} \frac{e^{-\frac{\left(\overrightarrow{r}_{12}+\overrightarrow{r}_2\right)^2+r_2^2}{2B}}}{(2\pi B)^2} = \frac{e^{-\frac{r_{12}^2}{4B}}}{2B}. \tag{3.22}$$

By using Eq. (3.22), we obtain the final expression for $\tilde{T}_n$:

$$\tilde{T}_n \equiv \frac{2}{B} \int dr_{12} r_{12} e^{-\frac{r_{12}^2}{4B}} J_n\left(k_1 r_{12}\right) J_n\left(k_2 r_{12}\right) J_{2n}\left(k_3 r_{12}\right). \tag{3.23}$$

For very small momenta (i.e. all $k_i \ll 1/B^{1/2}$), we obtain

$$\tilde{T}_n \simeq \frac{2^2 \left[B^2 \mathrm{Sym}\left(k_1 k_2 k_3^2\right)\right]^n}{(n!)^2}. \tag{3.24}$$

The details of calculation are given in Appendix A.

3.3.3 Numerical Results

The value of three-point cumulant is

$$ac_n = T_n/(N_c^2-1)^2 + \tilde{T}_n/(N_c^2-1), \tag{3.25}$$

where n is the harmonic number (we depict the cases $n = 2, 4$). We cannot calculate the integrals T_n and $\tilde{T}_n$ analytically, so we instead depict several types of behaviour of T_2, T_4, $\tilde{T}_2$ and $\tilde{T}_4$ as functions of momentum. Conversely, the correlators have a nontrivial structure as functions of k_1, k_2 and k_3, namely, they depend on the polar coordinates in a nontrivial way:

$$\begin{aligned} k_3 &= k_r \cos(\theta), \\ k_1 &= k_r \sin(\theta)\cos(\phi), \\ k_2 &= k_r \sin(\theta)\sin(\phi), \\ k_r &= \sqrt{k_1^2+k_2^2+k_3^2}. \end{aligned} \tag{3.26}$$

The value of the cumulant depends not only on k_r but also on θ and ϕ. Indeed, already for very small $k_1, k_2, k_3 \to 0$,

$$ac_2^3 \sim k_1^2 k_2^2 k_3^2 (k_1^2+k_2^2+k_3^2) \sim k_r^8 \sin(2\theta)^2 \sin(2\phi)^2 \sin(\theta)^2. \tag{3.27}$$

To better understand the structure of the cumulant we consider three cases:

Case I: All momenta are equal to each other: $k_1 = k_2 = k_3 = k$.

Case II: θ, $\phi = \text{const.}$, and we consider the cumulant and its parts as functions of k_r.

Case III: We consider the cumulant as a function of θ, ϕ for several values of k_r.

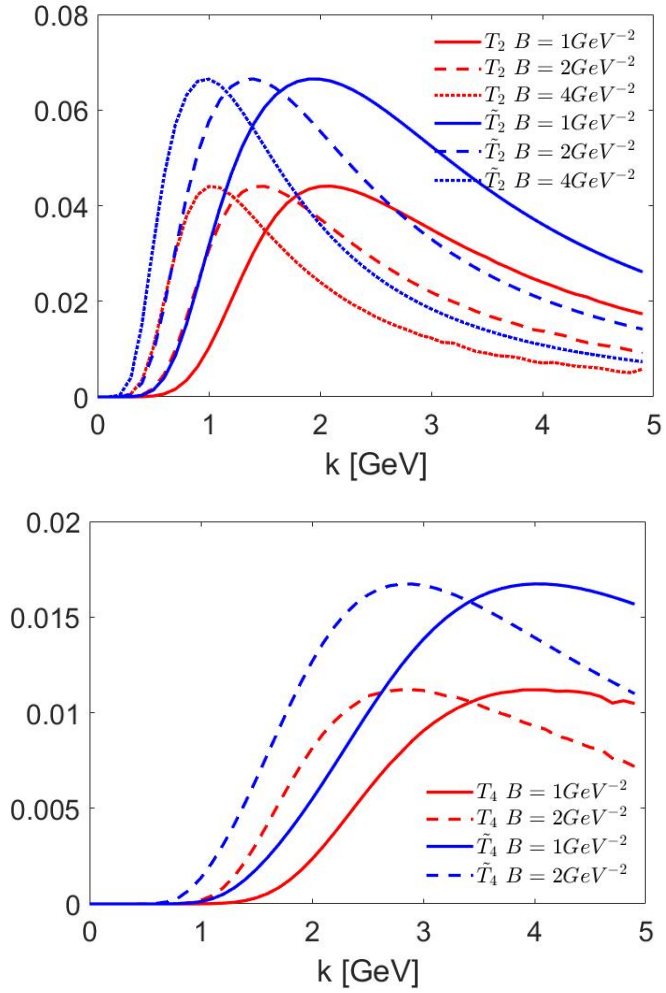

Figure 3.3: (top) Integrals T_2 and $\tilde{T}_2$ when all momenta are equal, $k_1 = k_2 = k_3 = k$ for different values of the parameter $B = 1(2, 4)$ GeV^{-2} in full (dashed, dotted) line. (bottom) Integrals T_4 and $\tilde{T}_4$ when all momenta are equal, $k_1 = k_2 = k_3 = k$ for different values of the parameter $B = 1(2)$ GeV^{-2} in full (dashed) line.

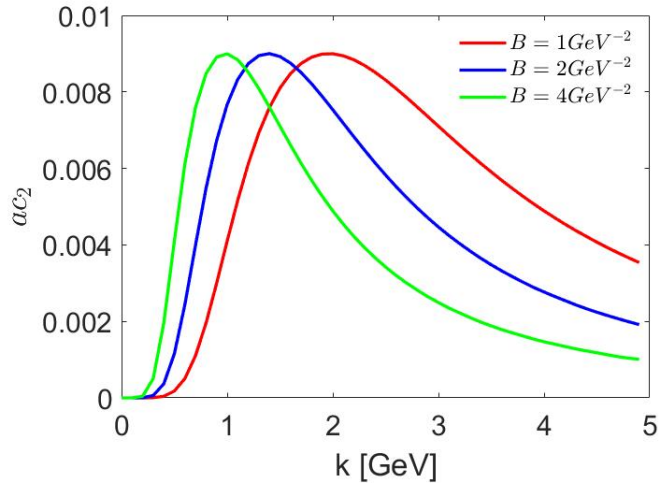

Figure 3.4: Cumulant ac_2 for $N = m = 3$, $N_c = 3$, $k_1 = k_2 = k_3$.

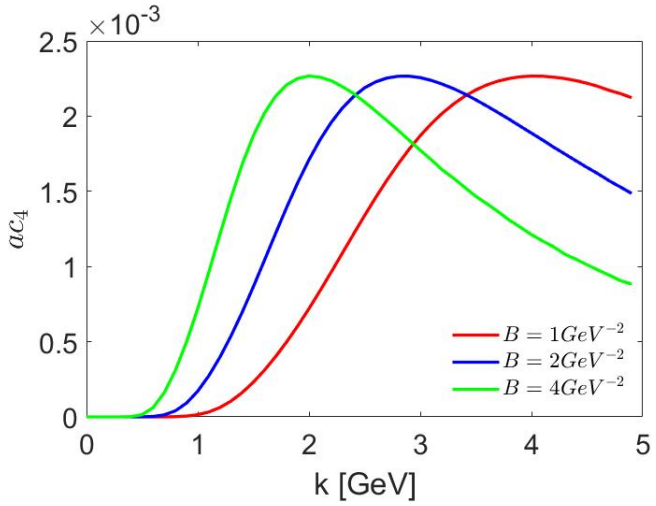

Figure 3.5: Cumulant ac_4 for $N = m = 3$, $N_c = 3$, $k_1 = k_2 = k_3$.

Figure 3.3 shows how T_2 and $\tilde{T}_2$ depend on k. For a given k, the integral increases up to k of order $1/\sqrt{B}$ and then slowly decreases, with maximum values of $T_2 \approx 0.04$ and $\tilde{T}_2 \approx 0.07$ that depend weakly on B. The maximum is located at approximately the same place where the maximum occurs for the similar graph for the symmetric cumulant (second harmonic), and they depend similarly on k.

Both integrals vanish at $k = 0$, and as $k \to \infty$ we get slowly $T_2 \to 0$ and $\tilde{T}_2 \to 0$. Both T_2 and $\tilde{T}_2$ peak at the same point, and they depend similarly on k.

Very similar behaviour occurs as a function of k for T_4 and $\tilde{T}_4$ in Fig. 3.3, except that the fourth harmonic is four to five times smaller and the maximum is shifted to larger k.

Figure 3.4 shows the corresponding full three-point cumulant ac_2 (i.e. the dependence on k of the second harmonic) for the model case $N = m = 3$. In this case, even for $N_c = 3$ the diagram with three gluons in a dipole dominates, accounting for 90% of the cumulant. Similarly, we depict ac_4 in Fig. 3.5.

An interesting feature of the momentum dependence of the cumulant is that the direction in (ϕ, θ) along which the cumulant is maximal is the direction corresponding to $k_1 = k_2 = k_3$. We illustrate this in Figs. 3.6 and 3.7 by considering the dependence of ac_2 and of tripole and dipole diagrams on the direction in k space.

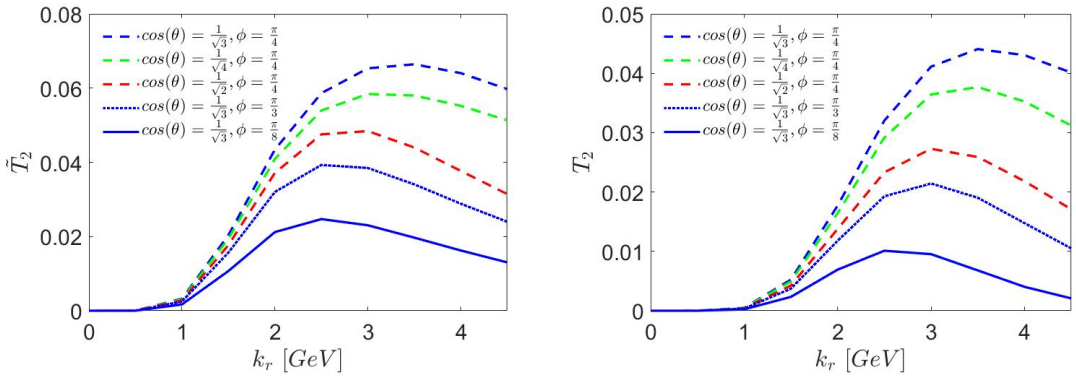

Figure 3.6: Integrals T_2 and $\tilde{T}_2$ for different directions, θ, $\phi = \text{const.}$, k_r varying.

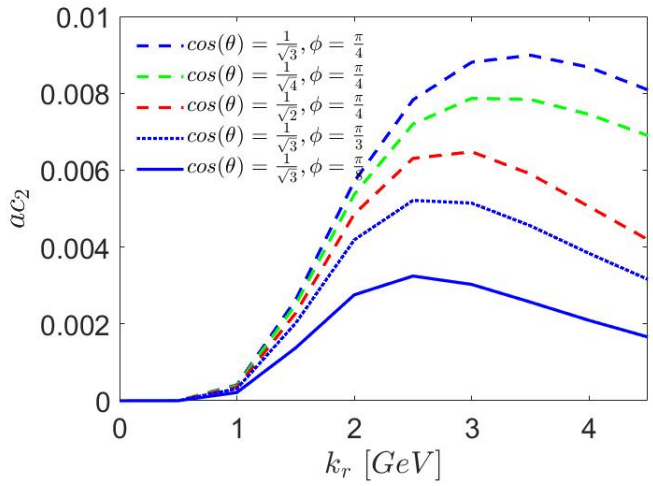

Figure 3.7: The full cumulant ac_2 for different directions, θ, $\phi = \text{const.}$, k_r varying. $B = 1$ GeV^{-2}.

Figures 3.6 and 3.7 show that the direction $k_1 = k_2 = k_3$ [i.e. $\cos(\theta) = 1/\sqrt{3}$, $\phi = \pi/4$] corresponds to an absolute maximum. Conversely, a common structure appears in each direction (i.e. increase up to a maximum value and then a slow decent depending on the direction). Figures 3.6 and 3.7 are for $B = 1$ GeV^{-2}; the behaviour is qualitatively similar for other values of B.

To better understand the two-dimensional structure, we also consider the behaviour of the cumulant as a function of θ, ϕ for $k_r = 2, 4, 6$ GeV. This is depicted in Figs. 3.8 and 3.9.

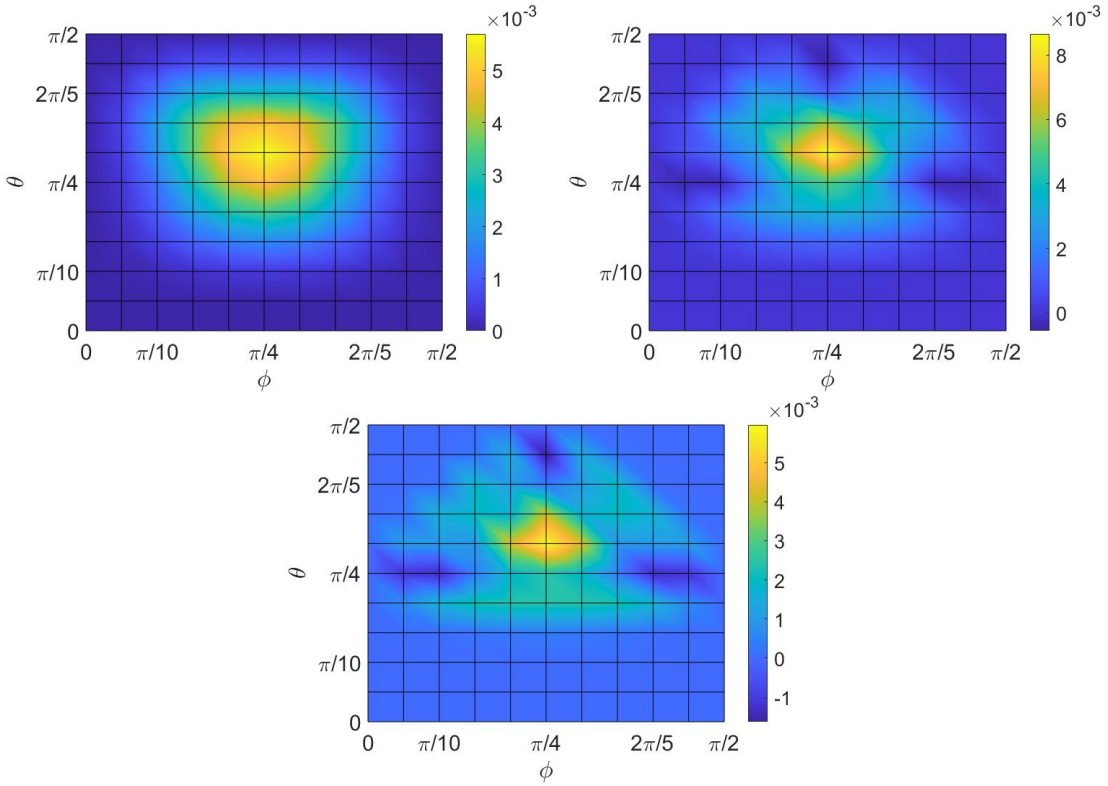

Figure 3.8: Cumulant ac_2 for $N = m = 3$, $N_c = 3$ when $k_r = 2, 4, 6$ GeV (for top left, top right and bottom, respectively) and $B = 1$ GeV^{-2}.

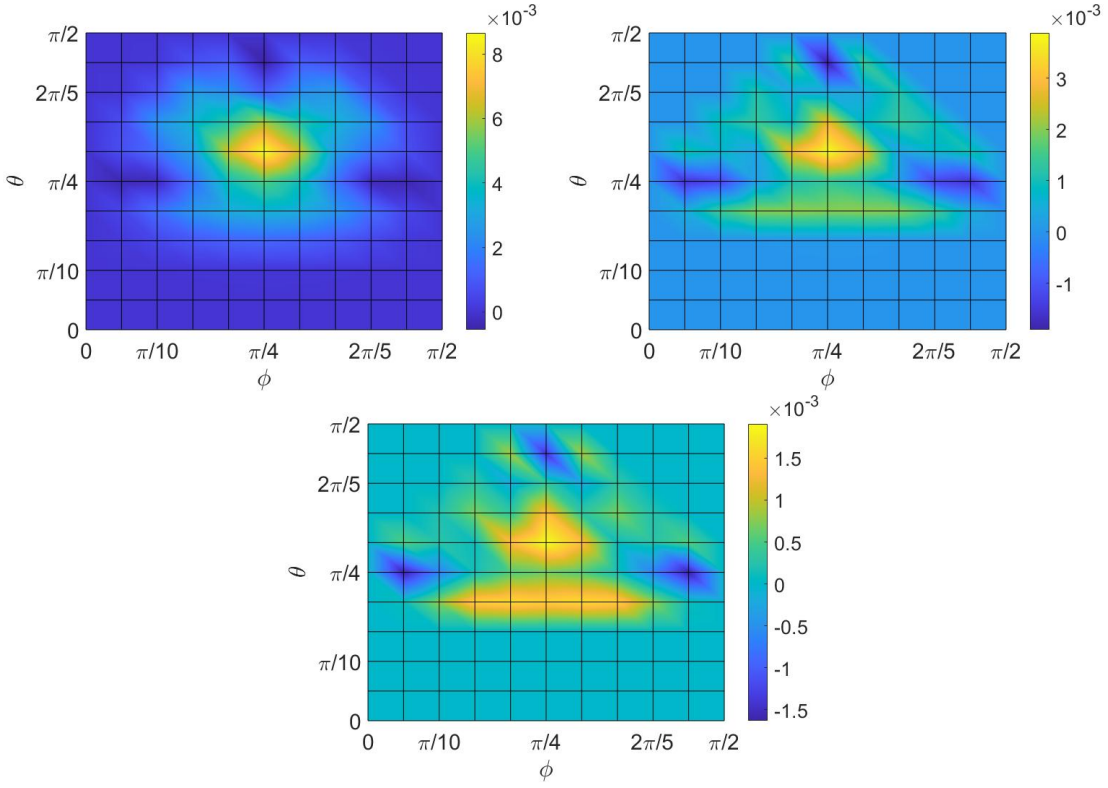

Figure 3.9: Cumulant ac_2 for $N = m = 3$, $N_c = 3$ when $k_r = 2, 4, 6$ GeV (for top left, top right and bottom, respectively) and $B = 4$ GeV^{-2}.

Recall that the case $B = 1$ GeV^{-2} corresponds to the best fit for even symmetric cumulants in Ref. [10], while $B = 4$ GeV^{-2} corresponds to the mean-field approach with the effective cross section for MPIs being twice as big as the experimental cross section. We limit ourselves by depicting the second harmonic. The structure of the cumulant for $B = 2$, 3 GeV^{-2} is very similar to the structure for $B = 1$ GeV^{-2}, so we do not show it here. The structure starts to change only for larger B, which corresponds to the effective DPS cross section being larger than the experimental cross section.

Given the very similar form of the k dependence of T_n and $\tilde{T}_n$ (except for their scale), the similar dependence on k will continue for arbitrary m, N (with different overall coefficients depending on N, m).

We also compare the numerical results for small momentum with the analytic expressions (3.19) and (3.24) and find that they coincide.

3.4 High Multiplicity

3.4.1 Higher-Order Diagrams

We now consider the general case of N, $m > 3$. We noted above that the leading behaviour in powers of $1/(N_c^2 - 1)$ [and a re-summation of the series in terms of $m^2/(N_c^2 - 1)$] corresponds to diagrams with one tripole and an arbitrary number of non-intersecting dipoles. However, in this case, the term contributing to the cumulant is suppressed by $1/N$ but is of first order in $1/(N_c^2-1)$. The corresponding re-summation, which is analogous to the re-summation for a tripole, includes the series corresponding to diagrams with one dipole with three off-diagonal gluons and up to $[N/2-1]$ non-intersecting dipoles, such that each of the sources has only two (or zero) gluons coming out. Numerically for $N_c = 3$ the term with three gluon dipoles is a dominant one up to very large multiplicities of order 100.

Consequently, there are three types of diagrams to consider:

Type (a): Diagrams with arbitrary number (up to $N/2$) of dipoles with two off-diagonal gluons. These diagrams were considered in detail in Ref. [11]. Such diagrams contribute to the total cross section $\hat{\sigma}$.

Type (b): One tripole and $d < N/2$ non-intersecting dipoles with two off-diagonal gluons.

Type (c): One dipole with three off-diagonal gluons and d non-intersecting dipoles with two off-diagonal gluons each.

Recall the calculation of the combinatorial coefficients for Type (a). We first select two gluons and two sources for each two-gluon dipole. From the gluons selected we get a factor of $\binom{1}{2}$:

$$\binom{m}{2}\binom{m-2}{2}\cdots\binom{m-2d+2}{2}\frac{1}{d!}=\frac{(m)!}{2^d d!\,(m-2d)!}. \tag{3.28}$$

The sources give us a similar factor of

$$\binom{N}{2}\binom{N-2}{2}\cdots\binom{N-2d+2}{2}=\frac{(N)!}{2^d\,(N-2d)!}. \tag{3.29}$$

For Type (b) diagrams, an additional multiplier comes from the number of choices of the three-gluon dipole and is given by

$$3\binom{m}{3}3!\binom{N}{2}. \tag{3.30}$$

For Type (c) the number of choices for the tripole produces a factor

$$3\binom{m}{3}3!\binom{N}{3}. \tag{3.31}$$

Only diagrams of Types (b) and (c) contribute to harmonics of $n>0$, so we can write

$$\begin{aligned}\frac{d^3\hat{\sigma}}{\prod_{i=1}^{i=3}d\Gamma_i} \;\propto\; & N_c^m(N_c^2-1)^N N^m\prod_{i=1}^{i=3}\left|\overrightarrow{f}\left(\boldsymbol{k}_i\right)\right|^2 \\ & \times\Bigg\{\sum_{d=0}^{\lfloor(N-2)/2\rfloor}\left(\frac{\hat{D}_0F_{\mathrm{corr}}^{(2)}(N,m)}{N^2(N_c^2-1)}\right)^d\frac{2^3 3!F_{\mathrm{corr}}^{(3)}(N,m)}{N^3 4(N_c^2-1)} \\ & \times\frac{m!N!}{d!3!2!(m-2d-3)!(N-2d-2)!} \\ & \times\int_\rho\cos\left(\mathbf{k}_1\cdot\mathbf{r}_{12}\right)\cos\left(\mathbf{k}_2\cdot\mathbf{r}_{12}\right)\cos\left(\mathbf{k}_3\cdot\mathbf{r}_{12}\right) \\ & +\sum_{d=0}^{\lfloor(N-3)/2\rfloor}\left(\frac{\hat{D}_0F_{\mathrm{corr}}^{(2)}(N,m)}{N^2(N_c^2-1)}\right)^d\frac{2^3 3!F_{\mathrm{corr}}^{(3)}(N,m)}{N^3(N_c^2-1)^2} \\ & \times\frac{m!N!}{d!(3!)^2(m-2d-3)!(N-2d-3)!} \\ & \times\int_\rho\cos\left(\mathbf{k}_1\cdot\mathbf{r}_{12}\right)\cos\left(\mathbf{k}_2\cdot\mathbf{r}_{23}\right)\cos\left(\mathbf{k}_3\cdot\mathbf{r}_{31}\right)\Bigg\}.\end{aligned} \tag{3.32}$$

Here we defined the integral $\hat{D}_0$ corresponding to the off-diagonal dipole component of the wave function of the nucleon fully integrated out (i.e. integrated over both

the source positions and the momenta of the gluons):

$$\hat{D}_0 \equiv \int (r_{12} dr_{12}) \left(\prod_{j=1,2} k_j dk_j \left(\left| \overrightarrow{f}(\mathbf{k}_j) \right| \right)^2 \right) \frac{e^{-\frac{r_{12}^2}{4B}}}{2B} J_0(k_1 r_{12}) J_0(k_2 r_{12}) . \tag{3.33}$$

This integral is determined by a normalised radiation amplitude $\vec{f}$ and, as in Ref. [11], can be considered as a free parameter (coinciding with the free parameter in Ref. [11]). This integral is expected to be between zero and one [11].

As mentioned above, Ref. [10] shows that the diagonal gluons contribute to the interference diagrams by renormalising them [i.e. multiplying by factors $F(m,N)$ that are easily calculated]. For renormalisation factors $F^{(2)}$ and $F^{(3)}$ connected with diagonal gluons for dipole and tripole diagrams relevant to our discussion, we have the explicit expression

$$F^{(3)}(N,m) = \frac{(m-3)!}{m!}[6(m-2N)N^2 + 6(N-1)^{m-1}N^{3-m}(-2+m+2N)]. \tag{3.34}$$

In the limit $N \to \infty$, $m \to \infty$, $m/N = \bar{m} = \text{const.}$, we have

$$F^{(3)}(N,m) \to F^{(3)}(\bar{m}) = 6\frac{e^{-\bar{m}}(2+\bar{m})}{\bar{m}^3} + 6\frac{\bar{m}-2}{\bar{m}^3}. \tag{3.35}$$

In the same way, Ref. [10] obtained

$$F^{(2)}(N,m) = \frac{2N^{1-m}[N(N-1)^m + mN^m - N^{1+m}]}{m(m-1)}, \tag{3.36}$$

and in the limit $N \to \infty$, $m \to \infty$, $m/N = \bar{m} = \text{const.}$, we have

$$F^{(2)}(N,m) \to F^{(2)}(\bar{m}) = \frac{2\bar{m} + 2e^{-\bar{m}} - 2}{\bar{m}^2}. \tag{3.37}$$

For the three-gluon dipole we get a correction factor that is the same as $F^{(3)}(N,m)$, as calculated in Appendix B. For non-intersecting dipoles and tripoles, we can prove that the corresponding renormalisation factors factorize.

To find the differential multiplicity, we must find the total cross section $\hat{\sigma}$ to the same approximation. This cross section is

$$\begin{aligned}
\hat{\sigma} \quad \propto \quad & N_c^m (N_c^2-1)^N N^m \\
& \times \left\{ \sum_{d=0}^{\lfloor N/2 \rfloor} \left(\frac{\hat{D}_0 F^{(2)}_{\text{corr}}(N,m)}{N^2(N_c^2-1)} \right)^d \frac{m!N!}{d!\,(m-2d)!\,(N-2d)!} \right. \\
& + \frac{3^3 F^{(3)}_{\text{corr}}(N,m)\,\hat{\tilde{T}}_0}{N^3(N_c^2-1)} \sum_{d=0}^{\lfloor (N-2)/2 \rfloor} \left(\frac{\hat{D}_0 F^{(2)}_{\text{corr}}(N,m)}{N^2(N_c^2-1)} \right)^d \frac{m!N!}{d!2!3!\,(m-2d-3)!\,(N-2d-2)!} \\
& \left. + \frac{3^3 F^{(3)}_{\text{corr}}(N,m)\,\hat{T}_0}{N^3(N_c^2-1)^2} \sum_{d=0}^{\lfloor (N-3)/2 \rfloor} \left(\frac{\hat{D}_0 F^{(2)}_{\text{corr}}(N,m)}{N^2(N_c^2-1)} \right)^d \frac{m!N!}{d!(3!)^2\,(m-2d-3)!\,(N-2d-3)!} \right\},
\end{aligned} \tag{3.38}$$

where we define the integrals

$$\hat{\tilde{T}}_0 \equiv \frac{2}{3^3}\int (r_{12}dr_{12})\prod_{j=1}^{3} k_j dk_j \left|\overrightarrow{f}\,(\mathbf{k}_j)\right|^2 \frac{e^{-\frac{r_{12}^2}{4B}}}{B} J_0\left(k_1 r_{12}\right) J_0\left(k_2 r_{12}\right) J_0\left(k_3 r_{12}\right), \tag{3.39}$$

$$\hat{T}_0 \equiv \frac{2^2}{3^5}\int \left(d^2 r_{12} d^2 r_{23}\right)\prod_{j=1}^{j=3} k_j dk_j \left|\overrightarrow{f}\,(\mathbf{k}_j)\right|^2 \frac{e^{-\frac{r_{12}^2+\overrightarrow{r}_{12}\cdot\overrightarrow{r}_{23}+r_{23}^2}{3B}}}{(2\pi B)^2}$$

$$\times J_0\left(k_1 r_{12}\right) J_0\left(k_2 r_{23}\right) J_0\left(k_3\left|\overrightarrow{r}_{12}+\overrightarrow{r}_{23}\right|\right), \tag{3.40}$$

corresponding to the integrated-out tripole and dipole with three off-diagonal gluons. The radiation amplitude $\vec{f}$ determines the values of $\hat{T}_0$ and $\hat{\tilde{T}}_0$ (i.e. they are no longer free parameters of the model). The values of $\hat{T}_0$ and $\hat{\tilde{T}}_0$ are correlated with the value of $\hat{D}_0$.

For the differential multiplicity, we obtain

$$\begin{aligned}
\frac{d^3N}{d\Gamma_1 d\Gamma_2 d\Gamma_3} &= \frac{d^3\sigma}{\sigma d\Gamma_1 d\Gamma_2 d\Gamma_3} \\
&\approx \left(\prod_{i=1}^{i=3}\left|\overrightarrow{f}\,(\boldsymbol{k}_i)\right|^2\right)\hat{\sigma}^{-1} \\
&\quad\times\left[\frac{2F_{\mathrm{corr}}^{(3)}(N,m)}{N^3\left(N_c^2-1\right)}\sum_{d=0}^{\lfloor (N-2)/2\rfloor}\left(\frac{\hat{D}_0 F_{\mathrm{corr}}^{(2)}(N,m)}{N^2\left(N_c^2-1\right)}\right)^d \frac{m!N!}{d!2!3!\,(m-2d-3)!\,(N-2d-2)!}\right. \\
&\quad\times\int_\rho \cos\left(\mathbf{k}_1\cdot\mathbf{r}_{12}\right)\cos\left(\mathbf{k}_2\cdot\mathbf{r}_{12}\right)\cos\left(\mathbf{k}_3\cdot\mathbf{r}_{12}\right) \\
&\quad+\frac{2^3 F_{\mathrm{corr}}^{(3)}(N,m)}{N^3\left(N_c^2-1\right)^2}\sum_{d=0}^{\lfloor (N-3)/2\rfloor}\left(\frac{\hat{D}_0 F_{\mathrm{corr}}^{(2)}(N,m)}{N^2\left(N_c^2-1\right)}\right)^d \frac{m!N!}{d!(3!)^2\,(m-2d-3)!\,(N-2d-3)!} \\
&\quad\left.\times\int_\rho \cos\left(\mathbf{k}_1\cdot\mathbf{r}_{12}\right)\cos\left(\mathbf{k}_2\cdot\mathbf{r}_{23}\right)\cos\left(\mathbf{k}_3\cdot\mathbf{r}_{31}\right)\right],
\end{aligned} \tag{3.41}$$

where

$$\hat{\sigma}\equiv\sum_{d=0}^{\lfloor N/2\rfloor}\left(\frac{\hat{D}_0 F_{\mathrm{corr}}^{(2)}(N,m)}{N^2\left(N_c^2-1\right)}\right)^d \frac{m!N!}{d!\,(m-2d)!\,(N-2d)!} \tag{3.42}$$

is the total cross section. We have shown by direct numerical calculation that the contribution to the total cross section of the integrated-out three-gluon dipole and of the integrated-out tripole are negligible compered with the two-gluon dipole terms, so we can ignore the dependence on $\hat{T}_0$ and $\hat{\tilde{T}}_0$.

For the differential one-gluon distribution, we have, in this approximation,

$$\frac{dN}{d\Gamma} = m\left|\overrightarrow{f}\,(\boldsymbol{k})\right|^2. \tag{3.43}$$

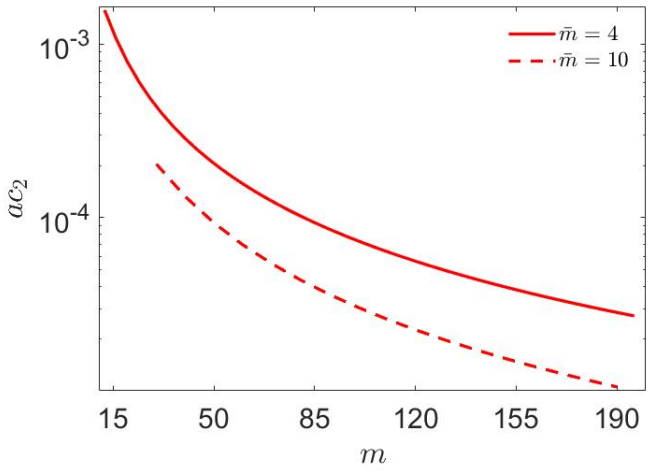

Figure 3.10: The maximum value of ac_2 (as a function of momentum) as a function of multiplicity m for different values of $\bar{m}$, where $\hat{D}_0 = 0.1$ and $N_c = 3$.

We can now write the parts corresponding to the three-gluon dipole and the tripole contribution:

$$
\begin{aligned}
ac_n^{3,2}\{3\} &= \frac{3^3 F^{(3)}_{\rm corr}(N,m)}{\binom{m}{3}\hat{\sigma}N^3(N_c^2-1)}\tilde{T}_n/3 \\
&\quad \times \sum_{d=0}^{\lfloor (N-2)/2 \rfloor} \left(\frac{\hat{D}_0 F^{(2)}_{\rm corr}(N,m)}{N^2\left(N_c^2-1\right)}\right)^d \frac{m!N!}{d!2!3!(m-2d-3)!(N-2d-2)!}, \\
ac_n^{3,3}\{3\} &= \frac{3^3 F^{(3)}_{\rm corr}(N,m)}{\binom{m}{3}\hat{\sigma}N^3(N_c^2-1)^2}T_n \\
&\quad \times \sum_{d=0}^{\lfloor (N-3)/2 \rfloor} \left(\frac{\hat{D}_0 F^{(2)}_{\rm corr}(N,m)}{N^2\left(N_c^2-1\right)}\right)^d \frac{m!N!}{d!(3!)^2(m-2d-3)!(N-2d-3)!}, \\
ac_n &= ac_n^{3,2}\{3\} + ac_n^{3,3}\{3\}\,. \qquad (3.44)
\end{aligned}
$$

Note that by taking $\hat{D}_0 = 0$, or equivalently, only the $d = 0$ term in the expansion for $\hat{\Sigma}$ is return to the result [Eq. (3.11)] for $N = m = 3$ of the previous section.

3.4.2 Numerical Results

We now look at ac as a function of the multiplicity for different values of $\bar{m} \equiv m/N$. We first look at ac_2 as a function of m for fixed values of $\bar{m} = 4, 10$. Figure 3.10 shows, as a function of m, the maximum value of ac_2 as function of transverse momentum. The value of ac_2 decreases slowly with multiplicity, and the characteristic scale of ac_2 for moderate $m \approx 50$ is of the order 2×10^{-4}.

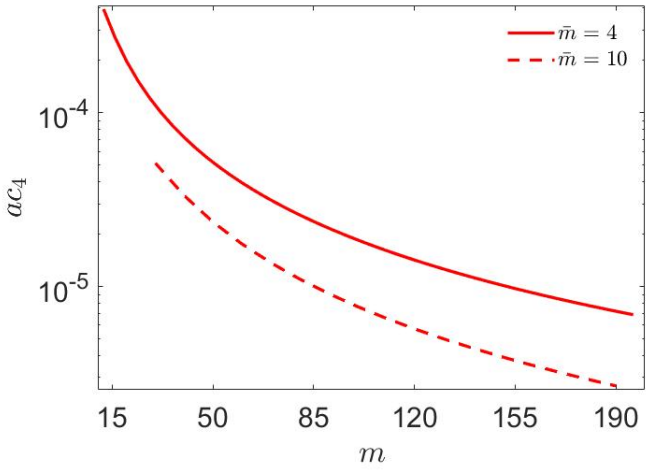

Figure 3.11: The maximum value of ac_4 (as a function of momentum) as a function of multiplicity m for different values of $\bar{m}$, where $\hat{D}_0 = 0.1$ and $N_c = 3$.

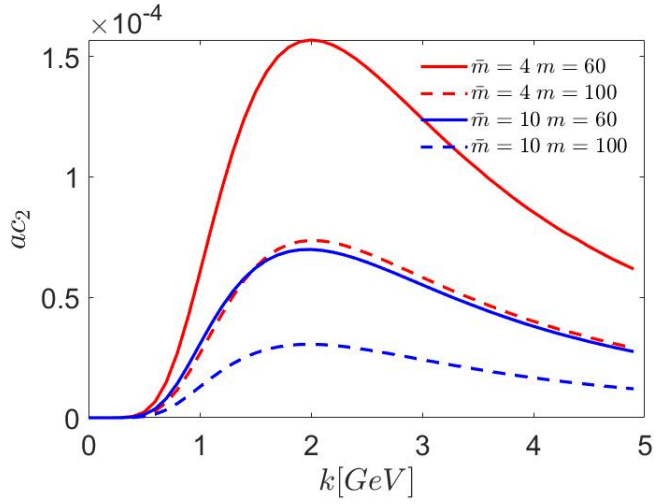

Figure 3.12: Form of ac_2 for $k_1 = k_2 = k_3$ and for different values of multiplicity m, with $\hat{D}_0 = 0.1$, $B = 1$ GeV^{-2}, $N_c = 3$.

The scale of two-point correlator $v_2^2 \equiv sc_2\{2\}$, calculated in Ref. [11], was ≈4–5×10^{-3} [i.e. a decrease of order $2(N_c^2 - 1)$ occurs upon going from v_2^2 to ac_2], and the ratio between the two depends weakly on multiplicity.

Figure 3.11 shows the analogous dependence of ac_4, and Fig. 3.12 shows how ac_2 depends on k for various multiplicities m. The k dependence is practically independent of multiplicity (up to an overall scaling factor) and is the same as for the case $N = m = 3$.

3.4.3 Comparison with Experimental Results

Here we compare our results with recent experimental data [12]. In Ref. [12], the second harmonic was averaged over the experimental data with momentum varying in two different kinematic regions: $k \in [0.3, 3]$ GeV and $k \in [0.5, 5]$ GeV.

Recall that, in the form of $\tilde{T}_n$ and T_n, we can completely separate the dependence of the momentum and n and the dependence on all other parameters such as multiplicity, number of sources, N_c and the model constant $\hat{D}_0$. It is convenient to define

$$\begin{aligned} R^{3,2}\left(N, m, N_c, \hat{D}_0\right) &\equiv \frac{ac_n^{3,2}\{3\}}{\tilde{T}_n}, \\ R^{3,3}\left(N, m, N_c, \hat{D}_0\right) &\equiv \frac{ac_n^{3,3}\{3\}}{T_n}. \end{aligned} \tag{3.45}$$

Since all of the dependence on the momentum in our model is contained in the k-dependent functions $T_n(k_1, k_2, k_3)$ and $\tilde{T}_n(k_1, k_2, k_3)$, we can calculate the averages:

	$B = 1$ GeV^{-2}	$B = 2$ GeV^{-2}	$B = 4$ GeV^{-2}
$\langle T_2\rangle_{0.3-3GeV} = \frac{\int_{0.3}^{3} dk_1 dk_2 dk_3 T_2}{(3-0.3)^3}$	9.4×10^{-3}	6.5×10^{-3}	2.7×10^{-3}
$\left\langle \tilde{T}_2\right\rangle_{0.3-3GeV} = \frac{\int_{0.3}^{3} dk_1 dk_2 dk_3 T_2}{(3-0.3)^3}$	2.1×10^{-2}	1.6×10^{-2}	1.1×10^{-2}
$\langle T_2\rangle_{0.5-5GeV} = \frac{\int_{0.5}^{5} dk_1 dk_2 dk_3 T_2}{(5-0.5)^3}$	4.1×10^{-3}	1.4×10^{-3}	1.5×10^{-3}
$\left\langle \tilde{T}_2\right\rangle_{0.5-5GeV} = \frac{\int_{0.5}^{5} dk_1 dk_2 dk_3 T_2}{(5-0.5)^3}$	1.4×10^{-2}	8.7×10^{-3}	5.0×10^{-3}

Table 3.1: Averages of the integrals for different ranges of k_1, k_2, k_3 and values of B.

The value of the cumulant is obtained by calculating

$$\langle ac_2\{3\}\rangle = R^{3,2}\left\langle \tilde{T}_2\right\rangle + R^{3,3}\langle T_2\rangle, \tag{3.46}$$

and the results are shown in Fig. 3.13.

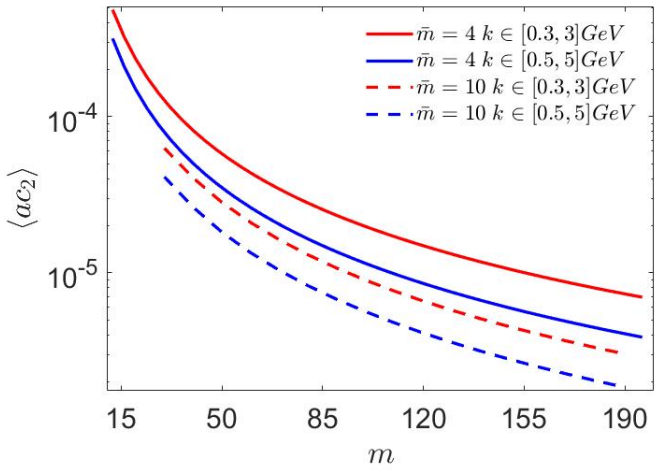

Figure 3.13: Three-point cumulant ac^3 averaged over $0.5 < k_i < 3$ and $0.5 < k_i < 5$ $(i = 1, 2, 3)$.

Figure 3.14 shows the theoretical value of the second harmonic (integrated over the region $0.5 \leq k \leq 3$ together with experimental data, namely, the ATLAS result after additional analysis to eliminate non-flow effects; see Ref. [56]). Note that the values of m that are obtained here by using the LPHD concept correspond to a total number of soft hadrons of $m \approx 1.5 N_{\text{charged}}$, where N_{charged} is a number of charged particles measured in the ATLAS experiment. The high-multiplicity sample used by ATLAS is dominated by π mesons [57], the factor $\frac{3}{2}$ then comes from isotopic invariance since π mesons form a triplet in the isotopic space. The two different types of data are depicted, with or without gap, which means that the gap of 0.5 units between subevents to limit non-flow is taken or not are depicted. Please refer to Ref. [12, 56] for the details of the experimental analysis.

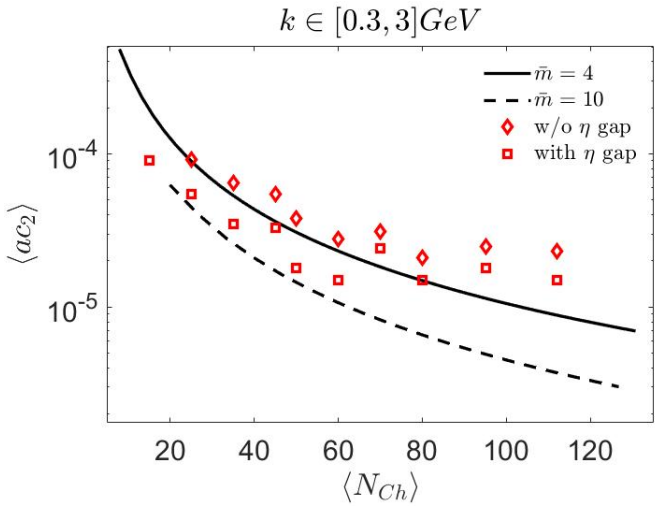

Figure 3.14: Three-point cumulant ac_2 averaged over $0.5 < k_i < 3$ and $0.5 < k_i < 3$ $(i = 1, 2, 3)$ and compared with experimental data. The experimental data have

been additionally analysed [56] by the ATLAS Collaboration to minimize non-flow effects, where the two types of experimental points correspond to analysis with and without the 0.5-unit gap between subevents.

The results for $m \leq 120 (N_{\text{charged}} \leq 80)$ are consistent with the experimental data if we average over region $0.5 \leq k \leq 3$ GeV. However, for higher multiplicities, the theoretical result decreases with total multiplicity m rather rapidly, contrary to the experimental data, for which ac is independent of multiplicity for large m. In addition, the ATLAS data for average ac_2 over the region $0.5 \leq k \leq 5$ GeV tend to increase relative to the average over $0.5 \leq k \leq 3$ GeV, whereas Fig. 3.13 shows the opposite trend. However, these averages are very sensitive to explicit k dependence, so even a small inaccuracy in the k dependence leads to a rather large inaccuracy in the average. Moreover, our results may be less accurate for large transverse momentum, where the soft-gluon approximation is less accurate.

Chapter 4

Conclusions

We have studied how colour interference and colour flow affect the three-point asymmetric cumulants by using the model of Refs. [10, 11].

The results for our asymmetric correlator are qualitatively consistent with the scale of available experimental data [12], at least for moderate multiplicities $m \approx 100$. Note that only integrated experimental data are available, which hinders a detailed comparison with the experimental results. These data seem to be very sensitive to precise transverse momentum dependence, so a detailed comparison between theoretical and experimental results must await further measurements, in particular a detailed study of transverse momentum dependence, as done already for symmetric correlators.

We provide herein a detailed study of the transverse momentum dependence and characteristic scale of the correlator.

A discrepancy with the experimental data takes the form of a decrease of the ac cumulant with multiplicity m at high multiplicities, and analogous behaviour also occurs for symmetric cumulants [11]. The experimental data indicate that cumulants are virtually independent of multiplicity. Conversely, significant uncertainties related to the separation of the flow and non-flow effects may exist in the experimental data [56]. We expect that further study of the model, in particular inclusion of higher suppressed diagrams (such as quadrupole-like diagrams), will improve the dependence on multiplicity both for symmetric and asymmetric correlators [58].

Appendix A

Small-Momentum Limit

Consider the case of very small transverse momentum for a tripole. Looking at very small momentum, $k_j \ll B^{-1/2}$ for all three momenta, we Taylor expand the Bessel functions

$$J_n(z) \simeq \frac{z^n}{n!2^n} \tag{A.1}$$

to find

$$\begin{aligned} T_n \simeq & \frac{2^{4(1-n)}\left(k_1k_2k_3^2\right)^n}{3^2\left(n!\right)^2(2n)!\left(2\pi B\right)^2}\int dr_{12}dr_{23}d\alpha_{12}d\alpha_{23}r_{12}^{1+n}r_{23}^{1+n}\exp\left(-\frac{r_{12}^2+\overrightarrow{r}_{12}\cdot\overrightarrow{r}_{23}+r_{23}^2}{3B}\right) \\ & \times\left[\cos\left(\alpha_{12}\right)+\sin\left(\alpha_{12}\right)\right]^n\left[\cos\left(\alpha_{23}\right)+\sin\left(\alpha_{23}\right)\right]^n \\ & \times\left\{r_{12}\cos\left(\alpha_{12}\right)+r_{23}\cos\left(\alpha_{23}\right)-i\left[r_{12}\sin\left(\alpha_{12}\right)+r_{23}\sin\left(\alpha_{23}\right)\right]\right\}^{2n}. \end{aligned} \tag{A.2}$$

From dimensional analysis for small momentum,

$$ac_n \propto \left(B^2k_1k_2k_3^2\right)^n. \tag{A.3}$$

Simplifying the integral [Eq. (A.2)] we obtain in the limit of small k_i:

$$\begin{aligned} T_n \simeq & \frac{(3B)^2\,2^{4(1-n)}\left(3^2B^2k_1k_2k_3^2\right)^n}{3^2\left(n!\right)^2(2n)!\left(2\pi B\right)^2}\int_{R^4}dx_1dx_2dy_1dy_2 \\ & \times\frac{\partial^n}{\partial\alpha^n}\frac{\partial^n}{\partial\beta^n}\frac{\partial^{2n}}{\partial\gamma^{2n}}e^{-\left(x_1^2+x_1x_2+x_2^2+y_1^2+y_1y_2+y_2^2\right)+\alpha(x_1+iy_1)+\beta(x_2+iy_2)+\gamma[x_1+x_2-i(y_1+y_2)]}\Big|_{\alpha=\beta=\gamma=0} \\ = & \frac{2^{4(1-n)}\left(3^2B^2k_1k_2k_3^2\right)^n}{\left(n!\right)^2(2n)!\left(2\pi\right)^2}\,\frac{\partial^n}{\partial\alpha^n}\frac{\partial^n}{\partial\beta^n}\frac{\partial^{2n}}{\partial\gamma^{2n}}\frac{4\pi^2}{3}e^{\frac{2}{3}\gamma(\alpha+\beta)}\Big|_{\alpha=\beta=\gamma=0} \\ = & \frac{2^{4(1-n)}\left(3^2B^2k_1k_2k_3^2\right)^n}{3\left(n!\right)^2(2n)!}(2n)!\left(\frac{2}{3}\right)^{2n}=\frac{2^{4+2n}\left(B^2k_1k_2k_3^2\right)^n}{3\left(n!\right)^2}. \end{aligned} \tag{A.4}$$

All expressions above are understood to be symmetrized over gluons 1, 2, 3 (i.e. equal to $\frac{1}{3}\sum_{1,2,3}$).

We can also use the same approximation to obtain

$$\tilde{T}_n \simeq \frac{2^{1-4n}\left[\mathrm{Sym}\left(k_1 k_2 k_3^2\right)\right]^n}{B\left(n!\right)^2(2n)!}\int dr_{12} r_{12}^{1+4n} e^{-\frac{r_{12}^2}{4B}}. \tag{A.5}$$

This leaves us with an integral that may be solved by using $u = \frac{r_{12}^2}{4B}$, which gives

$$\tilde{T}_n \simeq \frac{2^2\left(B^2 k_1 k_2 k_3^2\right)^n}{\left(n!\right)^2}. \tag{A.6}$$

Appendix B

Three-Gluon Dipole Correction

We obtain the correction factor for the three-gluon dipole in the same way as was done in Ref. [10]. To make an ordered list of emitted gluons with only three off-diagonal gluons to make a three-gluon dipole, we can divide the diagonal gluons into four types. If the off-diagonal gluons are 1, 2, 3, then the diagonal gluons can be before 1, between 1 and 2, between 2 and 3 and after 3. The ones between 1 and 2 and between 2 and 3 will produce a factor of $\frac{1}{2}$ if they are from the same sources as the off-diagonal gluons; otherwise they produce a factor of one. We first need the number of incoherent diagrams, which is

$$\begin{aligned} N_{\text{incoh}} &= \sum_{j_{12}=0}^{m-3} \sum_{j_{23}=0}^{m-3-j_{12}} N^{m-3-j_{12}-j_{23}}(m-2-j_{12}-j_{23}) \\ &\quad \times \sum_{l_{12}=0}^{j_{12}} \left(\begin{array}{c} j_{12} \\ l_{12} \end{array} \right) 2^{l_{12}} (N-2)^{j_{12}-l_{12}} \\ &\quad \times \sum_{l_{23}=0}^{j_{23}} \left(\begin{array}{c} j_{23} \\ l_{23} \end{array} \right) 2^{l_{23}} (N-2)^{j_{23}-l_{23}} \\ &= \frac{m!}{3!(m-3)!} N^{m-3}, \end{aligned} \tag{B.1}$$

where j_{ab} counts the number of diagonal gluons between a and b and l_{ab} counts how many of them are on the same gluons as the three-gluon dipole.

The correction coefficient is then calculated by taking into account the factor of $(\frac{1}{2})^l$ that comes from the identity $T^a T^b T^a = T^b/2$:

$$\begin{aligned} F^{(3,2)}(N,m) &= \frac{1}{N_{\text{incoh}}} \sum_{j_{12}=0}^{m-3} \sum_{j_{23}=0}^{m-3-j_{12}} N^{m-3-j_{12}-j_{23}}(m-2-j_{12}-j_{23}) \\ &\quad \times \sum_{l_{12}=0}^{j_{12}} \left(\begin{array}{c} j_{12} \\ l_{12} \end{array} \right) 2^{l_{12}} (N-2)^{j_{12}-l_{12}} 2^{-l_{12}} \end{aligned}$$

$$\times \sum_{l_{23}=0}^{j_{23}} \left(\begin{array}{c} j_{23} \\ l_{23} \end{array} \right) 2^{l_{23}} (N-2)^{j_{23}-l_{23}} 2^{-l_{23}}$$

$$= \frac{(m-3)!}{m!}[6(m-2N)N^2 + 6(N-1)^{m-1}N^{3-m}(-2+m+2N)]. \tag{B.2}$$

This is exactly $F^{(3)}(N,m)$, as we can see from Ref. [10].

Bibliography

[1] V. Khachatryan *et al.* [CMS Collaboration] JHEP **1009** (2010) 091 doi:10.1007/JHEP09(2010)091 [arXiv:1009.4122 [hep-ex]].

[2] V. Khachatryan *et al.* [CMS Collaboration], Phys. Lett. B **765** (2017) 193 doi:10.1016/j.physletb.2016.12.009 [arXiv:1606.06198 [nucl-ex]].

[3] M. Aaboud *et al.* [ATLAS Collaboration] JHEP **03** (2017) 157 doi:10.1007/JHEP03(2017)157

[4] J. Kim *et al.* [ALICE Collaboration], PoS EPS-HEP2019 (2020) 293 doi:10.22323/1.364.0293

[5] M.Aaboudetal *et al.*. [ATLAS Collaboration], Eur. Phys. J. **C77** (2017) no.6,428 [arXiv:1705.04176[hep-ex]].

[6] M. Aaboud *et al.* [ATLAS Collaboration] Eur. Phys. J. C **78** (2018) 997 [arXiv:1808.03951 [nucl-ex]].

[7] G. Aad *et al.* [ATLAS Collaboration] Phys. Rev. C **101** (2020) 024906 [arXiv:1911.04812v2 [nucl-ex]].

[8] K.Aamodtetal *et al.*, [ALICE Collaboration], Phys. Rev. Lett. **107** (2011) 032301 [arXiv:1105.3865[nucl-ex]].

[9] B.B.Abelevetal *et al.*, [ALICE Collaboration], Phys. Rev. **C90** (2014) no.5,054901 [arXiv:1406.2474[nucl-ex]].

[10] B. Blok, C. D. Jakel, M. Strikman, U. A. Wiedemann, J. High Energy Phys. **1712** (2017) 074 [arXiv:1708.08241 [hep-ph]].

[11] B. Blok, U. A. Wiedemann, Phys. Lett. B **795** (2019) 259-265 [arXiv:1812.04113[hep-ph]].

[12] M. Aaboud *et al.* [ATLAS Collaboration], Phys. Lett. B **789** (2019) 444-471 [arXiv:1807.02012v2 [nucl-ex]].

[13] U. Heinz, M. Jacob [arXiv:0002042 [nucl-th]].

[14] A. Bilandzic, R. Snellings, S. Voloshin, Phys. Rev. C **83** (2011) 044913 doi:10.1103/PhysRevC.83.044913 [arXiv:1010.0233 [nucl-ex]].

[15] S. S. Padula PoS ICHEP2016 **358** (2016) doi:10.22323/1.282.0358

[16] S. Acharya *et al.* [ALICE Collaboration], JHEP **09** (2018) 006 [arXiv:1805.04390 [nucl-ex]].

[17] N. Borghini, P. M. Dinh and J. Y. Ollitrault, Phys.Rev. C **63** (2001) 054906 [arXiv:nucl-th/0007063].

[18] N. Borghini, P. M. Dinh and J. Y. Ollitrault, Phys. Rev. C **64** (2001) 054901 doi:10.1103/PhysRevC.64.054901 [nucl-th/0105040].

[19] C. Zhang, J. Jia, J. Xu, Phys. Lett. B **792**, 138–141 (2019). [arXiv:1812.03536v3 [nucl-th]].

[20] S. Alekhin, J. Blümlein, S. Moch, R. Placakyte Phys. Rev. D **96**, 014011 (2017) doi:10.1103/PhysRevD.96.014011 [arXiv:1701.05838 [hep-ph]]

[21] B. Blok, M. Strikman, Adv. Ser. Direct. High Energy Phys. **29** (2019) 63–99, [arXiv:1709.00334 [hep-ph]].

[22] L. Frankfurt, M. Strikman, C. Weiss Ann.Rev.Nucl.Part.Sci. **55**:403-465 (2005) [arXiv:hep-ph/0507286]

[23] L. Frankfurt, C. E. Hyde, M. Strikman and C. Weiss, Phys. Rev. D 75 (2007) 054009 doi:10.1103/PhysRevD.75.054009 [hep-ph/0608271].

[24] J. Kuechler [ALICE and ATLAS and CMS Collaborations], PoS LHCP **2016** (2016) 133.

[25] M. Aaboud *et al.* [ATLAS Collaboration], JHEP **1611** (2016) 110 doi:10.1007/JHEP11(2016)110 [arXiv:1608.01857 [hep-ex]].

[26] P. Gunnellini [CMS Collaboration], "Study of high pT particle production from double parton scatterings at the CMS experiment," 23-27 Nov 2015, Trieste, Italy. (http://indico.ictp.it/event/a14280/)

[27] M. Y. Azarkin, I. M. Dremin and M. Strikman, Phys. Lett. B **735** (2014) 244 doi:10.1016/j.physletb.2014.06.040 [arXiv:1401.1973 [hep-ph]].

[28] V.Khachatryan *et al.*, [CMS Collaboration], Phys. Rev. Lett. **115** (2015) no.1,012301 [arXiv:1502.05382[nucl-ex]].

[29] A.Adareetal *et al.* [PHENIX Collaboration], Phys. Rev. Lett. **114** (2015) no.19,192301 [arXiv:1404.7461[nucl-ex]].

[30] L.Adamczyketal *et al.*. [STAR Collaboration], Phys. Lett. **B747** (2015) 265 [arXiv:1502.07652[nucl-ex]].

[31] P. Romatschke and U. Romatschke, doi:10.1017/9781108651998 [arXiv:1712.05815 [nucl-th]].

[32] N. Borghini and C. Gombeaud, Eur. Phys. J. C **71** (2011), 1612 doi:10.1140/epjc/s10052-011-1612-7 [arXiv:1012.0899 [nucl-th]].

[33] J. Xu and C. M. Ko, Phys. Rev. C **83** (2011), 034904 doi:10.1103/PhysRevC.83.034904 [arXiv:1101.2231 [nucl-th]].

[34] J. Uphoff, F. Senzel, O. Fochler, C. Wesp, Z. Xu and C. Greiner, Phys. Rev. Lett. **114** (2015) no.11, 112301 doi:10.1103/PhysRevLett.114.112301 [arXiv:1401.1364 [hep-ph]].

[35] A. Kurkela, U. A. Wiedemann and B. Wu, Eur. Phys. J. C **79** (2019) no.9, 759 doi:10.1140/epjc/s10052-019-7262-x [arXiv:1805.04081 [hep-ph]].

[36] A. Kurkela, A. Mazeliauskas and R. Törnkvist, [arXiv:2104.08179 [hep-ph]].

[37] A. Buckley, J. Butterworth, S. Gieseke, D. Grellscheid, S. Hoche, H. Hoeth, F. Krauss, L. Lonnblad, E. Nurse and P. Richardson, *et al.* Phys. Rept. **504** (2011), 145-233 [arXiv:1101.2599 [hep-ph]].

[38] N. Fischer and T. Sjöstrand, JHEP **01** (2017), 140 doi:10.1007/JHEP01(2017)140 [arXiv:1610.09818 [hep-ph]].

[39] C. Bierlich, G. Gustafson and L. Lönnblad, Phys. Lett. B **779** (2018), 58-63 doi:10.1016/j.physletb.2018.01.069 [arXiv:1710.09725 [hep-ph]].

[40] M. Mace, V. V. Skokov, P. Tribedy and R. Venugopalan, Phys. Rev. Lett. **121** (2018) no.5, 052301 [erratum: Phys. Rev. Lett. **123** (2019) no.3, 039901] [arXiv:1805.09342 [hep-ph]].

[41] A. Bzdak, B. Schenke, P. Tribedy and R. Venugopalan, Phys. Rev. C **87** (2013) no.6, 064906 doi:10.1103/PhysRevC.87.064906 [arXiv:1304.3403 [nucl-th]].

[42] T. Altinoluk, N. Armesto, G. Beuf, A. Kovner and M. Lublinsky, Phys. Lett. B **751** (2015), 448-452 doi:10.1016/j.physletb.2015.10.072 [arXiv:1503.07126 [hep-ph]].

[43] T. Altinoluk and N. Armesto, Eur. Phys. J. A **56** (2020) no.8, 215 doi:10.1140/epja/s10050-020-00225-6 [arXiv:2004.08185 [hep-ph]].

[44] J.R. Gaunt and W.J. Stirling, JHEP **1003**, 005 (2010) [arXiv:0910.4347 [hep-ph]].

[45] B. Blok, Yu. Dokshitzer, L. Frankfurt and M. Strikman, Phys. Rev. D **83**, 071501 (2011) [arXiv:1009.2714 [hep-ph]].

[46] M. Diehl, PoS D **IS2010** (2010) 223 [arXiv:1007.5477 [hep-ph]].

[47] J.R. Gaunt and W.J. Stirling, JHEP **1106**, 048 (2011) [arXiv:1103.1888 [hep-ph]].

[48] B. Blok, Yu. Dokshitser, L. Frankfurt and M. Strikman, Eur. Phys. J. C **72**, 1963 (2012) [arXiv:1106.5533 [hep-ph]].

[49] M. Diehl, D. Ostermeier and A. Schafer, JHEP **1203** (2012) 089 [arXiv:1111.0910 [hep-ph]].

[50] B. Blok, Y. Dokshitzer, L. Frankfurt and M. Strikman, Eur. Phys. J. C **74** (2014) 2926 [arXiv:1306.3763 [hep-ph]].

[51] M. Diehl, J. R. Gaunt and K. Schönwald, JHEP **1706** (2017) 083 doi:10.1007/JHEP06(2017)083 [arXiv:1702.06486 [hep-ph]].

[52] A. V. Manohar and W. J. Waalewijn, Phys. Rev. D **85** (2012) 114009 doi:10.1103/PhysRevD.85.114009

[53] P. Bartalini and J. R. Gaunt, editors, "Multiple Parton Interactions at the LHC," Adv. Ser. Direct. High Energy Phys. **29** (2018), pp.1-450 doi:10.1142/10646

[54] Y. L. Dokshitzer, V. A. Khoze, A. H. Mueller and S. I. Troian, "Basics of perturbative QCD," Gif-sur-Yvette, France: Ed. Frontieres (1991) 274 p..

[55] Bateman, H., Erdelyi, A., Higher Transcendental Functions, Vol.I-III. McGraw-Hill Book Company, New York 1953.

[56] C. Zhang, J. Jia and J. Xu, Phys. Lett. B **792** (2019), 138-141 doi:10.1016/j.physletb.2019.03.035 [arXiv:1812.03536 [nucl-th]].

[57] J. Jia, private communication.

[58] B. Blok and R. Segev, in preparation.

המרכזי המתאים. המונמט המרכזי של מספר זוגי של חלקיקים נקרה המומנט הסמטרי, עבור מספר אי-זוגי של חלקיקים המומנט המרכזי נקרה אסימטרי מכיוון שהוא מחייב שנסתכל על הרמוניות שונות עבור החלקיקים השונים.

התזה הזו מסודרת בצורה הבאה:

במבוא אנחנו מסבירים את המטרות של המחקר שלנו.

בפרק השני אנחנו נותנים סיקור של הרעניונות הבסיסיים של הדרך חשיבה החדשה עבור אירועים בעלי מספר תוצרים גבוהה בהתנגשויות פרוטון-פרוטון בהתבסס על התאבכות קוונטית ואינטרקציה מרובת פרטונים. ספציפית אנחנו מסבירים את הגאומטריה של התנגשות מרובת תוצרים ואת הכלים מניסיניים והמתמטיים שנשתמש בהם כדי לתאר את התלות האופקית בין החלקיקים, אז אנחנו מסכמים את הרעיונות הבסיסיים של אינטרקציה מרובת פרטונים, ואז מפרטים את הפרטים של המודל בו נשתמש כדי לחשב את המומנט האסימטרי של שלושה חלקיקים.

בפרק שלוש אנחנו מבצעים את החישוב של המומנט האסימטרי המתקבל עבור שלושה חלקיקיסת וחוקרים את התלות של מומנט זה בתנע של החלקיקים ומספר החלקיקים הנפלטים, ולבסוף משווים את החישוב לתוצאות אשר נמדדו ב-LHC. ספציפית אנחנו מתחילים מלבסס מחדש את הבעיה המרכזית ולהזיג אותה בתור הכלים של המודל שאנחנו עובדים איתו, ואז אנחנו מסכמים את הכלים של המודל שאנחנו צריכים בשביל לחשב את המונמט האסימטרי של שלושה חלקיקים, לאחר מכן אנחנו מחשבים את המומנט האסימטרי של שלושה חלקיקים כתלות בתנע של החלקיקים עבור המקרה הפשוט של שלוש אינטרקציות פרטוניות ושלושה חלקיקים שנפלטו, ולבסוף אנחנו מוצאים את התלות של המומנט האסימטרי עבור שלושה חלקיקים במספר החלקיקים שנפלטו ומשווים את התוצאות למדידות הקיימות.

פרק ארבע מציג את מסקנות המחקר.

תקציר

התצפיות האחרונות מראות תלות אופקית לא טריוויאלית בהתנגשויות פרוטון-פרוטון (החלקיקים הנפלטים מההתנגשות מראים קשר בכיוונים שלהם במישור המאונך לציר ההתנגשות) בעלות מספר תוצרים גבוהה במאיץ ההדרונים הגדול (LHC), תלות זו מכונה גם תופעת **רכס**. תצפיות אלו העלו התעניינות משמעותית. התעניינות זו עלתה מכיוון שתלות דומה נצפה לפני כן בהתנגשויות של יונים כבדים ב-LHC ובמאיץ היונים הכבדים היחסותיים (RHIC), כאשר עבור יונים כבדים תופעת הרכס נחשבה לסימן חשוב ליצירה של פלזמת קווארק-גלואונים (QGP). תופעת הרכס נראת טבעית במסגרת של QGP, בגלל האינטרציה החזקה בין החלקיקים הנוצרים במצב הסופי שלהם, אבל בהתנגשויות פרוטון-פרוטון שטח החתך הקטן יותר והצפיפיות הנמוכה מהווים קושי עבור הסבר על ידי QGP, בנוסף התנגשויות פרוטון-פרוטון מתאימות לתוצאות של יוצרי מונטה-קרלו שמניחים כי החלקיקים הנפלטים לא תלויים אחד בשני. זה הוביל למחקרים של מודלים חדשים שיסבירו את תופעת הרכס, ספציפית פותח מודל חדש שמבוסס על התאבכות קוונטית ואינטרקציה מרובת פרטונים (MPI). עד כו הפורמליזם הזה שומש בהצלחה לחישוב התלות הסימטרית.

בחיבור זה אנחנו חוקרים את ההשפעה של התאבכות קוונטית וזרימת צבע על התלות בין שלושה חלקיקים שמתוארת על ידי המומנט האסימטרי באירועים בעלי מספר תוצרים גבוהה בהתנגשויות פרוטון-פרוטון. אנחנו משתמשים במודל שפותח לאחרונה לחקירת ההתנהגות הקולקטיבית במומנטים הסימטריים. אנחנו מראים שהמומנט האסימטרי המתקבל עבור שלושה חלקיקים מתאים איכותית לתוצאות שנמדדו כאשר מתשמשים באותם פרמטרים בהם השתמשו כדי לחשב את המומנטים הסימטריים. התוצאות שלנו מראות שהתלות במצב ההתחלתי של החלקיקים הסופיים חייבת להיות משמעותית, ואולי אפילו שולטת בהסבר של התלות עבור אירועים בעלי מספר תוצרים גבוהה בהתנגשויות פרוטון-פרוטון.

על מנת לחקור את התלות האופקית בין החלקיקים ביותר פרטים, נהוג לפתח צפיפות החלקיקים במרחב התנע כסדרת פורייה עבור הזווית האופקית, כאשר המקדמים של הסדרה הזו נקראים הרמוניות זרימה, טכניקה זו נקרת אנליזת זרימה. הקשר בין ההרמוניות זרימה והתלות האופקית נהיה מדוייק יותר כאשר מסתכלים על תלות בין כמה שיותר חלקיקים, אבל כאשר מסתכלים על מספר חלקיקים גבוהה צריך להפחית את התלות של תתי הקבוצות, הגודל שנותן לנו את הרמוניית הזרימה הוא המומנט

הדרכה

המחקר נעשה בהנחיית פרופסור בלוק בוריס בפקולטה לפיזיקה.

אני מודה לטכניון על התמיכה הכספית הנדיבה בהשתלמותי.

חישוב מומנט אסימטרי עבור שלושה חלקיקים בהתנגשויות פרוטון-פרוטון מרובות תוצרים ב-LHC

חיבור על מחקר

לשם מילוי חלקי של הדרישות לקבלת התואר מגיסטר למדעים בפיזיקה

רן שגב

הוגש לסנט הטכניון - מכון טכנולוגי לישראל
אדר א' ה'תשפ"ב, חיפה, פברואר 2022

חישוב מומנט אסימטרי עבור שלושה חלקיקים בהתנגשויות פרוטון-פרוטון מרובות תוצרים ב-LHC

רן שגב